Electrochemical and surface studies of the effect of naphthalene-based additives on tin electrodeposition

Aranzales Ochoa, D.M.

Cover Page

The handle http://hdl.handle.net/1887/3151629 holds various files of this Leiden University dissertation.

Author: Aranzales Ochoa, D.M.
Title: Electrochemical and surface studies of the effect of naphthalene-based additives on tin electrodeposition
Issue date: 2021-03-17

Electrochemical and surface studies of the effect of naphthalene-based additives on tin electrodeposition

Proefschrift

ter verkrijging van

de graad van Doctor aan de Universiteit Leiden,

op gezag van Rector Magnificus Prof. Dr. ir. H.Bijl,

volgens besluit van het College voor Promoties

te verdedigen op woensdag 17 maart 2021

klokke 15:00 uur

door

Diana Marcela Aranzales Ochoa

Geboren te Bogota in 1988

Promotiecommissie

Promotor

Prof. Dr. Marc T. M. Koper (Universiteit Leiden)

Co-promotor

Dr. Jacques Wijenberg (Tata Steel, IJmuiden)

Overige leden

Prof. Dr. E. Bouwman (Universiteit Leiden)

Prof. Dr. H. S. Overkleeft (Universiteit Leiden)

Prof. Dr. J. M. C. Mol (Technische Universiteit Delft)

Prof. Dr. A. Hubin (Vrije Universiteit Brussel)

Dr. D.G.H. Hetterscheid (Universiteit Leiden)

A Dios por hacerme testigo de la magnificencia de su obra,

A mis padres y hermanos

Table of contents

_____

List of Abbreviations

SA	-	Sulfuric Acid
MSA	-	Methane Sulfonic Acid
ML	-	Monolayer
UPD	-	Underpotential Deposition
OPD	-	Overpotential Deposition
XRD	-	X-ray Diffraction
STM	-	Scanning Tunnelling Microscopy
RE	-	Reference Electrode
RHE	-	Reversible Hydrogen Electrode
NHE	-	Normal Hydrogen Electrode
CE	-	Counter Electrode
RDE	-	Rotating Disk Electrode
SEM	-	Scanning Electron Microscopy
HER	-	Hydrogen Evolution Reaction
LSV	-	Linear sweep Voltammetry
CV	-	Cyclic Voltammetry
NPT	-	Naphthalene
NPTS	-	Naphthalene Sulfonic Acid
HNPTS	-	Hydroxy Naphthalene Sulfonic Acid
ENSA	-	Ethoxylated α-napthalenesulfonic acid
SERS	-	Surface Enhanced Raman Spectroscopy
DFT	-	Density Functional Theory
DL	-	Double Layer
BDD	-	Boron Doped Diamond
j	-	Current density
$D_{Sn^{2+}}$	-	Diffusion coefficient Sn (II)
SH	-	Scharifker and Hills model
N	-	Number of nuclei

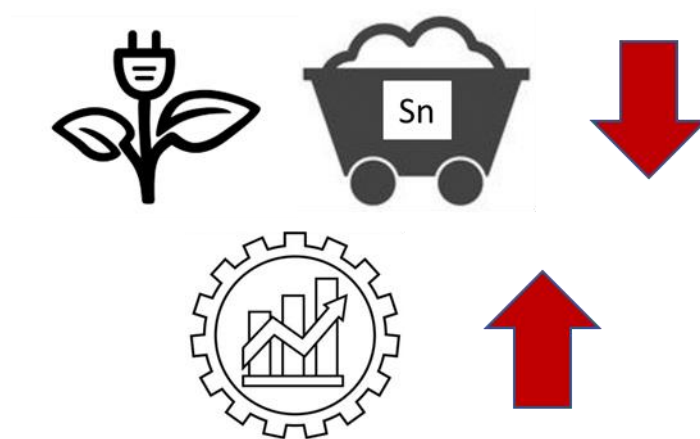**List of Abbreviations**

_____

N_0 -   Number of actives sites

A -   Rate constant

AN_0 -   Steady state nucleation rate

Introduction

_____

1.1 Electrodeposition

Electrodeposition of metals is a process that has profoundly influenced the world, allowing the improvement of properties of metals or other materials by protecting and enhancing their functionality. Electrodeposition is used in many diverse industries, including home appliances, jewellery, automotive, aircraft and airspace, batteries and electronics, both for decorative and engineering applications. Electrodeposition has a strong technological and economic significance, which has evolved over the years. Nowadays, decorative applications have diminished, primarily due to added expenses and problems associated with plant effluent control and waste treatment; on the other hand, applications in engineering, electroforming and electronics are continuously increasing.

Electroplating as a process started in 1772 with Giovanni Beccaria, who decomposed metal salts using the charge of a Leyden jar to supply a pulse of current[1]. Later, in 1803, Luigi Brugnatelli officially invented the electroplating process by successfully plating a thin layer of gold onto a silver coin[2]. Initially, the development of electroplating was slow because of the limitations of electricity sources. Alessandro Volta's invention of the "Volta's pile" in 1796 did not prove to be an appropriate source of energy for commercial electroplating[3]. However, shortly afterwards, in 1836, the understanding of electricity allowed the development of the first electricity generators, and subsequently it led J.F Daniell to invent the self-polarizing cell, a more reliable source of electricity. Finally in 1840, George Elkington patented an improved method of gilding copper, brass and other metals or alloys of metals[1].

1.2 Tin plating

Multiple metals are currently used in electroplating processes. However, there is a metal that stands out as one of the earliest metals to be known and used since the earliest periods of urban civilization: Tin[4]. It is a soft metal, ductile, with a low melting point. Tin finds application as a metal and in chemical compounds. As a metal, it is mainly used as an alloy or coating, and its chemical compounds are of high relevance in agricultural, plastics and pharmaceutical products. Currently, tin plays an important role in daily life, being used in food packaging, jewellery, also in modern technology in electric vehicles, aerospace, batteries, photovoltaics cells, among others[5]. Tin coatings are used to protect from air oxidation, to enhance corrosion resistance, to improve solderability, for decorative purposes and as anode material for Li-ion batteries[6, 7].

1.2 Tin plating

_____

The development of tin plating was independent on the electrodeposition process during the early stages. The origin of tinplate can be traced to the tinning of hammered iron sheet in Bavaria in the 14th century. Later on, the tinplate industry spread to Dresden (Germany), and tinplate articles were exported to many countries, including England. In 1720, a tinplate factory was set up in South Wales - UK, where the incorporation of mechanical tinning machines allowed to extend and increase the productivity. Subsequently, tinplate reached the United States, and later on Asia. During the first half of the 20th century continuous advancements in the tinplate process were achieved, from hot-dipping to electrotinning.

Electrotinning became popular giving the advantages of producing thinner, more uniform tin coatings and lower manufacturing cost than the hot-dipping process. However, it was not until World War II, when tin supplies were scarce, that electrotinning process was widely implemented. Currently, the majority of tin electroplating is done over steel sheets (thin mild steel)[8].

Three electroplating processes were developed according to the type of electrolyte and design of the processing units: alkaline tin (IV) oxide hydrate salts, ferrostan (phenolsulfonic acid or 4-Hydroxybenzenesulfonic Acid), and halogen (fluoride and chloride). Most commercial tin electroplating lines in the world use the ferrostan process, which is based on a sulfonic acid electrolyte[9]. Figure 1 shows the schematic arrangement of the handling and processing units of the three types of electrotinning lines.
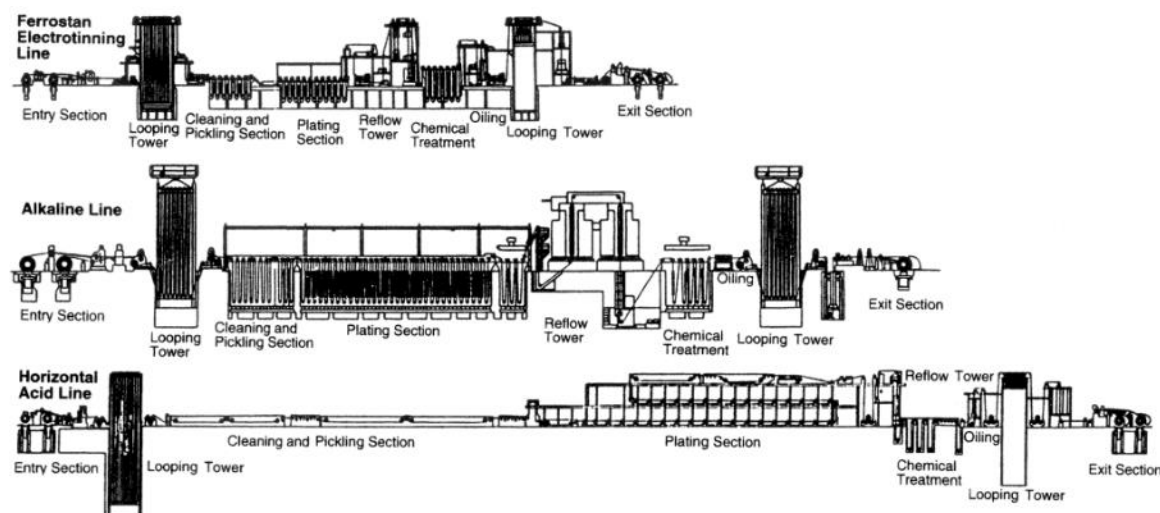

Figure 1. Schematic arrangement of handling and processing units of three types of electrotinning lines[9]

Regardless of the different electrolytes and design of the electrotinning lines, a series of common steps are present in the electroplating processes:

- Cleaning and pickling:

The strips are thoroughly cleaned by oxidation of the surface in acidic media and subsequent washing. This process is followed by pickling that removes oxides and rust layers. It also etches the surface for better deposition of tin.

- Electroplating:

Tin is electrodeposited usually via galvanostatic method. This process can be made from different electrolytes, using different tin salts and additives. This topic will be discussed in detail in the following section.

- Thermal treatment:

The tin coated strip is flow-melted by resistance heating to a temperature just above the melting point of tin and followed by a water quenching. This procedure generates a reflective surface and creates iron-tin intermetallic compounds, which play an important role in the stability of the material.

- Passivation:

The tin coated strip is passivated by immersion in dichromate solution which deposits a very thin chromate film of chromium on the surface.

- Organic coating:

A thin film of oil is applied to the surface in order to preserve the surface from attack and also to enhance the lubrication properties.

1.3 Tin electroplating baths

Although the composition of electroplating baths used in tin electrodeposition process is quite diverse, almost every single bath consists of: electrolyte, tin salts, and additives. Physical and chemical properties of the tin deposits are strongly dependent on the electrolytes, tin salts, and additives used during the process.

1.3.1 Electrolytes

Electrolytes for tin deposition can be acidic or alkaline. Currently, most of the tin electrodeposition in the industry is carried out under acidic conditions.

Alkaline baths are usually hydroxides, they do not require additives and they are known as not corrosive to steel (due to the passivation of the Fe). Alkaline baths are composed by a tin (IV)

oxide hydrate which must be heated above 65 ^{0}C during the deposition, because at lower temperatures Sn (IV) precipitates as a SnO_2. Tin electrodeposition from alkaline tin (IV) oxide hydrate solution leads to low maximum current density[5] and requires twice as much electric charge necessary to deposit the same mass of tin from tin (II) salt solutions[10]. Currently, this type of bath is obsolete.

Acidic baths are often composed of sulfate or sulfonate electrolytes using tin (II) salts. Acidic solutions offer faster deposition rates at ambient temperature. However, Sn (II) easily oxidizes and produces SnO_2 that precipitates in the plating tanks. To avoid Sn (II) oxidation and to stabilize the acidic bath, inorganic and organic additives have to be added in the solution. The most used acidic electrolytes are:

- Phenol sulfonic acid (PSA) electrolyte:

The PSA electrolyte consists of a solution of PSA, tin (II) salts solutions and additive agents that ensure the quality of the deposits over a wide current density range[11]. This bath was one of the first to be developed, and it is still present in some parts of the world; nonetheless, it has been gradually substituted due to environmental regulations.

- Halogen electrolyte:

The halogen electrolyte consists of a solution of tin chloride, sodium and potassium fluoride, chloride salts and organic additives. It is a widely employed electrolyte bath; it has the distinction that it operates with a different type or design of electroplating line, having horizontal rather than vertical plating tanks, which enables lines to be run faster. It was developed by E. I. du Pont de Nemours, Weirton Steel and Wean Engineering.

- Flouroboric acid electrolyte:

The fluoroboric acid electrolyte contains tin fluoroborate, fluoroboric acid and boric acid. Boric acid is known to prevent hydrolysis of the fluoroborate ions. It was developed by Rasselstein in the late 1940's; this bath did not become popular due to commercial restrictions.

- Methane sulfonic acid electrolyte:

The use of methane sulfonic acid as electrolyte in the electroplating of tin and tin alloys started in the early 1980's. MSA easily gained an important market and spread in the electroplating industry with wide acceptance, owing to its many advantages, which include: high conductivity, biodegradability, less Sn (II) oxidation and high current density. The wide approval of MSA generated additional developments for applications in mass scale process. In 1989, the first commercial tinplate production line using a patented MSA process (Ronastan) was implemented in IJmuiden, The Netherlands.

Studies of tin electrodeposition using deep eutectic solvents have also been performed[12, 13]. Deep eutectic electrolytes offer advantages such as high metal salt solubility and the ability to tailor redox properties of the metal ions through choice of the anion. This type of bath has

been used for tin alloys, where it is very difficult to control alloy composition because of the large differences in the redox potentials for the metal ions, or because of other effects, such as different kinetics of deposition of the two metals with respect to each other and the substrate[13]. Deep eutectic solvents are formed between a variety of quaternary ammonium salts and carboxylic acids.

Recent years have shown constant improvements of the tin electroplating process from MSA electrolyte and other electrolytes, allowing to get thinner thickness in the tin deposits, tailoring morphology and decreasing the amount of sludge formed during the process. However, many questions remain unsolved about the effect of the electrolyte at the electrode-electrolyte interface and in the solution, as well.

1.3.2 Additives

Tin electrodeposition in acidic conditions require the use of organic additives, as tin coatings plated without additives in the electrolyte are non-adherent, coarse, porous, and exhibit dendrites[14]. The use of additives in the electroplating baths allows to tailor and improve properties of the deposits, fulfilling the required characteristics for the different uses of tin electroplated surfaces. Some studies have also reported adverse effect of additives by organic co-deposition on the coatings[15, 16].

The chemical structure of the organic additives employed in tin electrodeposition is quite diverse and complex including aromatic sulfonates, amine derivatives, phenol derivatives, unsaturated carbonyl compounds, polyoxyethylene and polyoxypropylene, glue, gelatin, wood tar, resins, among others. The development of these organic additives has been mainly empirical and their mechanism of action remains not fully understood. In contrast to what is seen for copper electrodeposition, where a widely accepted classification of the additives has been established (i.e., accelerator, suppressor, leveler), the classification of additives used in tin electrodeposition based on their effect is still under discussion. Nonetheless, one of the classifications for additives used in tin and tin-lead alloy plating baths is given by Jordan[17].

Jordan classified the organic additives as surface active agents, oxidation inhibitors, grain refiners and brighteners[17].

Surface active species are known to have strong polarizing effects on tin deposition. They also act as emulsifying agents for brighteners, meaning that they facilitate their dissolution. Some of the most characteristic compounds are: polyethylene glycol, polypropylene glycol, fatty acid ethoxylates, alkylphenol ethoxylates, α or β naphthol ethoxylates, poly alcohols, among others. The most characteristic effect of surface-active species is to produce tin deposits free of dendrites, with smaller grain size that generates matt to satin-bright deposits.

Oxidation inhibitors or stabilizers are added to the acidic baths in order to avoid or minimize the oxidation rate of Sn^{2+} to Sn^{4+}. Sn (IV) ions easily form SnO_2 that precipitates and forms

sludge in the plating tanks, generating technical and economic problems. Some of the molecules that are used as oxidation stabilizers are hydroquinone, hydrazine, ascorbic acid and sulfonic acid. 2-hydroxy-6-methylbenzenesulfonic acid (cresol sulfonic acid) seems to be one of the first compounds to be used as an oxidation stabilizer in tin electrodeposition[18] .

Grain refiners are compounds that generates a decrease of the size of the metal features. Some of the typical grain refiners are aromatics such phenol sulfonic acid, 2–naphthol based compounds, also alkyl sulfonic acids, among others.

Brighteners lead also to a significant grain refining and increase the reflectivity of the metal deposit surface. Reflective surfaces are characterized by crystallite sizes at the surface of less than 0.3 μm^2. Kanani[19] describes two types of brighteners. The first group generates a decrease in the grain size but it does not generate mirror-finish deposits; sulfonamides, alkyl sulfonic acids are in this group. The second group of brighteners impart a near mirror finish deposit, even at very low concentrations; thiourea, thiocarbazone mercaptoalkylsulfonic belong to this group[19].

4-phenylbut-3-ene-2-one (an alpha beta unsaturated ketone) is also known as a model brightener reagent that generates very smooth and bright tin deposits by inhibiting the metal growth by its strong adsorption or the adsorption of its reaction products on the substrate[17]. Other compounds are also broadly used as brighteners, such as aromatic amines and aliphatic aldehydes.
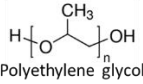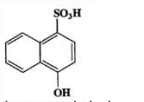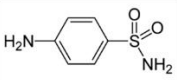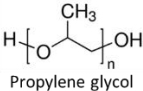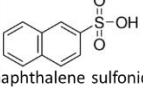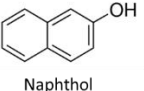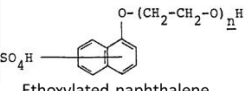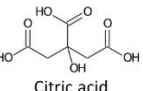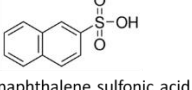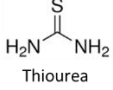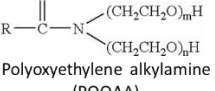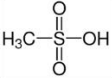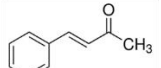
The broad variety of current applications of tin coatings in technological and daily life products and its potential future uses has triggered an important increase of tin electrodeposition studies in the last 25 years. Multiple studies about the influence of the electrolytes, tin salts and additives have been performed; these studies have been mainly focused on the characteristics of the tin deposits, therefore properties such as smoothness, brightness, adhesion, grain size, crystalline orientation, wear resistance have been meticulously considered for tin electrodeposition on different substrates and in the presence of different electrolytes and mixes of additives. On the other hand, the studies that consider single additives and their role in the initial stages of the tin electrodeposition process are much fewer.

The development in the composition of the plating baths has been mostly empirical and ad hoc, which explains why there are fewer studies that consider baths with single additives and their influence in the initial stages of the deposition process. Further, a considerable percentage of plating baths composition remains undisclosed by the companies.

A proper understanding of the initial stages of tin electrodeposition process and the influence of the electrolyte and additives would allow an extension of the current applications and an improvement of the process. Nonetheless, many questions remain unsolved, such as the influence of the electrolyte and additives on the metal ions species in solution, the mechanisms of interaction of the electrolyte and additives with the substrate, on the kinetics

of nucleation and growth, the evolution of the morphology during the nucleation and growth, the chemical composition of the deposit, among others.

Table 1. Some of the most common additives used on tin electrodeposition process

Surface active species	Oxidation inhibitors	Grain refiners	Brighteners
Polyethylene glycol	Hydroquinone	Hydroxy naphthalene sulfonic acid (HNPTS)	4-amino benzene sulfonamide
Propylene glycol	2- naphthalene sulfonic acid	Naphthol	Alkyl sulfonates
Ethoxylated naphthalene sulfonic acid (ENSA)	Citric acid	2 - naphthalene sulfonic acid	Thiourea
Polyoxyethylene alkylamine (POOAA)	Methanesulfonic acid		4-phenylbut-3-ene-2-one

1.4 Outline of this thesis

The aim of this thesis is a fundamental approach to the understanding of the effect of electrolytes and additives on the mechanism of tin electrodeposition process, and the corresponding thermodynamics and kinetics parameters of the nucleation and growth processes. The work provides insights for the improvement of the tin electrodeposition process and also for electrodeposition of other metals.

In Chapter 2, we study tin electrodeposition on polycrystalline gold electrodes from two different supporting electrolytes: sulfuric acid (SA) and methanesulfonic acid (MSA), both of them commonly used in the industry. We show electrodeposition of tin takes place via three different mechanisms: irreversible adsorption, underpotential deposition and overpotential deposition. Our results show tin overpotential deposition is faster in the presence of sulfate than in methanesulfonate anions, presumably due to complex formation. Static and hydrodynamic measurements also show methanesulfonate anions lead to a more homogenous tin coverage than sulfate.

Subsequently, in Chapter 3 we build upon on the findings obtained in the previous chapter, and we study the effect of naphthalene derivatives: naphthalene (NPT), naphthalenesulfonate (NPTS), hydroxynaphthalenesulfonate (HNPTS), and ethoxylated napthalenesulfonic acid

1.4 Outline of this thesis

_____

(ENSA), a commonly used additive in the industry, on the tin electrodeposition process on a gold electrode. We conclude the formation of (condensed) films of NPT, NPTS, HNPTS and ENSA. We show tin electrodeposition is strongly affected by the presence of the naphthalene derivatives films. Tin bulk electrodeposition is inhibited in the presence of NPT and NPTS, but promoted in the presence of HNPTS. Tin deposits grown in the presence of NPT and NTPS seem to have the same morphology, but the tin deposit grown in the presence of HNPTS exhibits markedly smaller features. ENSA exhibits a similar behaviour to NPT and NPTS during the tin deposition process in terms of the measured voltammetry: a suppression of the bulk Sn electrodeposition, but essentially no effect on the AuSn alloy formation. Furthermore, sulfonated additives lead to some form of sulfur incorporation in the AuSn alloys.

In Chapter 4, we continue the study of the effect of naphthalene-based additives on the kinetics of tin electrodeposition on a boron doped diamond electrode. Current transients in the presence of NPT, NPTS and HNPTS are analysed with the standard Scharifker-Hills model determining the steady state nucleation rate (AN_0) and the number density of nucleation sites (N_0). In the absence of additives, the nucleation process is shown to transition from progressive to instantaneous with increasingly negative potential. A decrease in the nucleation kinetics of tin deposition on BDD is observed in the presence of naphthalene-based additives: NPT showed the smallest effect on the reduction of the kinetics, followed by NPTS, and the strongest effect is observed in the presence of HNPTS. Moreover, we show that Sn (II) is not complexed by the additives and charge transfer kinetics is not influenced by the presence of the additives. Additives only affect the nucleation process. Furthermore, the behavior of ethoxylated α-napthalenesulfonic acid (ENSA) exhibits an identical behavior that on gold, i.e., a strong inhibition of the tin deposition process.

Finally, in Chapter 5 we use the gathered knowledge of the effect of naphthalene-based additives on tin electrodeposition on more stable substrates, i.e., gold and boron doped diamond electrodes, to provide insights of the interaction of the additives with iron and their effect on the overall tin deposition process on an iron electrode. We showed the effect of NPT and NPTS on tin electrodeposition remains mainly independent of the substrate. HNPTS shows a stronger decrease of tin deposition, in agreement with has been previously observed on tin deposition on a BDD electrode. Furthermore, we showed that transport of Sn (II) ions from the bulk to the electrode surface is not affected by NPT, NPTS and HNPTS. We verified that ENSA-6 forms a thick film on the iron surface, a behavior correlated with the results on the gold and BDD surfaces. Lastly, ENSA-6 also exhibits the strongest inhibition of tin deposition on iron.

1.5 References

(1)   Raub, C. The History of Electroplating. In _Metal Plating and Patination_; Elsevier, 1993; pp 284–290.

(2)   Hunt, L. B. The Early History of Gold Plating - A Tangled Tale of Disputed Priorities. _Gold Bull._ 1973, _6_ (1), 16–27.

(3)   de Santillana, G. Alessandro Volta. _Sci. Am._ 1965, _212_ (1), 82–91.

(4)   Barry, B. T. K. Tin Processing. _Encyclopeadia Britannica_; Encyclopaedia Britannica, inc., 2017.

(5)   Walsh, F. C.; Low, C. T. J. A Review of Developments in the Electrodeposition of Tin. _Surf. Coatings Technol._ 2016, _288_, 79–94.

(6)   Hassoun, J.; Scrosati, B. A High-Performance Polymer Tin Sulfur Lithium Ion Battery. _Angew. Chemie - Int. Ed._ 2010, _49_ (13), 2371–2374.

(7)   Zhou, X.; Bao, J.; Dai, Z.; Guo, Y.-G. Tin Nanoparticles Impregnated in Nitrogen-Doped Graphene for Lithium-Ion Battery Anodes. _J. Phys. Chem. C_ 2013, _117_ (48), 25367–25373.

(8)   ITRA Ltda. Guide to Tinplate. 2001, pp 1–124.

(9)   Schlesinger, M. Paunovic, M. _Modern Electroplating_, 5th editio.; Wiley: New Jersey, 2014.

(10)   He, A.; Liu, Q.; Ivey, D. G. Electrodeposition of Tin: A Simple Approach. _J. Mater. Sci. Mater. Electron._ 2008, _19_ (6), 553–562.

(11)   Morgan, E. Tinplate and Modern Canmaking Technology; Pergamon: Oxford, 1985; pp 5–73.

(12)   Abbott, A. P.; Capper, G.; McKenzie, K. J.; Ryder, K. S. Electrodeposition of Zinc-Tin Alloys from Deep Eutectic Solvents Based on Choline Chloride. _J. Electroanal. Chem._ 2007, _599_ (2), 288–294.

(13)   Abbott, A. P.; Alhaji, A. I.; Ryder, K. S.; Horne, M.; Rodopoulos, T. Electrodeposition of Copper-Tin Alloys Using Deep Eutectic Solvents. _Trans. Inst. Met. Finish._ 2016, _94_ (2), 104–113.

(14)   Aragón, A.; Figueroa, M. G.; Gana, R. E.; Zagal, J. H. Effect of a Polyethoxylate Surfactant on the Electrodeposition of Tin. _J. Appl. Electrochem._ 1992, _22_ (6), 558–562.

(15)   Hill, J. S.; MacLachlan, D. F. A.; Stoddart, C. T. H. The Structure and Superconductive Properties of Electrodeposited Tin Films. _Br. J. Appl. Phys._ 1966, _17_ (4), 513–520.

(16)   Jaén, J.; Vértes, A.; Tjutina, K. M.; Kasmodamianskaya, L. V.; Kiss, L.; Shepeleva, E. V. Mössbauer Studies on Electrodeposited Tin-Copper Alloys. _Electrochim. Acta_ 1985, _30_ (4), 535–539.

(17)   Jordan, M. _The Electrodeposition of Tin and Its Alloys_; ASM International, 1999.

(18)   Hothersall, A. W.; Bradshaw, W. N. The Electrodeposition of Tin from Acid Sulfate Solutions. _Trans. IMF_ 1936, _12_ (1), 113–128.

(19)   Kanani, N. _Electroplating: Basic Principles, Processes and Practice_, 1st editio.; Elsevier science: Berlin, 2004.

Voltammetric study of tin electrodeposition on polycrystalline gold from sulfuric and methanesulfonic acid

Chapter 2: Voltammetric study of tin electrodeposition on polycrystalline gold from sulfuric and methanesulfonic acid

_____
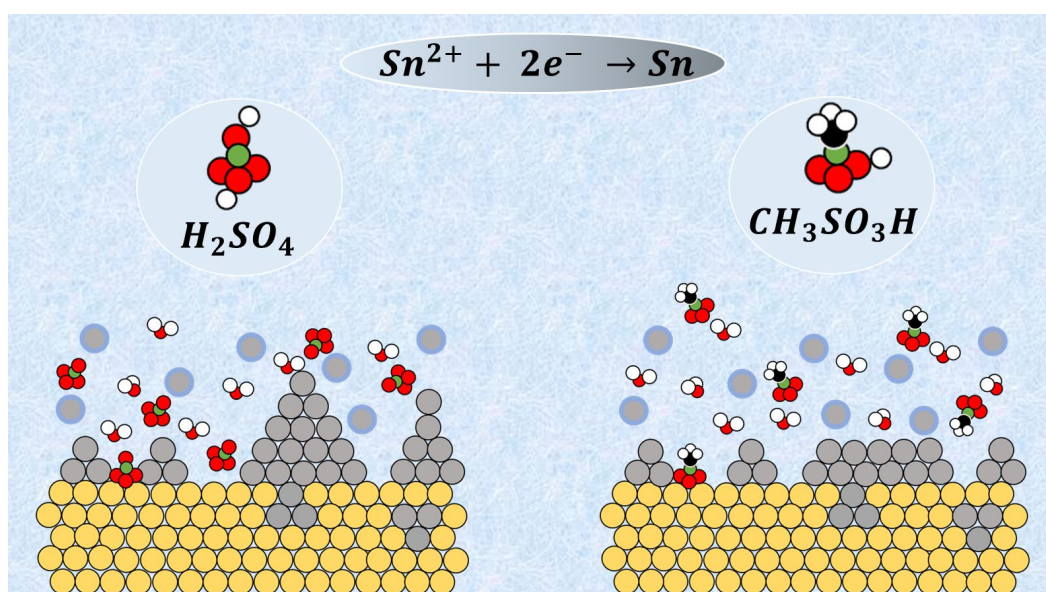
Abstract

In this work, we have studied tin electrodeposition on polycrystalline gold electrodes from two different supporting electrolytes: sulfuric acid (SA) and methanesulfonic acid (MSA), both of them commonly used in the industry. This work aims to understand the effect of the different electrolyte anions on the deposition process. We show at least three different tin deposition mechanisms on gold: irreversible adsorption, underpotential deposition, and overpotential (bulk) deposition. Underpotential deposition leads to the formation of a layer of tin in SA and MSA with a coverage around $\theta_{Sn(H_2SO_4)} = 0.45\ ML$ (monolayer) and $\theta_{Sn(CH_3SO_3H)} = 0.42\ ML$, respectively. The UPD Sn layer is however somewhat uncharacteristic as it is associated with island formation and surface alloying. Cyclic voltammograms in an extended potential range showed five distinct peaks: two cathodic peaks associated with tin underpotential and overpotential deposition, and three main anodic peaks, corresponding to the oxidation of the bulk Sn, of the AuSn intermetallic layer, and of the adsorbed Sn (II) to Sn (IV). Both voltammetric and rotating disk electrode measurements show that the kinetics of tin electrodeposition in MSA is slower than in SA, which we ascribe to Sn-MSA complex formation in solution. Slow Sn deposition in MSA promotes AuSn formation, in contrast to SA in which bulk tin deposition is more prominent. Complete Levich-type mass transport control of tin deposition in SA and MSA was only reached at low scan rate due to concurrent HER on the uncovered gold surface during the deposition process at higher scan rates. An unexpected surface-confined passivation process is observed in both electrolytes.

_____

2.1 Introduction

Tin electrodeposition has become one of the most popular surface coating processes due to several applications in different industrial sectors, such as packaging, microelectronics, automotive and industrial, jewelry and other decorative purposes, batteries for electrochemical storage, amongst many others[1]. Tin electroplating offers many important properties to the substrate because of its good wettability, solderability and compatibility. It is also one of the few metals that is suitable for being in contact with food and chemical products. Exhaustive studies about the science and technology of tin electrodeposition have been performed and reviewed[1,2].

In spite of the large number of studies about electrolytes[3,4], tin salts, and additives[5, 6, 7, 8, 9, 10] used in tin electrodeposition, there is still lack of information about the fundamental aspects of the initial stages of the tin deposition process. It is not fully clear how initial stages are affected by electrolytes, additives and how those stages influence the whole process. A good understanding of the initial stages of tin electrodeposition will allow an improvement of the process and an extension of the current applications of tin deposition, and it can also give insights into the electrodeposition process for other metals.

Fundamental studies of tin electrodeposition have been performed on copper[11], gold[12] and carbon substrates[13]. Although gold is considered an inert metal electrode material, previous studies of tin electrodeposition on gold electrodes have shown that the process is complex. Sn (II) cations are adsorbed irreversibly on gold electrodes. At the surface they presumably undergo different reactions producing oxygenated Sn species such as SnO or Sn (OH)$_2$. With more negative electrode potential, the Sn (II) ad species are reduced to Sn(0), in a reversible surface-confined redox couple[14]. However, this Sn underpotential deposition (UPD) process is unusual in the sense that it does not yield a dense ordered Sn adlayer. Rather, in situ STM studies have shown the formation of clusters of electrodeposited tin[15]. At potentials more negative than UPD, overpotential deposition (OPD) takes place following a diffusion-controlled nucleation and growth process[12]. Multilayer tin deposition on gold is also associated with (surface) alloy formation, as evidenced by XRD, in situ STM and in situ surface conductance measurements[12, 15, 16]. Anodic stripping of electrodeposited tin takes place in (at least) three discernible oxidation peaks, corresponding to the oxidation of the bulk Sn, of the AuSn intermetallic layer, and of the adsorbed Sn (II) to Sn (IV)[12, 17].

In this work, we study the different electrodeposition mechanisms (underpotential deposition UPD, overpotential deposition OPD and irreversible adsorption) from two different acidic supporting electrolytes: sulfuric (SA) and methanesulfonic acid (MSA). Sulfuric acid has been used for many years in the electroplating industry because it is a low-cost electrolyte. Methanesulfonic acid presents an excellent metal salt solubility, high conductivity, stability, wide operating window[18], a relatively low toxicity and good biodegradability[3]. Our study aims

Chapter 2: Voltammetric study of tin electrodeposition on polycrystalline gold from sulfuric and methanesulfonic acid

_____

at investigating how the tin electrodeposition process on a model gold electrode surface differs between these two acidic electrolyte solutions, in order to understand in more detail, the effect of the MSA electrolyte. Although gold is not a practical substrate material for tin electrodeposition, we believe that our results on the influence of the electrolyte may generalize to other substrates.

2.2 Experimental

All glassware was stored overnight in a solution of 1g L^{-1} $KMnO_4$ in 0.5 M H_2SO_4. Before use it was rinsed with water and 30% hydrogen peroxide solution in order to remove permanganate anions and trace impurities. Glassware was boiled in water four times before starting the experiments. The water used to clean glassware and to prepare solutions was demineralized and ultra-filtrated by a Millipore MilliQ system (18.2 MΩ cm). A gold wire was used as a counter electrode and a reversible hydrogen (RHE) was used as a reference, but all potentials are referred to the normal hydrogen electrode (NHE). Reference electrode was in contact with the electrolyte via a Luggin capillary; the gap between the RE Luggin capillary and the working electrode is about 2 cm.

A capacitor of 10 µF was connected to the gold wire and the RHE electrode in order to filter small currents produced in the RHE electrode and reduce the noise in measurements at low currents. The working electrode was either a gold hemispherical bead electrode (surface diameter ~ 2.5 mm) under static conditions, or a gold disk electrode (5 mm diameter, 4 mm thick) under hydrodynamic conditions (RDE experiments). Cyclic voltammetry experiments were performed using a potentiostat PGSTAT 12 (Metrohm-Autolab). RDE experiments were performed with a MSR rotating electrode (Pine Research) at rotation rates of 400, 900, 1600, 2500 rpm.

Before each measurement, the working electrode was cleaned electrochemically; the electrode was first oxidized in 0.1M sulfuric acid by applying 10 V for 20 s, using a graphite bar as a counter electrode and then the gold oxide formed was removed by dipping the working electrode in a 6 M HCl solution for 30 s. Subsequently, the electrode was rinsed and electropolished in a solution 0.1 M H_2SO_4 through 200 cycles between 0 to 1.8 V at 1 V s^{-1}. Additionally, before every measurement, cyclic voltammetry of the gold surface was recorded at potentials between 0 to 1.8 V at 50 mV s^{-1} to test the quality and cleanliness of the surface and the solution. The electrode potential was corrected for Ohmic drop during the measurements, by using 85% of the ohmic resistance measured by electrochemical impedance spectroscopy. Ohmic drop was compensated at 85% in order to avoid overcompensation and/or associated instabilities due to possible changes in the solution resistance during the measurements.

All solutions were prepared from chemicals with the highest purity commercially available: H_2SO_4 (96% ultrapure, Merck), $HClO_4$ (60%, Merck – EMSURE® ACS), Na_2SO_4 (99.995% - metal basis, Alfa Aesar), CH_3SO_3H (≥99.0%, Sigma Aldrich), Sn $(CH_3SO_3)_2$ (50 wt. % in H_2O, Sigma Aldrich), $SnSO_4$ (≥ 95%, Sigma Aldrich).

The production of Sn^{4+}, hydrolysis products and polymeric species formed in the bulk of the solution were avoided by working in an oxygen-free atmosphere (permanent Argon bubbling), at a pH lower than 2, and low Sn^{2+} concentrations. Nevertheless, the presence of hydrolysis products at or near the electrode surface cannot be excluded due to an increase in the local pH during hydrogen evolution on gold. However, once the substrate is fully covered by tin, this effect should be negligible.

2.3 Results and discussions

2.3.1 Tin underpotential and overpotential deposition and tin stripping

Figure 1 shows a comparison of the cyclic voltammograms (CV) of gold in sulfuric, methanesulfonic and perchloric acid in an extended potential region, including the Hydrogen Evolution Reaction (HER). The CV in perchloric acid was included as perchlorate anions are considered to be non-specifically adsorbed on the gold electrode. The onset potentials values for gold (hydr)oxides formation are ca. 1.29 V ($HClO_4$), 1.36 V (CH_3SO_3H) and 1.42 V (H_2SO_4), suggesting that methanesulfonate anions adsorb more strongly than perchlorate anions but more weakly than sulfate anions. The charges corresponding to gold oxide formation and reduction (ca. 390 $\mu C\ cm^{-2}$) were calculated in sulfuric acid (SA) and methanesulfonic acid (MSA), respectively.

These charges are almost the same for both electrolytes, indicating that the oxide formation and reduction are not strongly affected by the anions of the electrolyte. Hydrogen evolution currents at negative potentials are similar for all three electrolytes. In brief, there are only small differences in oxidation and reduction profiles at the gold surface in these electrolytes.

Chapter 2: Voltammetric study of tin electrodeposition on polycrystalline gold from sulfuric and methanesulfonic acid

_____

Figure 1. Cyclic voltammograms of a polycrystalline gold disc electrode, 0.1 M H_2SO_4 (red line) and 0.1 M CH_3SO_3H (black line) and 0.1 M $HClO_4$ (green line) recorded between -0.34 to 1.81 V in SA and -0.33 to 1.82 V vs. NHE in MSA at 50 mV s^{-1}.

Figure 2. Cyclic voltammograms of tin electrodeposition on a polycrystalline gold electrode for different switching anodic potentials at 30 mV s^{-1}. a) 0.1 M H_2SO_4, 0.1 Mm $SnSO_4$ b) 0.1 M CH_3SO_3H, 0.1 Mm Sn $(CH_3SO_3)_2$.

Figures 2a and 2b show that tin electrodeposition on gold from both electrolytes takes place via two cathodic peaks (C1 and C2) and (at least) three anodic peaks (A1, A2 and A3). Peaks C1 and C2 have been ascribed to UPD and OPD of tin[12,17]. UPD charges were calculated between 0.009 to 0.199 V in SA and 0.021 to 0.211 V in MSA V vs. NHE (0.009 and 0.021 V are

18

_____

more positive than standard equilibrium potential of the Sn^{2+}/Sn couple), as indicated in the inset of Figures 3a and 3b, giving charge density values for Q_{Sn-UPD} of 175 µC cm^{-2} and 165 µC cm^{-2} in H_2SO_4 and CH_3SO_3H, respectively. These values agree with earlier values determined by Rodes et al.[19], and correspond to a tin coverage onto the gold surface of $\theta_{Sn(H_2SO_4)} = 0.45$ ML and $\theta_{Sn(CH_3SO_3H)} = 0.42$ ML, assuming a full discharge of two electrons leading to 1 ML$_{Sn}$= 390 µC cm^{-2}, and the absence of the influence of anions. We note that there is some ambiguity in determining the UPD charge and consequently the corresponding tin coverage, as there is no clearly distinguishable UPD onset potential due to the nature of the polycrystalline substrate, and to the contribution of double layer charging. The charge density values, as well as previous work on Sn electrodeposition on gold and our own SEM images (see Fig.A1 in the appendix A), suggest that the Sn layer is not dense but rather forms clusters[15]. To illustrate this effect using an electrochemical measurement, we make use of the fact that the HER has a much higher overpotential on Sn than on Au[20]. Figure 3 shows the HER current on Sn-modified gold electrodes prepared with different amounts of tin at different potentials. Tin deposited in the middle and at the end of UPD region, i.e., at 0.009 and -0.08V in SA and 0.021 and -0.07 V and MSA, resp., leads to a lowering of the HER current, but no complete blockage is observed. Even for Sn deposited at -0.141 V in SA and -0.129 V in MSA, i.e., in the OPD region, there is still no complete blockage compared to the situation where Sn has been deposited at -0.541 V in SA and -0.529V in MSA. Remarkably, Sn deposition in MSA electrolyte leads to a better blockage of the HER current than Sn deposition in SA electrolyte. This suggests a denser Sn layer generated in MSA, although, as we will see below, Sn deposition in MSA is generally slower than in SA. Probably the slower growth leads to a more homogeneous coverage of tin on the gold electrode.
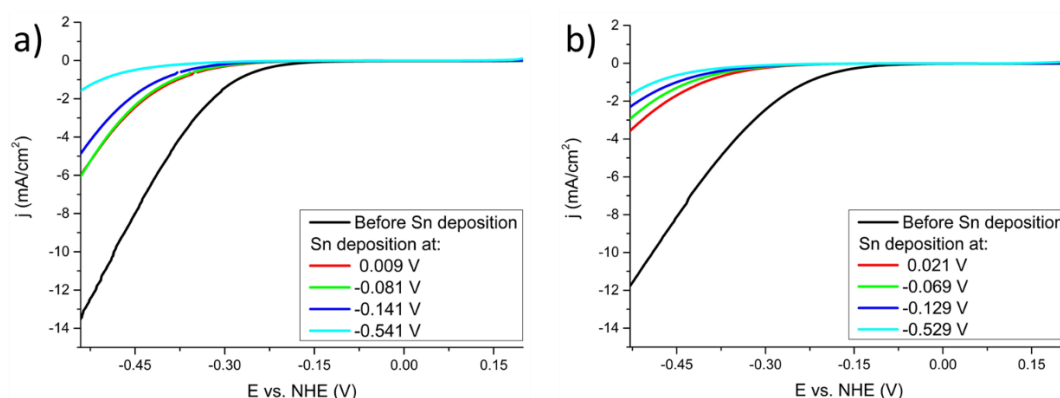
Figure 3. H$_2$ evolution activity of polycrystalline gold electrode before and after tin deposition at different potentials. Tin deposition was carried out through LSV, with different final potentials: (-0.05, -0.14, -0.20 and -0.60 V vs RHE). After each tin deposition, electrode was transferred to a tin free-electrolyte solution at -0.101V in SA and -0.09 V in MSA. Linear sweep voltammograms were recorded at 30 mV s^{-1}, from 0.199 to -0.541 V in SA and 0.211 to -0.529 V in MSA. a) 0.1 M H$_2$SO$_4$ b) 0.1 M CH$_3$SO$_3$H

Chapter 2: Voltammetric study of tin electrodeposition on polycrystalline gold from sulfuric and methanesulfonic acid

_____

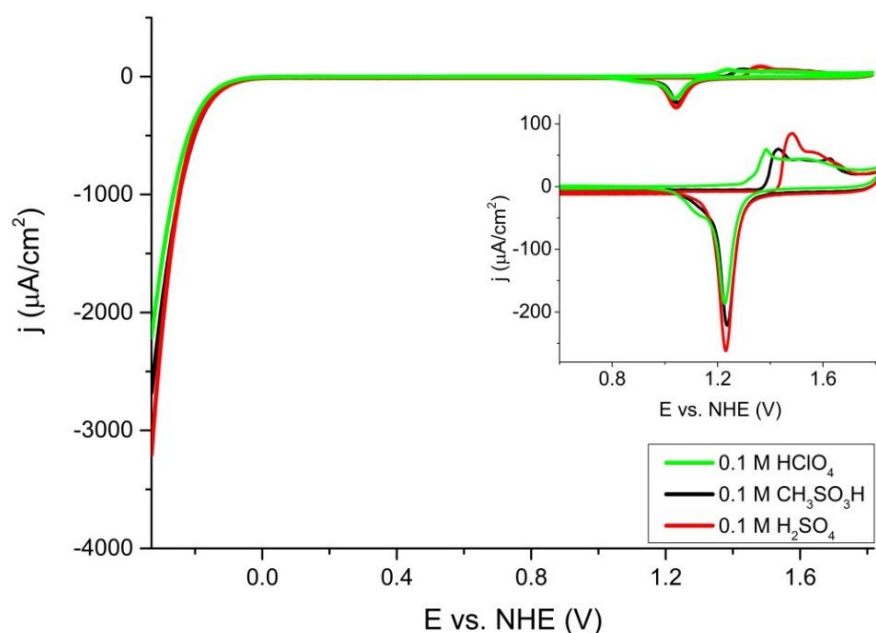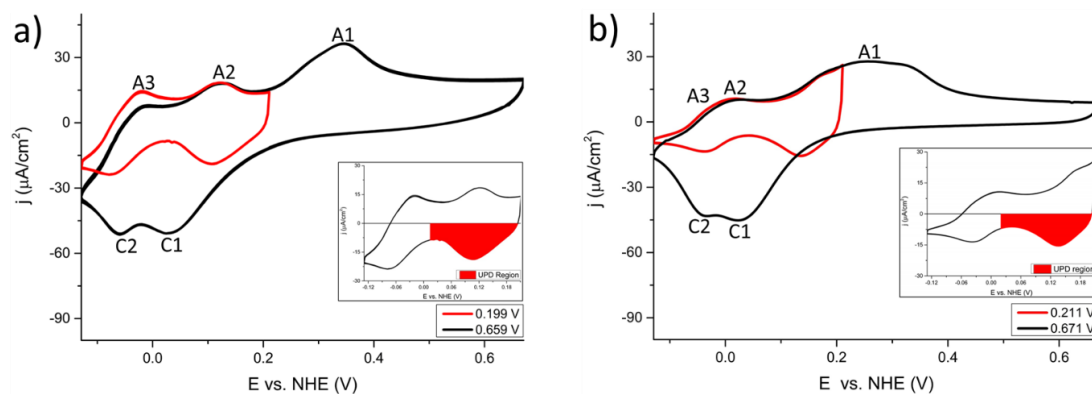**Figure 4.** Cyclic voltammograms of a polycrystalline gold electrode, different switching cathodic potentials at 10 mV s^{-1}. a) 0.1 M H$_2$SO$_4$ - 0.1 mM SnSO$_4$ b) 0.1 M CH$_3$SO$_3$H - 0.1 mM Sn (CH$_3$SO$_3$)$_2$

Figures 4a and 4b show the tin electrodeposition and subsequent anodic stripping as a function of different cathodic potential limits, in the underpotential, overpotential and hydrogen evolution region. The most positive potential was ke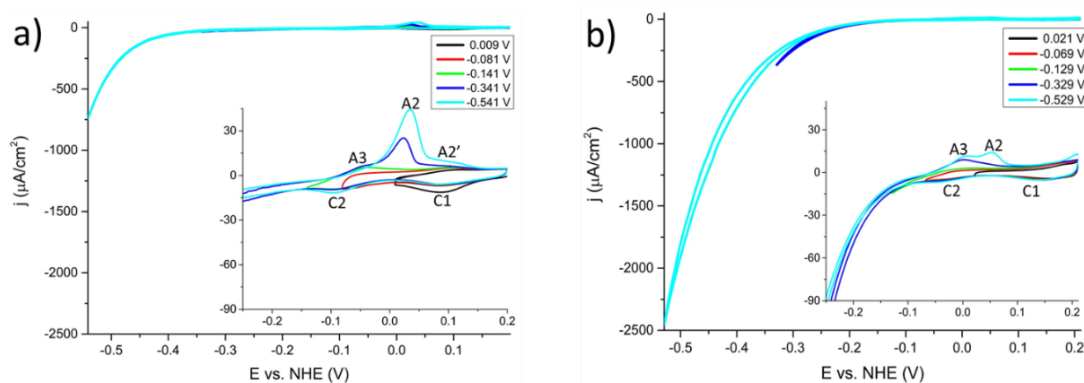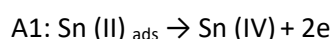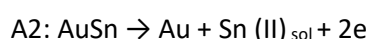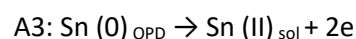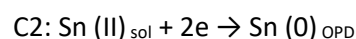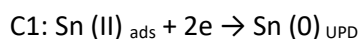pt below 0.199 V in SA and 0.211 V in MSA in order to avoid oxidation of Sn (II) to Sn (IV); therefore peak A1 (see Fig.2), which has been attributed to the oxidation of Sn (II)$_{ads}$ to Sn (IV)[12] , is not included in these voltammograms.

The insets in Figures 4a and 4b show the development of peaks A3 and A2 in SA and MSA. The peaks develop faster in SA than in MSA, suggesting that the amount of tin deposited is higher in SA. In SA, peak A2 develops a shoulder (A2') around 0.09 V vs. NHE, which is absent in MSA. Previous reports[12,15,16] have suggested that peak A2 corresponds to stripping of Au-Sn alloys, while peak A3 corresponds to stripping of bulk deposited tin. Tin – gold alloy formation can be associated to underpotential deposition in the sense that the interaction between both Sn adatoms and dissolved Sn with the gold substrate exceeds the binding energy between the Sn atoms[21]. As a result, Sn UPD on gold also leads to place exchange and consequently surface alloying[22].

In summary, the peaks in Figure 4 would correspond to the following surface reactions:

$$C1: Sn \text{ (II) }_{ads} + 2e \rightarrow Sn \text{ (0) }_{UPD}$$

$$C2: Sn \text{ (II) }_{sol} + 2e \rightarrow Sn \text{ (0) }_{OPD}$$

$$A3: Sn \text{ (0) }_{OPD} \rightarrow Sn \text{ (II) }_{sol} + 2e$$

$$A2: AuSn \rightarrow Au + Sn \text{ (II) }_{sol} + 2e$$

$$A1: Sn \text{ (II) }_{ads} \rightarrow Sn \text{ (IV) } + 2e$$

In these equations, AuSn is formed by the dissolution of Sn$_{UPD}$ and Sn$_{OPD}$ into the gold lattice.

_____

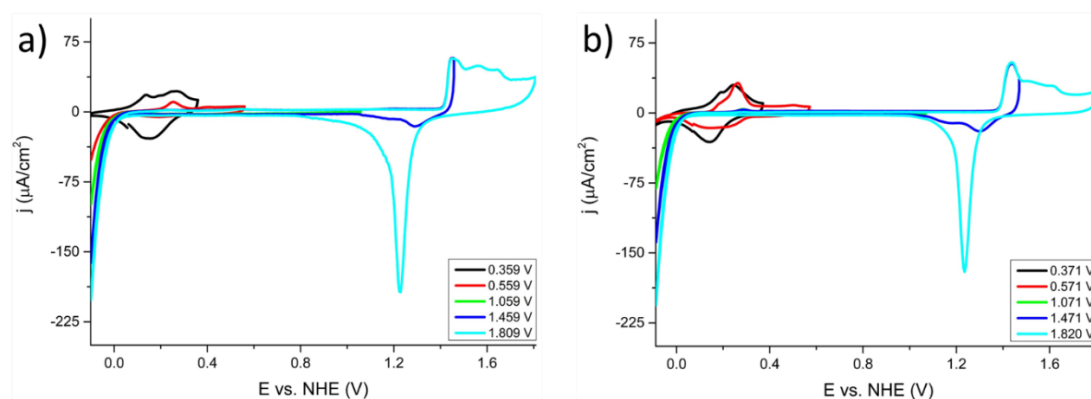## 2.3.2 Irreversible adsorption of tin

Figure 5. Voltammetric desorption of tin adspecies in the test electrolyte. Tin was adsorbed from a deaerated tin solution of 1 mM $SnSO_4$ (A) and $Sn (CH_3SO_3)_2$ (B) and then transferred to a test solution a) 0.1M H_2SO_4 and b) 0.1 M CH_3SO_3H.

Figures 5a and 5b compare the voltammetry of irreversibly adsorbed tin on the polycrystalline gold surface in SA and MSA. Tin was adsorbed on the gold electrode by bringing the electrode in contact with a Sn (II) solution at open circuit potential (0.84 and 0.68 V for SA and MSA, respectively, for 30 seconds). Subsequently, the gold electrode was transferred to a SA or MSA solution which did not contain tin with the potential at -0.101 V in SA and -0.09 V in MSA. From the cyclic voltammograms in the -0.059 to 0.31 V (SA) and 0.071 to 0.32 V (MSA) windows, it is observed that irreversible adsorption takes place in both electrolytes, giving rise to a quasi-reversible surface-confined redox couple, in agreement with earlier results by Rodes et al.[14]. A decrease of tin coverage or complete removal of the tin layer is observed when more positive switching potentials are applied, as also illustrated in Fig.5.

From pH dependent measurements, Rodes et al. [14, 19] have suggested that the irreversibly adsorbed Sn(II) species is an oxygenated species, i.e. SnO or $Sn(OH)_2$. Once the potential is positive enough such that Sn (IV) is formed, the adsorbed species dissolves into the electrolyte. They also suggested that anion adsorption takes place in or on the adsorbed tin layer,[19] in agreement with the small differences observed in the shape of the redox peaks in Figure 5a (SA) and 5b (MSA).

2.3.3 Anodic stripping of deposited tin

Cyclic voltammograms were recorded at a rotating disk electrode (RDE) in an extended range of potential (-0.541 to 0.659 V in SA and -0.529 to 0.671 V in MSA) to study the nature of the deposited layer, as revealed by the anodic stripping voltammogram. Results are shown in

Chapter 2: Voltammetric study of tin electrodeposition on polycrystalline gold from sulfuric and methanesulfonic acid

_____

Figures 6a and 6b, showing CVs obtained at different rotation rates for SA and MSA electrolytes. Figure 6 shows higher stripping currents and charges in SA than in MSA, which agrees with the previous conclusion that Sn (II) electrodeposition is faster in SA than in MSA (and hence more tin is deposited in SA). Additionally, figure 6 shows that the relative ratio between peaks A2 and A3 is higher in MSA than in SA, even if the kinetics of Sn (II) deposition is slower in MSA than in SA. This observation suggests that AuSn alloy formation is relatively more important in MSA, suggesting that slow deposition leads to more AuSn alloy formation, in contrast to fast deposition which leads to more bulk Sn formation.
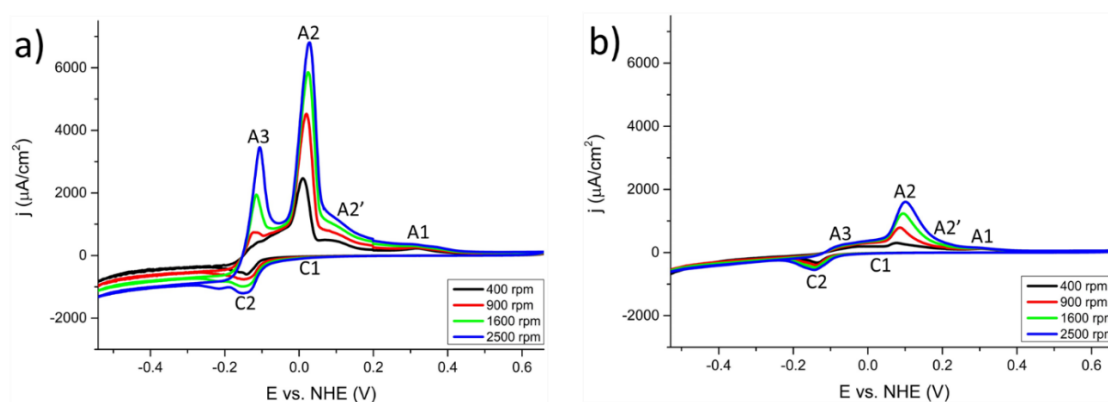
Figure 6. Cyclic voltammograms of tin deposition from sulfuric and methanesulfonic acid at a rotating gold disc electrode. Concentration of solution Sn^{2+} 0.6 mM a) 0.1 M H_2SO_4 b) 0.1 M CH_3SO_3H. Scan rate 30 mV s^{-1}; rotation rate indicated in the figures

Figure 7. Stripping voltammograms of tin deposition from sulfuric acid. Concentration of solution Sn^{2+} 0.1 mM. 30 mV s^{-1} and 900 rpm from 0.1 M H_2SO_4. Potential was kept at -0.541V during different periods of time, -0.541 V was chosen as starting potential.

_____

In order to study this effect further, cyclic voltammograms were recorded with different waiting times at the most negative potential of -0.541 V. In the series of experiments shown in Figure 7, performed in sulfuric acid, the concentration of Sn (II) in solution is lower than in Fig.6 (0.1 mM vs. 0.6 mM), to study the evolution of the stripping voltammogram for lower amounts of deposited Sn. The charges of peak A3, A2, A2' and A1 were calculated for the different waiting times, by the deconvolution and integration of the corresponding peaks.

The charges corresponding to both peaks A3 and A2 are affected by the deposition time, whereas the charge of peak A1 is not. Initially (for 0 and 30 seconds), only peak A2' is observed, whereas peak A2 grows in after 60 seconds and peak A2' becomes a shoulder. Both peaks A2 and A2' are assigned to stripping of AuSn alloy formed during the deposition process. The potential region of peak A2' is clearly separate from peak A2, and appears to be associated with a small amount of Sn on the Au electrode, associated with the early stages of the electrodeposition process and the last stages of AuSn electrodissolution[23]. The fact that the charge of peak A1 is independent of deposition time agrees well with the supposition that it corresponds to surface-confined process, i.e. Sn $(II)_{ads}$ oxidation to Sn (IV)[12].

Figure 8. Stripping voltammograms of tin deposition from methanesulfonic acid. Concentration of solution Sn^{2+} 0.1 mM. 30 mV s^{-1} and 900 rpm from 0.1 M CH_3SO_3H. Potential was kept at -0.529V during different periods of time, -0.529 V was chosen as starting potential.

Figure 8 shows the same series of stripping cyclic voltammograms for tin deposition as in Fig.7, but from the MSA electrolyte. As observed in Fig.6, the charge of peak A2 relative to A3 is higher for tin deposition from MSA than from SA, suggesting that AuSn alloy formation is enhanced in methanesulfonic acid. Peak A2' is not well resolved in MSA. As in Fig.7, Peak A1 does not depend on the waiting time, which agrees with Sn$(II)_{ads}$ to Sn(IV)[12] being a superficial process.

Chapter 2: Voltammetric study of tin electrodeposition on polycrystalline gold from sulfuric and methanesulfonic acid

_____
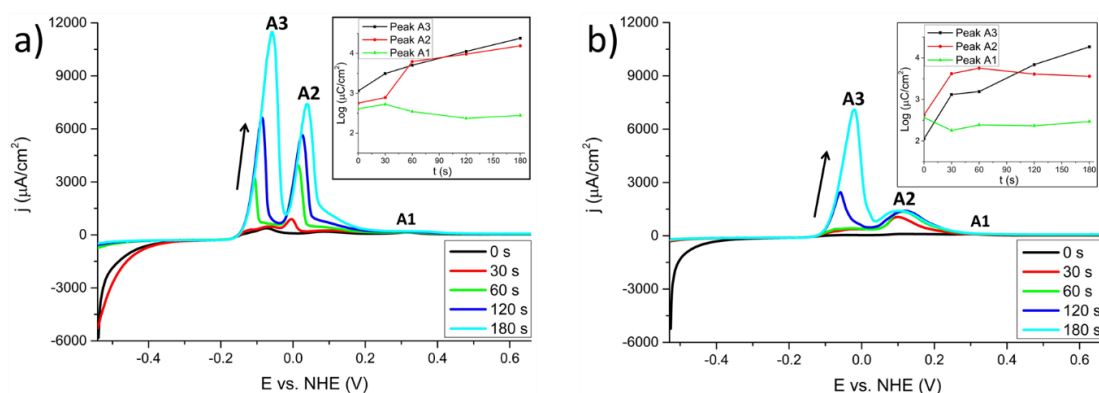
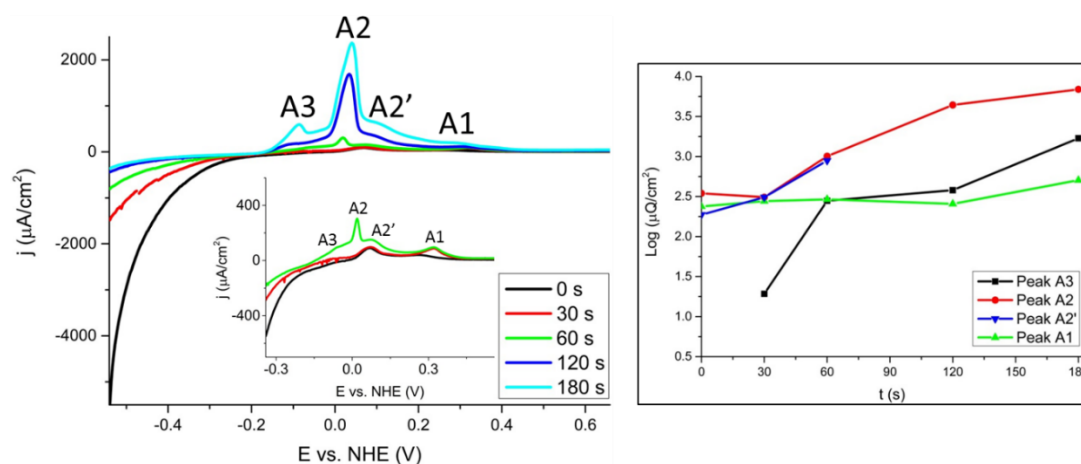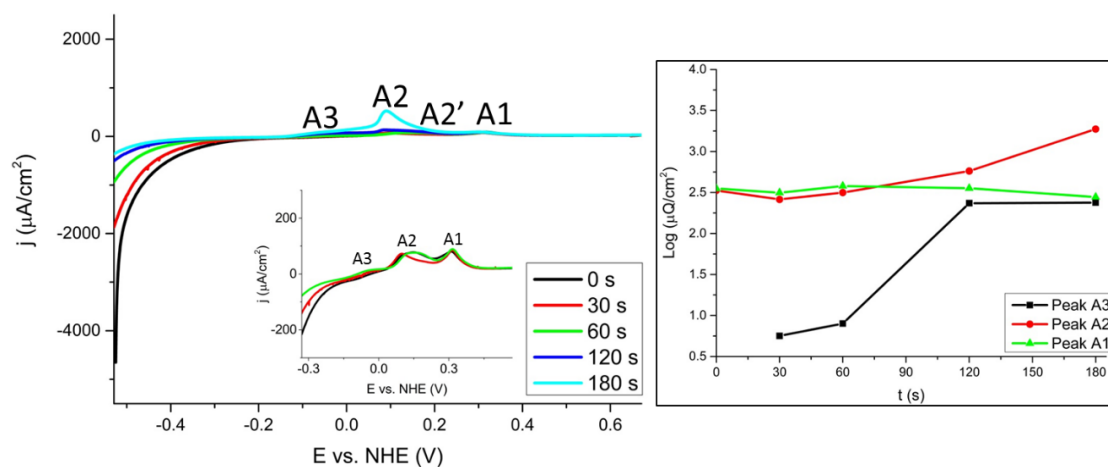**Figure 9.** Stripping voltammograms of tin deposition from sulfuric and methanesulfonic acid. Concentration of solution Sn^{2+} 0.6 mM. 30 mV s^{-1} and 900 rpm from 0.1 M H_2SO_4/CH_3SO_3H. Potential was kept at -0.541 V (SA) and -0.529 V (MSA) during different periods of time, previous potentials were chosen as starting potentials.

Figure 9 shows stripping cyclic voltammograms for tin layers deposited in sulfuric and methanesulfonic acid recorded at a higher tin concentration (0.6 Mm Sn^{2+}) and different waiting times. Peak A3 assigned to the stripping of bulk deposition is now larger than the A2 peak in both SA and MSA, showing that at a higher concentration of tin, bulk deposition is promoted in both electrolytes. On the other hand, in SA, both the A2 and the A3 are affected by the waiting time, whereas in MSA, the A2 peak seems to plateau. We speculate that this could be related to a more homogeneous deposition of Sn on the Au surface in MSA.
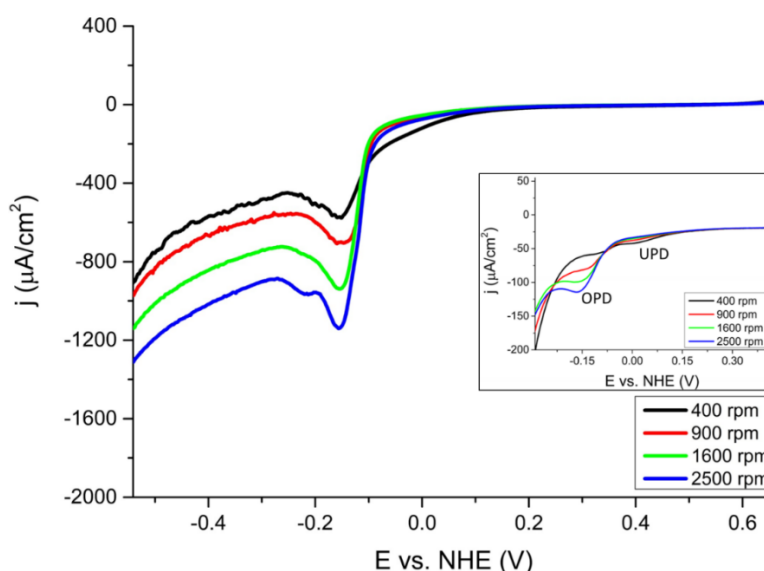
Figure 10. Linear sweep voltammograms of tin deposition from sulfuric acid on a gold rotating disc electrode. Concentration of solution Sn^{2+} 0.6 mM. Scan rate 30 mV s^{-1}; rotation rate 400, 900, 1600 and 2500 rpm inset, tin deposition from 0.1 mM $SnSO_4$, 0.1 M H_2SO_4.

_____
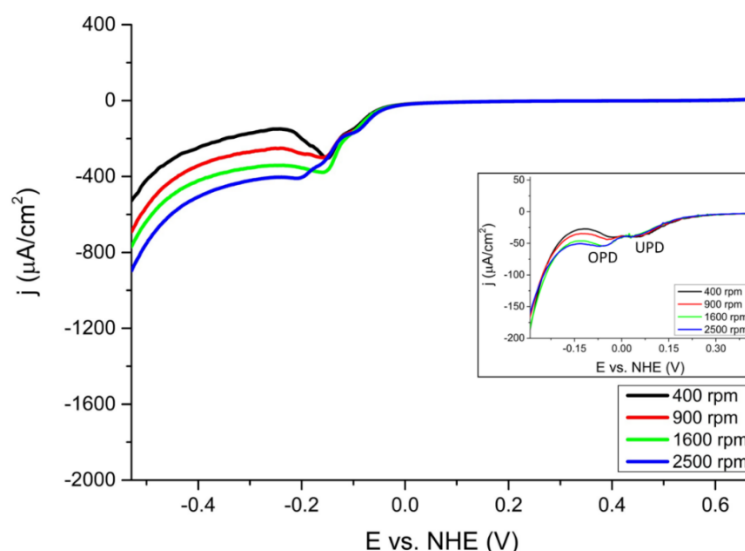
Figure 11. Linear sweep voltammograms of tin deposition from methanesulfonic acid on a gold rotating disc electrode. Concentration of solution Sn^{2+} 0.6 mM, 0.1 M CH_3SO_3H. Scan rate 30 mV s^{-1}; rotation rate 400, 900, 1600 and 2500 rpm. Inset tin deposition from 0.1 mM Sn $(CH_3SO_3)_2$, 0.1M CH_3SO_3H

2.3.4 RDE voltammetry

Linear sweep RDE voltammetry measurements were also performed in order to obtain information about the electrodeposition mechanism under controlled mass-transport conditions. Underpotential deposition from sulfuric and methanesulfonic acid are not affected by the rotation speed, which also agrees with the fact that irreversible adsorption takes place in SA and MSA: Sn (II) species are previously adsorbed as Sn (II)$_{ads}$ species and then reduced to Sn (0) during underpotential deposition process. This UPD peak is only seen at very low Sn (II) concentration ~0.1 mM, as at a higher concentration it is hidden by the higher currents from the bulk deposition (insets of Fig. 10 and 11). On the other hand, Figures 10 and 11 show that tin overpotential deposition is affected by rotation speed, regardless of the nature of the supporting electrolyte. This is in agreement with the previous findings of Petersson and Ahlberg[13, 12]. The onset potential for tin bulk deposition ($Sn^{2+} \rightarrow Sn$) is almost the same for SA and MSA. Tin deposition OPD currents near the onset potential are generally higher in SA, suggesting that the kinetics of tin deposition from MSA is slower than from SA. Previous studies about complex formation between methanesulfonate and different ions such as Pb^{2+} [18] would suggest that this phenomenon may be due to complex formation between Sn^{2+} and methanesulfonate anions.

Figures 10 and 11 also show at 30 mV s^{-1} the current-voltage curves are not completely sigmoidal, and the plateau current does not vary linearly with the square root of the rotation rate in the Koutecky-Levich plots (see Fig. A2 and A3). However, linear sweep voltammograms recorded at very low scan rate (2 mV s^{-1}) show mass transport-controlled currents in

Chapter 2: Voltammetric study of tin electrodeposition on polycrystalline gold from sulfuric and methanesulfonic acid

_____

agreement with the expected Levich dependence on rotation rate, as shown in Figure 12 (See Koutecky-Levich plots in the Fig. A4 and A5 in the appendix A). Low scan rate leads to more tin deposition and subsequently a complete coverage of the gold surface, avoiding any concurrent non-desirable side reaction, such as HER on gold. Therefore, the unusual behavior shown in Figures 10 and 11 is ascribed to a concurrent HER on the gold surface during the deposition process, which is likely to cluster formation, leading to a partial coverage of the surface.
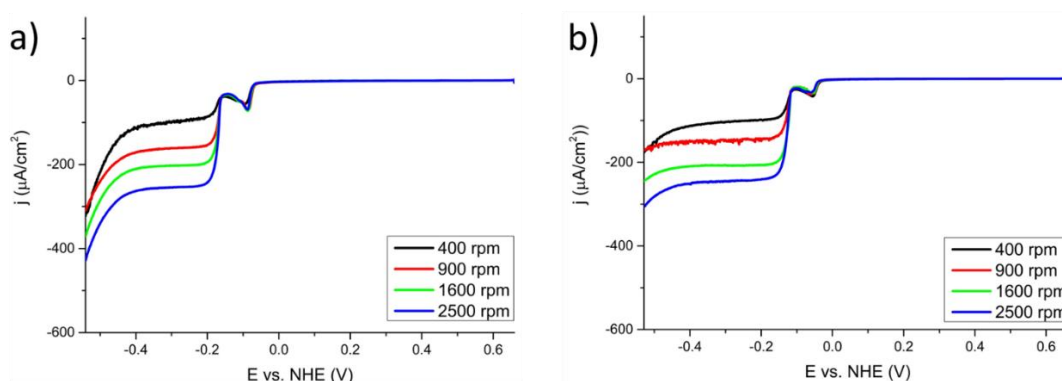
Figure 12. Linear sweep voltammograms of tin deposition from sulfuric and methanesulfonic acid on a gold rotating disc electrode. Concentration of solution a) Sn^{2+} 0.6 mM, 0.1 M H_2SO_4 and b) 0.1M CH_3SO_3H. Scan rate 2 mV s^{-1}; different rotation rates.

Figure 12a and 12b exhibit a distinctive region between -0.071 and -0.16 V vs. NHE (SA) and -0.029 and -0.12 V vs. NHE (MSA), respectively, in which the Sn (II) exhibits a kind of pre-peak, where the current density decreases by ca. 50%, before it reaches the diffusion-limited value at more negative potentials. Figure 13 shows that the passivation phenomenon is sensitive to pH, and it is essentially absent at pH=3. Previous studies have shown passivation processes during tin electroplating in acid medium[24], though in the presence of organic additives. Passivation during anodic electro dissolution of metals, including tin, is well known, and typically associated with formation of oxide films [25,26].

The nature of the cathodic prepeak remains elusive. Given the potential where the prepeak occurs, surface hydrogen or hydride formation might be possible,[27] inhibiting further tin deposition. Passivation by surface hydrogen is known to lead to inhibit the cathodic reduction of nitrate on copper[28] and platinum[29] electrodes. However, hydride formation on tin surface seems unlikely due to the weakness of the M-H bond[30], leading to the low catalytic activity of Sn for HER[20]. Given the sensitivity of the prepeak to pH, we tentatively relate the effect to the pH -dependent formation of electroactive Sn species in solution.

_____
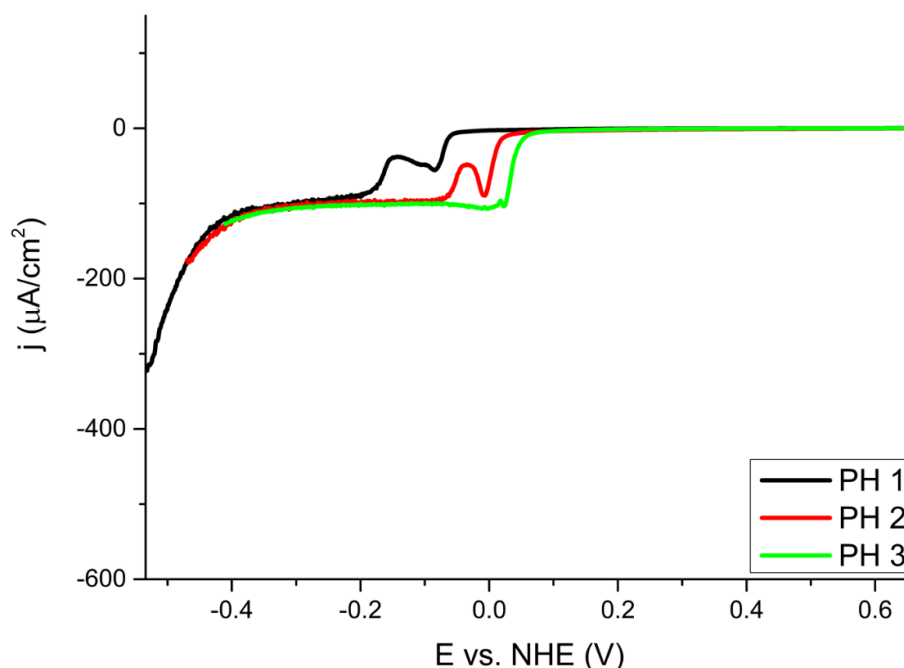
Figure 13. Linear sweep voltammograms of tin deposition from sulfuric acid at different pHs (1, 2, 3) on a gold rotating disc electrode. Concentration of solution: Sn^{2+} 0.6 mM, scan rate 2 mV s^{-1}; rotation rate 900 rpm.

2.4 Conclusions

In this work, we have compared tin electrodeposition on gold from sulfuric acid (SA) and methanesulfonic acid (MSA) electrolytes. Voltammetric studies show that electrodeposition in SA and MSA follows three different stages: irreversible adsorption, underpotential deposition (UPD), and overpotential deposition (OPD). The irreversible adsorption of tin takes place at potentials positive of its electrochemical discharge, and involves an oxygenated adspecies such as SnO or Sn (OH)$_2$, interacting with electrolyte anions. The UPD of Sn differs from the traditional UPD in the sense that (tin) clusters are formed on the surface instead of a monolayer, which we assume to be related to the driving force for Sn UPD on Au being the AuSn surface alloy formation. Our results show that tin OPD electrodeposition is faster in SA than in MSA, which we ascribe to a complexation effect of the Sn^{2+} in MSA solution. The exact nature of the electroactive Sn (II) complex in both SA and MSA would require further study. The lower deposition rate in MSA leads to a lower amount of Sn deposited under the same (kinetically-limited) conditions compared to SA. At higher overpotentials, Sn OPD is mass-transport limited in both SA and MSA. The lower deposition rate in MSA also leads to a more homogeneous coverage of the gold by tin, as observed by the more extensive blockage of

Chapter 2: Voltammetric study of tin electrodeposition on polycrystalline gold from sulfuric and methanesulfonic acid

_____

hydrogen evolution on the remaining gold surface. In MSA, the Au-Sn surface alloy formation is more prominent, presumably because of the lower deposition rate, which leads to a relatively faster surface alloying. Finally, an unexpected prepeak is observed at low scan rates and low pH. Further studies would be required to disclose the nature of this process related to this prepeak.

# 2.5 References

(1)   Walsh, F. C.; Low, C. T. J. A Review of Developments in the Electrodeposition of Tin. *Surf. Coatings Technol.* 2016, *288*, 79–94.

(2)   M. Jordan, E. G. L. *Electrodeposition of Tin and Its Alloys*; Saulgau, Germany, 1995.

(3)   Bengoa, L. N.; Pary, P.; Conconi, M. S.; Egli, W. A. Electrodeposition of Cu-Sn Alloys from a Methanesulfonic Acid Electrolyte Containing Benzyl Alcohol. *Electrochim. Acta* 2017, *256*, 211–219.

(4)   Torrent-Burgues, J.; Guaus, E.; Sanz, F. Initial Stages of Tin Electrodeposition from Sulfate Baths in the Presence of Gluconate. *J. Appl. Electrochem.* 2002, *32* (2), 225–230.

(5)   Bakkali, S.; Touir, R.; Cherkaoui, M.; Ebn Touhami, M. Influence of S-Dodecylmercaptobenzimidazole as Organic Additive on Electrodeposition of Tin. *Surf. Coatings Technol.* 2015, *261*, 337–343.

(6)   Lee, J.-Y.; Kim, J.-W.; Chang, B.-Y.; Tae Kim, H.; Park, S.-M. Effects of Ethoxylated α-Naphtholsulfonic Acid on Tin Electroplating at Iron Electrodes. *J. Electrochem. Soc.* 2004, *151* (5), C333–C341.

(7)   Low, C. T. J.; Walsh, F. C. Electrodeposition of Tin, Copper and Tin-Copper Alloys from a Methanesulfonic Acid Electrolyte Containing a Perfluorinated Cationic Surfactant. *Surf. Coatings Technol.* 2008, *202* (8), 1339–1349.

(8)   Low, C. T. J.; Walsh, F. C. The Stability of an Acidic Tin Methanesulfonate Electrolyte in the Presence of a Hydroquinone Antioxidant. *Electrochim. Acta* 2008, *53* (16), 5280–5286.

(9)   Martyak, N. M.; Seefeldt, R. Additive-Effects during Plating in Acid Tin Methanesulfonate Electrolytes. *Electrochim. Acta* 2004, *49* (25), 4303–4311.

(10)   Sekar, R.; Eagammai, C.; Jayakrishnan, S. Effect of Additives on Electrodeposition of Tin and Its Structural and Corrosion Behaviour. *J. Appl. Electrochem.* 2010, *40* (1), 49–57.

(11)   Low, C. T. J.; Walsh, F. C. The Influence of a Perfluorinated Cationic Surfactant on the Electrodeposition of Tin from a Methanesulfonic Acid Bath. *J. Electroanal. Chem.* 2008, *615* (2), 91–102.

(12)   Petersson, I.; Ahlberg, E. Kinetics of the Electrodeposition of Pb-Sn Alloys: Part II. At Polycrystalline Gold Electrodes. *J. Electroanal. Chem.* 2000, *485*, 178–187.

(13)   Petersson, I.; Ahlberg, E. Kinetics of the Electrodeposition of PbSn Alloys. Part I. At Glassy Carbon Electrodes. *J. Electroanal. Chem.* 2000, *485* (2), 166–177.

(14)   Rodes, A.; Feliu, J. M.; Aldaz, A. Irreversible Tin Adsorption on Polyoriented Gold Electrodes. *J. Electroanal. Chem* 1988, *256*, 455–462.

(15)   Mao, B. W.; Tang, J.; Randler, R. Clustering and Anisotropy in Monolayer Formation under Potential Control: Sn on Au(111). *Langmuir* 2002, *18* (14), 5329–5332.

(16)   Fonticelli, M.; Tucceri, R. I.; Posadas, D. Deposition and Stripping Processes of Tin on Gold Film Electrodes Studied by Surface Conductance. *Electrochim. Acta* 2004, *49* (28), 5197–5202.

(17)   Collazo, A.; Figueroa, R.; Nóvoa, X. R.; Pérez, C. Electrodeposition of Tin from a Sulfate Bath: An EQCM Study. *Surf. Coatings Technol.* 2015, *280*, 8–15.

(18)   Capelato, M. D.; Nóbrega, J. A.; Neves, E. F. A. Complexing Power of Alkanesulfonate Ions: The Lead-Methanesulfonate System. *J. Appl. Electrochem.* 1995, *25* (4), 408–411.

(19)   Rodes, A.; Herrero, E.; Feliu, J. M.; Aldaz, A. Structure Sensitivity of Irreversibly Adsorbed Tin on Gold Single-Crystal Electrodes in Acid Media. *J. Chem. Soc. Faraday Trans.* 1996, *92* (20), 3769–3776.

(20)   Azizi, O.; Jafarian, M.; Gobal, F.; Heli, H.; Mahjani, M. G. The Investigation of the Kinetics and Mechanism of Hydrogen Evolution Reaction on Tin. *Int. J. Hydrogen Energy* 2007, *32* (12), 1755–1761.

(21)   H. Ibach. *Physics of Surfaces and Interfaces*, 1st ed.; Springer - Verlag Berling Heidelberg, 2006.

(22)   Milchev, A.; Staikov, G. Atomistic Aspects of Electrochemical Alloy Formation: A Review of Nucleation and Growth of Nano-Clusters and Thin Films. *Indian J. Chem.* 2005, *44A* (5), 899–912.

(23)   Clavilier, J.; Feliu, J. M.; Aldaz, A. An Irreversible Structure Sensitive Adsorption Step in Bismuth Underpotential Deposition at Platinum Electrodes. 1988, *243*, 419–433.

(24)   M. and Bernie, J. A. C. Abnormal High Throwing Power and Cathode Passivity in Acid Tin Plating Baths. *Electrochim. Acta* 1967, *12* (April 1967), 205–212.

(25)   Palacios-Padrós, A.; Caballero-Briones, F.; Díez-Pérez, I.; Sanz, F. Tin Passivation in Alkaline Media: Formation of SnO Microcrystals as Hydroxyl Etching Product. *Electrochim. Acta* 2013, *111*, 837–845.

(26)   Kapusta, S. & Hackerman, N. Optical Studies of the Anodic Passivation of Tin. *J. Electrochem. Soc.* 1982, *129* (9), 1886–1889.

(27)   Gabe, D. R. The Role of Hydrogen in Metal Electrodeposition Processes. *J. Appl. Electrochem.* 1997, *27* (8), 908–915.

(28)   Pérez-gallent, E.; Figueiredo, M. C.; Katsounaros, I.; Koper, M. T. M. Electrochimica Acta Electrocatalytic Reduction of Nitrate on Copper Single Crystals in Acidic and Alkaline Solutions . *Electrochim. Acta* 2017, *227*, 77–84.

(29)   G. Horányi and E.M. Rizmayer. Role of Adsorption Phenomena in the Electrocatalytic Reduction of Nitric Acid at a Platinized Platinum Electrode. *J. Electroanal. Chem* 1982, *140*, 347–366.

(30)   Trasatti, S. Work Function, Electronegativity, and Electrochemical Behaviour of Metals. *J. Electroanal. Chem. Interfacial Electrochem.* 1972, *39* (1), 163–184.

CHAPTER 3

The effect of naphthalene-based additives on tin electrodeposition on a gold electrode

Chapter 3. The effect of naphthalene-based additives on tin electrodeposition on a gold electrode

_____
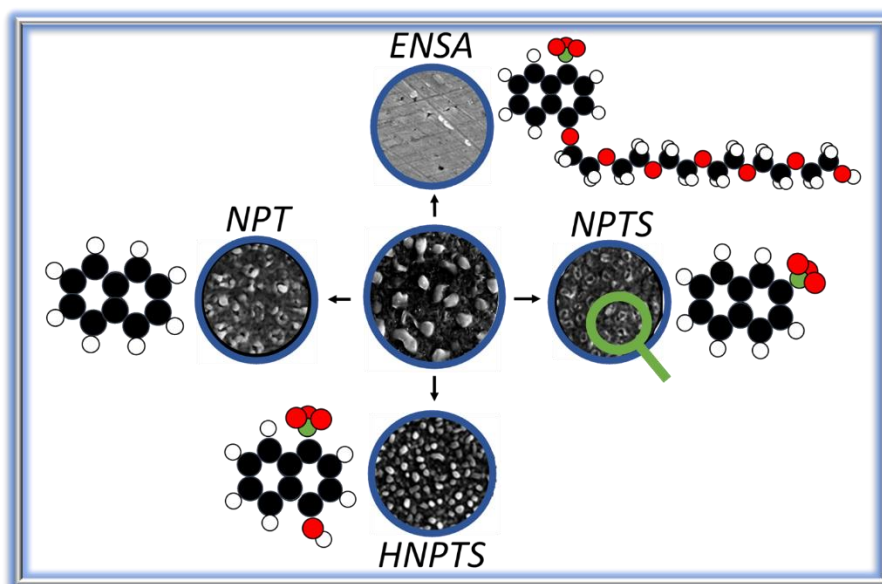
Abstract

In this work, we study the adsorption behavior of naphthalene derivatives: naphthalene (NPT), naphthalenesulfonate (NPTS), hydroxynaphthalenesulfonate (HNPTS) and ethoxylated α-napthalenesulfonic acid (ENSA, a commonly used additive in the tin electroplating industry), on gold electrodes and their effect on the tin electrodeposition process, by means of in situ and ex situ surface analysis techniques (cyclic voltammetry, in situ Surface Enhanced Raman Spectroscopy and ex situ Scanning Electron Microscopy). From experiments and density functional theory calculations, we conclude the formation of films of NPT, NPTS, HNPTS and ENSA, where NPT and NPTS lie flat on the gold surface and HNPTS and ENSA undergo oxidative polymerization. The nature and stability of the films are strongly dependent on the surface structure, interaction between the molecules, and applied potential. NPTS is observed to form a denser film than NPT due to attractive interactions between the adsorbed molecules on gold and tin. Tin electrodeposition is strongly affected by the presence of the NPT, NPTS, HNPTS and ENSA films. Tin bulk electrodeposition is inhibited in the presence of NPT and NPTS, but slightly promoted in the presence of HNPTS. Tin deposits grown in the presence of NPT and NTPS have the same morphology, and the characteristic size of the electrodeposited features is smaller than in their absence. The tin deposit grown in the presence of HNPTS exhibits markedly different and smaller features. Some amount of sulfur form is incorporated in the deposit as a result of the reductive desulfonation of NPTS, HNPTS and ENSA on the gold electrode. The effect of ENSA was compared to the results obtained with NPT, NPTS and HNPTS. ENSA exhibits a similar behavior to NPT, NPTS and HNPTS during tin deposition process in terms of the voltammetry of tin deposition, but it severely inhibits the bulk deposition. Naphthalene derivatives and ENSA have an effect on the tin bulk deposition process, but show no or little effect on the formation of AuSn (surface) alloys, which is ascribed to the slow nature of Sn UPD on gold and the SnAu alloying process.

_____

3.1 Introduction

Most of the plating solutions used in the electrodeposition of metals and alloys contain at least one inorganic or organic additive[1]. Additives play an important role in metal plating, such as reduction of substrate roughness, reduction of the grain size of the deposit, production of specific micro- and macro-structures, increase of the corrosion resistance, among others. Numerous studies have been performed in order to understand the role of the additives during metal deposition[2,3]. The effect of additives has been the most extensively studied for copper electrodeposition [4, 5, 6, 7, 8, 9, 10, 11], for instance by showing their strong influence on the surface structure of the substrate, the lifting of the reconstruction as a consequence of additive adsorption [4, 12], or the creation of surface vacancy islands[6]. Changes during the nucleation and growth are also common when organic molecules are added, such as an increase in the number of nuclei[7] and the decrease in the kinetics of electrodeposition[5].

Tin electrodeposition is a common electroplating process used in multiple applications: corrosion protection, electronics fabrication, packaging industry, and many others. During the past 20 years, developments in tin plating have allowed the extension of its applications to batteries and semiconductor industry[13]. High-quality tin coating baths require the addition of different compounds, especially organics, in order to have the desired chemical and physical properties of the deposit. Aromatic compounds are broadly used in tin electrodeposition, but the chemical structure of the common additives is quite diverse and complex, which makes understanding their exact effect difficult.

Previous work on the effect of aromatic carbonyls[14, 15, 16] has ascribed differences in the grain size and crystalline orientation of the tin deposits to the strong adsorption of the additives or their reduction products[15] onto the metal substrate, where additives block active sites and promote preferential tin growth. Martyak et al. studied glycol-type additives[17] and ascribed the increase of the tin (II) reduction overpotential to changes in the kinetics of the process. Barry et al. studied phenyl-2-butenalimine and formaldehyde and ascribed the same effect to changes in the nucleation and growth mechanism[18]. Studies of much more complex molecules such as the commonly used ethoxylated α-napthalenesulfonic acid (ENSA) have shown that it enhances the quality of tin deposits, which was ascribed to kinetic and mass transport limitations due to the formation of ENSA aggregates on the electrode[19, 20].

In this work we study the effect of naphthalene derivatives: naphthalene (NPT), naphthalenesulfonate (NPTS), hydroxynaphthalenesulfonate (HNPTS) and ethoxylated α-napthalenesulfonic acid (ENSA), on tin electrodeposition on a gold electrode. Gold was chosen as a substrate due to its a wide double layer window and weak chemisorbing properties. The electrochemistry of (single-crystal) gold has been well studied[12]. These properties facilitate

the understanding of molecular adsorption and metal deposition studies. We use the results obtained with NPT, NPTS and HNPTS (with simple chemical structures) as a model to obtain insights into the effect of a much more complex chemical structure, such as ENSA, a commonly used additive in industrial tin plating. Naphthalene derivatives and tin electrodeposition are studied by conventional electrochemical techniques as well as by means of in situ SERS (surface enhanced Raman spectroscopy), ex-situ SEM (scanning electron microscopy) and density functional theory calculations.

3.2 Experimental and computational details

3.2.1 Experimental details

All glassware was stored overnight in a solution of 1g L^{-1} $KMnO_4$ in 0.5 M H_2SO_4. Before use, it was rinsed with water and 30% hydrogen peroxide solution in order to remove permanganate anions and trace impurities. Glassware was boiled in water five times before starting the experiments. The water used to clean glassware and to prepare solutions was demineralized and ultra-filtrated by a Millipore MilliQ system (18.2 MΩ cm). A gold wire was used as a counter electrode and a reversible hydrogen electrode (RHE) was used as a reference, but all the potentials were converted to the normal hydrogen electrode (NHE), by using the following equation: $E_{RHE} = E_{NHE} - 0.0591pH$. The reference electrode was in contact with the electrolyte via a Luggin capillary. A capacitor of 10 μF was connected to an additional gold wire in solution and the RHE electrode to filter small currents produced in the RHE electrode and reduce the noise in measurements at low currents. The working electrode was either a gold single crystal disk electrode (diameter 7 mm, 1 mm thick), used in the hanging meniscus configuration, or a polycrystalline gold disk electrode (5 mm diameter, 4 mm thick) used in the rotating-disk electrode (RDE) setup under hydrodynamic conditions. Cyclic voltammetry experiments were performed using a potentiostat PGSTAT 12 (Metrohm-Autolab). RDE experiments were performed with a MSR rotating electrode (Pine Research) at a rotation rate of 1600 rpm. The electrode potential was corrected for Ohmic drop during the measurements, by using 85% of the Ohmic resistance measured by electrochemical impedance spectroscopy.

Single crystal gold electrodes were cleaned before each experiment by flame annealing for about 5 seconds, and subsequently cooled in air and quenched in deionized water; the procedure was repeated 10 times. To check the quality of the surface and cleanliness of the solution (0.1M H_2SO_4) a cyclic voltammogram was taken at potentials between 0.06 to 1.26 V at 50 mV s^{-1}. In the case of the polycrystalline gold surface, the electrode was cleaned electrochemically: first by oxidizing it in 0.1M sulfuric acid by applying 10 V for 20 s, using a graphite bar as a counter electrode, after which the gold oxide formed was removed by

dipping the working electrode in a 6 M HCl solution for 30 s. Subsequently, the polycrystalline gold electrode was mechanically polished by using diamond powder suspension (0.05 μm particle size) during 5 min, rinsed and transferred to an ultrasound bath with water. Finally, the electrode was electropolished in a 0.1 M H_2SO_4 solution by 200 cycles between 0.06 to 1.81 V at 1 V s^{-1}. Additionally, before every measurement, a cyclic voltammogram of the gold surface was recorded at potentials between 0.06 to 1.81 V at 50 mV s^{-1}. Scanning electron micrographs of the bare polycrystalline gold and gold single crystals surfaces prior to the experiments are presented in the Fig. B17.

In situ Surface Enhanced Raman Spectroscopy (SERS) measurements were performed with a confocal Raman microscope (LabRam HR, Horiba Yobin Yvon) with a 50x objective. A He/Ne laser of 633 nm was used as the excitation source. Reference and counter electrodes were the RHE and a gold wire, respectively. The working electrode was a roughened gold disk electrode of 4 mm diameter. The gold electrode was roughened as follows: The electrode was cleaned via mechanical polishing, electrochemical etching and electropolishing (see previous paragraph). Once the surface was clean, it was transferred to a separate cell containing 0.5 M KCl, and 50 cycles of step potentials were applied: 0.3 V during 15 s and 1.2 V during 5 s. Afterwards, the electrode was rinsed and transferred to the Raman cell to perform the in-situ spectroscopic measurements. A spectrum at 1.06 V was taken in the electrolyte without the presence of NPTS as a baseline.

The morphology of the metal deposits was observed by a scanning electron microscopy SEM. Micrographs were taken using the model JEOL 820 SEM at 15 kV. Energy Dispersive X-Ray Spectroscopy (EDS) measurements were taken at 15 kV, the reported percentage of tin was calculated from the average of relative ratio of tin from a line scan measurement of 0.5 μm length, over the tin features.

All solutions were prepared from chemicals with the highest purity commercially available: H_2SO_4 (96% ultrapure, Merck), $SnSO_4$ (≥ 95%, Sigma Aldrich), naphthalene (≥ 99%, Sigma Aldrich), 2-napthalenesulfonic acid sodium salt (99.6%, Sigma Aldrich), sodium thiosulfate (≥99.99%, Sigma Aldrich), 4-hydroxy-1-naphthalenesulfonic acid sodium salt (≥ 95 %, Santa Cruz Biotechnology) and ethoxylated α-napthalenesulfonic acid (73.6%, Pulcra chemicals). In the case of ENSA the main impurities are sulfuric acid with 8.7 %, and water with 2.4 %, other impurities were not provided by the supplier.

A low Sn^{2+} concentration (0.6 mM), an oxygen-free atmosphere (permanent argon bubbling), and a pH lower than 2, were chosen in order to avoid the contribution of polymeric Sn (II) species and hydrolysis products formed in the bulk of the solution [21, 22, 23, 24].

The number of deposited tin monolayers (ML) was calculated from the charge that flowed during the experiment, taking as reference the accepted value of the charge of a monolayer on polycrystalline gold surface: 390 ± 10 μC cm^{-2} [25]. The total charge of the deposit is the

addition of the cathodic charge calculated from the area under of the linear sweep voltammetry curve, between 0.659 to -0.241 V and the charge calculated from the product between the current at -0.241 V and the time that the potential was held (60 seconds) at it. The corresponding electrochemical experiments are shown in Figure B16 in the Appendix B. We assumed that the only reaction taking place in this range of potential is tin electrodeposition.

3.2.2 Computational details

The lateral interaction energy between naphthalene and naphthalenesulfonate on Au (111) and Sn (111) was calculated using density functional theory (DFT). DFT simulations were performed using the Vienna Ab-initio Simulations Package (VASP)[26, 27, 28] . A plane wave basis set was used with a cutoff energy of 450 eV. Ion core potentials were modeled using the Projector Augmented Wave (PAW) approach[29, 30] and the PBE exchange-correlation functional[31, 32] was used. Structural optimizations were carried out until the forces on each atom were below 0.02 eV Å^{-1}. Dipole corrections were applied in the surface normal direction[32]. The unreconstructed Au(111) surface was modeled in a 4x8 unit cell with a 5x3x1 Monkhorst-Pack[32] k-space sampling grid. The surface was comprised of four atomic layers with the bottom two layers frozen at the experimentally measured lattice constant of 4.08 Å[33]. The unreconstructed Sn(111) surface was modeled in a 3x6 unit cell with a 5x5x1 k-space grid, and was comprised of 8 atomic layers with the bottom two layers frozen at a lattice constant of 4.7Å (for α–Sn)[34]. Van der Waals interactions are approximated using the DFT-D3 method[35, 36] . Binding energies of naphthalene and naphthalenesulfonate are calculated for adsorption on Au (111) both without and with the van der Waals correction (all calculations of the lateral interaction energy include the correction).

To approximate the lateral interaction energy, both naphthalene and naphthalenesulfonate were first modeled on Au(111) in a (4x4) structure, as found experimentally by Wan et al. for naphthalene on Cu(111)[37], in a 4x8 unit cell, containing two naphthalene or naphthalenesulfonate molecules. The change in energy (0K DFT energy, neglecting entropy and vibrational energy) was then calculated for a similar structure but with the two molecules in the 4x8 unit cell brought closer together. This interaction was found to be attractive for both naphthalene and naphthalene sulfonate, however, the magnitude was very small (-0.02 eV) for naphthalene. A configuration where the sulfonate groups could hydrogen bond between the two naphthalene sulfonate molecules was also examined. In this case, one of the two naphthalene sulfonate acid molecules were rotated, so that the sulfonate groups were in close proximity. The hydrogen bonded configuration was found to be more stable. A similar procedure was used to study the lateral interactions on Sn (111), though an experimentally measured ad-layer structure on this surface could not be found in prior literature; a similar structure as that found on Au (111) was used.

_____

While only a small number of configurations were examined, the configurations examined for both naphthalene and naphthalenesulfonate were identical; the interactions were significantly more attractive for the naphthalenesulfonate than for the naphthalene. This interaction energy does not include the effect of the presence of solvent near the electrode surface (which could affect, for example, the energy gained on pairing/hydrogen-bonding neighboring naphthalenesulfonate molecules).

3.3 Results and discussions

Cyclic voltammetry measurements of polycrystalline gold in a wide potential window (-0.54 to 1.81 V) in the presence of naphthalene (NPT) and naphthalenesulfonate (NPTS) at different concentrations are shown in Figures 1 and 2, respectively. The measurements show that neither NPT or NPTS strongly modify the CV profile of the gold surface, in the sense that the onset potential and current profile for the gold (hydr-)oxide formation is not affected significantly (Figs. 1a and 2a), and the activity for the hydrogen evolution reaction (HER) is also not strongly affected. However, Fig. 1 and Fig.2 show new features in the double layer region between 0.58-0.62 V, which are dependent on the NPT and NPTS concentration. Simultaneously, a decrease in the current density and capacity in the double layer region between 0.2 and 0.5 V are also observed. Simultaneously, a decrease in the current density and capacity in the double layer region between 0.2 and 0.5 V are also observed.

Chapter 3. The effect of naphthalene-based additives on tin electrodeposition on a gold electrode

_____

Figure 1. Cyclic voltammograms of a polycrystalline gold disc electrode in 0.1 M H₂SO₄ at different NPT concentrations (a) CV recorded between -0.54 to 1.81 V at 50 mV s⁻¹. (b) Zoom-in of the double layer region, arrows show the decrease in the capacitive current (c) Zoom-in of the gold oxide formation and reduction region, arrows show the decrease in the peak currents (d) zoom-in of hydrogen evolution region (HER)
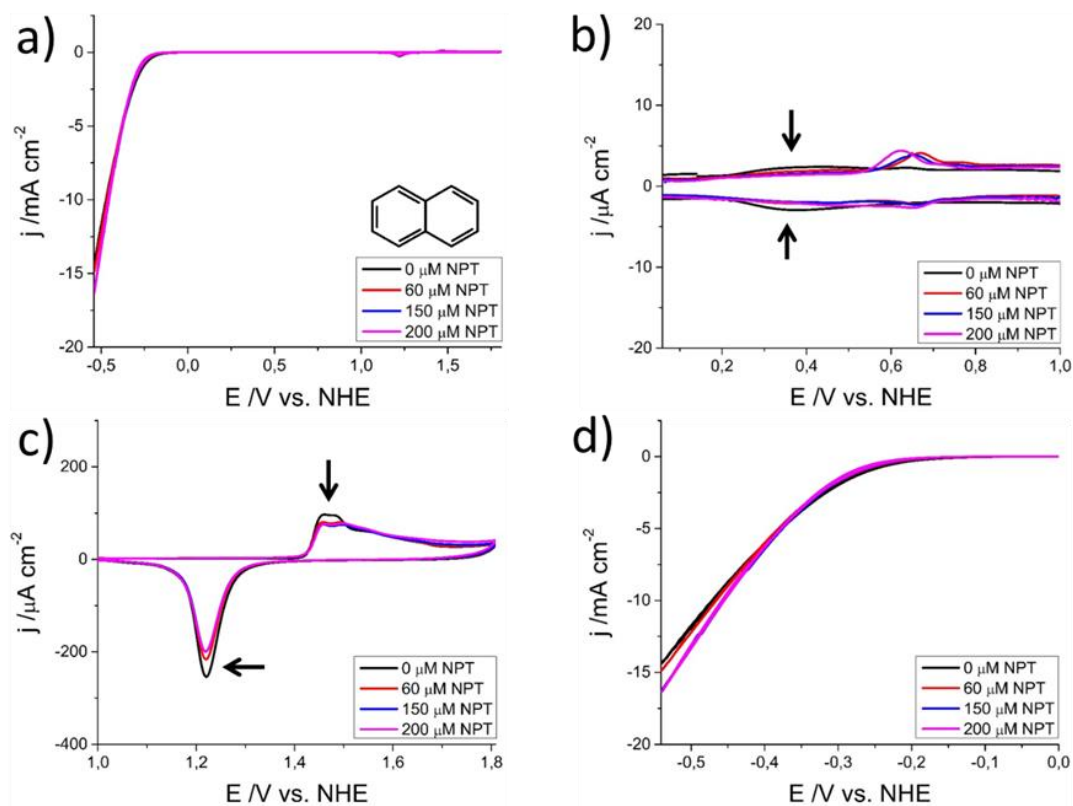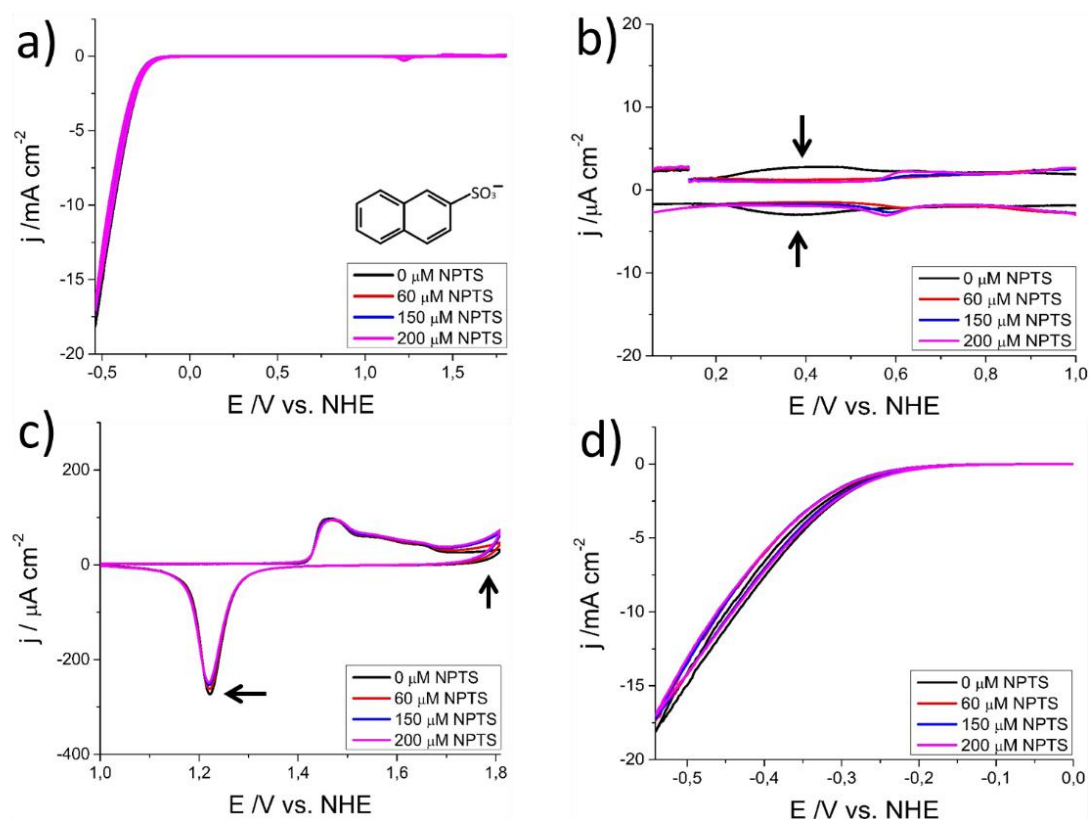
Figure 2. Cyclic voltammograms of a polycrystalline gold disc electrode in 0.1 M H_2SO_4 at different NPTS concentrations (a) CV recorded between -0.54 to 1.81 V at 50 mV s^{-1}. (b) Zoom-in of the double layer region, arrows show the decrease in the capacitive currents (c) Zoom-in of the gold oxide formation and reduction region, arrows show the decrease in the reduction area and the emergence of oxidative currents at very positive potentials (d) zoom-in of hydrogen evolution region (HER).

Although Figures 1 and 2 show only minor effects on the gold hydr(oxide) formation and reduction at positive potentials and the HER activity at negative potentials, both NPT and NPTS lead to changes in the current density in the double layer region, which may be explained by the formation of a film [38, 39]. It is known that organic molecules can be adsorbed at the metal surface by organizing spontaneously into monolayers. The formation of such films typically manifests in a characteristic decrease of the double layer capacity[39, 5].

Figure 3 shows cyclic voltammetry measurements of polycrystalline gold in a wide potential window (-0.54 to 1.81 V) in the presence of hydroxynaphthalenesulfonate (HNPTS) at different concentrations. The cyclic voltammogram exhibits some distinct features in comparison to NPT and NPTS. The double layer region presents at least three different peaks (A – C) that do not appear in the voltammetry of NPT and NPTS. These peaks exhibit a linear relationship between peak current and the scan rate, indicating that they involve adsorbed species. Above 1.1 V, there are two anodic peaks (D and E) that are not related to adsorption processes, as they do not have a reductive counterpart; instead, they seem associated to the oxidation of

Chapter 3. The effect of naphthalene-based additives on tin electrodeposition on a gold electrode

_____

HNPTS, likely involving oxidative polymerization of the naphthol, leading to the formation of a polymer film[40, 41, 42, 43]. The presence of this polymer film is confirmed by the considerably higher capacitance measured in the presence of HNPTS, suggestive of a thicker film that can store ions. Finally, hydrogen evolution is slightly hindered as a consequence of HNPTS adsorption, at least more than in the presence of NPT and NPTS.

In Figure 4, we show the cyclic voltammetry of a polycrystalline gold electrode in the presence of different concentrations of ENSA. The CVs are qualitatively more similar to the voltammetry in the presence of HNPTS than to the voltammetry in the presence of NTP and NTPS: there are new peaks in the voltammetry between 0.6 and 1.0 V (Fig.4b), which relate to surface adsorbed states, and there is an oxidation current above 1.1 V which does not have a reductive counterpart (Fig.4c). Together with the high double-layer capacitance (Fig.4b), this strongly suggests the formation of a polymer film formed oxidatively. Also, ENSA has a rather strong inhibitive effect on the hydrogen evolution (Fig.4d).

Figure 3. Cyclic voltammograms of a polycrystalline gold disc electrode in 0.1 M H_2SO_4 at different HNPTS concentrations (a) CV recorded between -0.54 to 1.81 V at 50 mV s^{-1}. (b) Zoom-in of the double layer region, arrows show the decrease in the capacitive currents and the rise of at least three anodic peaks (c) Zoom-in of the gold oxide formation and reduction region, arrows show the emergence of two anodic peaks (d) zoom-in of hydrogen evolution region (HER), arrow shows a slight decrease in the cathodic current.
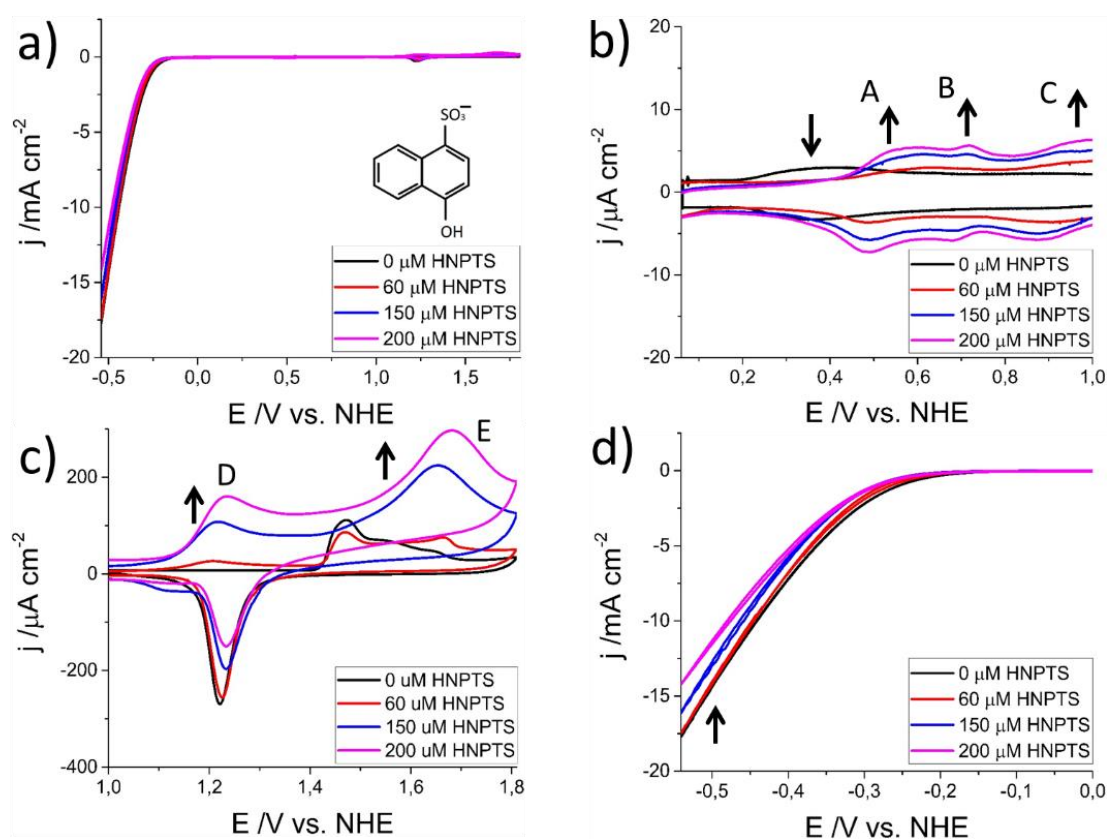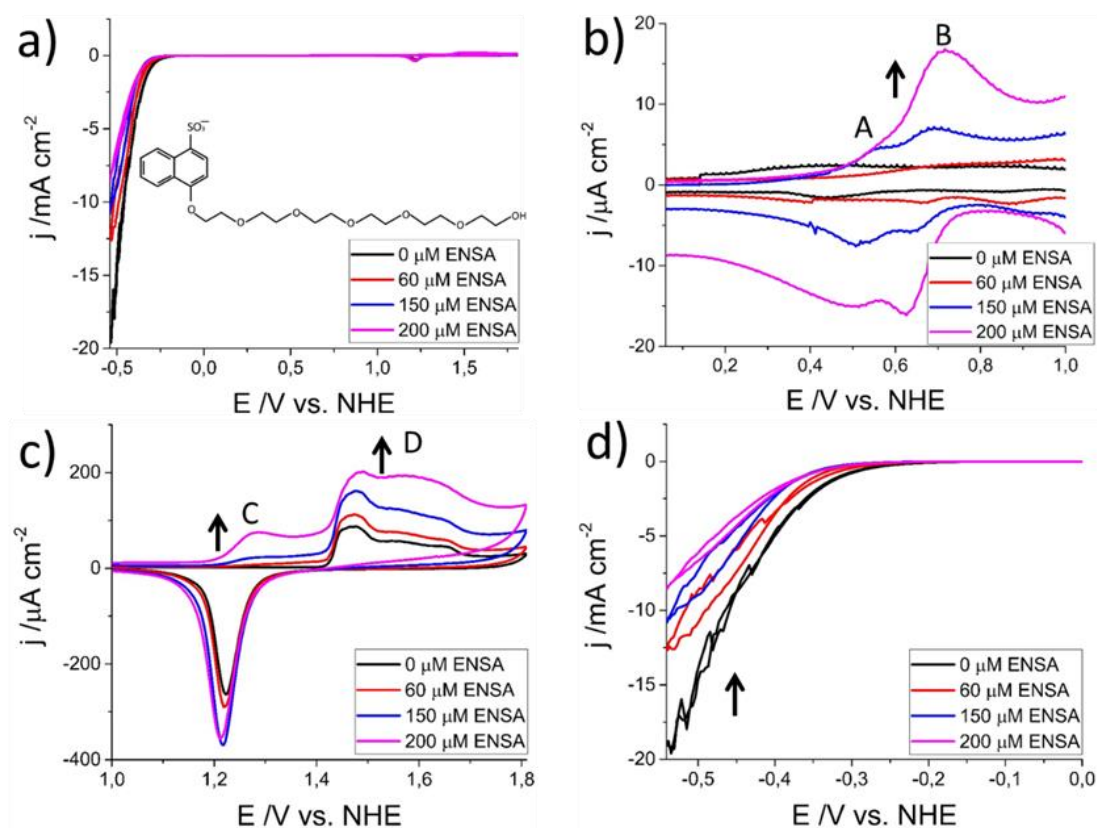
_____

Fig 4. Cyclic voltammograms of a polycrystalline gold disc electrode in 0.1 M H_2SO_4 at different ENSA concentrations (a) CV recorded between -0.54 to 1.81 V at 50 mV s^{-1}. (b) Zoom-in of the double layer region, arrow show the increase of a peak with the increasing ENSA concentration (c) Zoom-in of the gold oxide formation and reduction region, arrows show the emergence of oxidative currents at positive potentials (d) zoom-in of hydrogen evolution region (HER), arrow shows the strong decrease of HER

Since the nature and stability of electro-adsorbed organic films are strongly dependent on the crystalline surface structure, experiments on single-crystal Au surfaces were performed. Figures 5a-d show the cyclic voltammetry of Au (100) at different concentrations of NPT, NPTS, HNPTS and ENSA, respectively. We show here only results on Au (100), as the effects on this surface are the strongest, specifically on the surface reconstruction; results on Au (111) and Au (110) are shown in the Appendix B (see Fig. B1- B3, B5-B7).
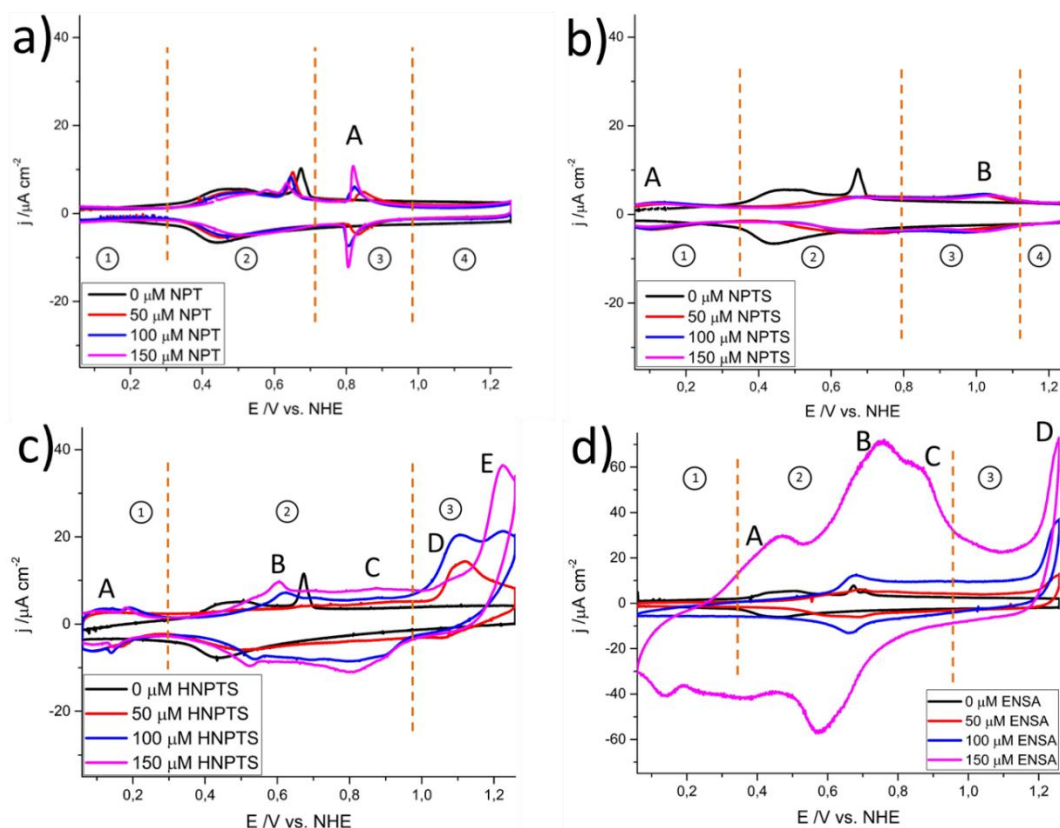
Figure 5. Cyclic voltammograms of Au (100), 0.1 M H_2SO_4 at different concentrations of (a) NPT (b) NPTS and (c) HNPTS (d) ENSA recorded between 0.06 to 1.26 V DL- region, at 50 mV s^{-1}.

The effect of NPT on Au (100) (Fig.5a) is primarily on the peak at 0.68 V, ascribed to the lifting of the (hex) reconstruction on Au(100)[12], which presents a decrease in its intensity, and a shift towards less positive potentials with an increase of NPT concentration. Since it is well known that on Au(100), the lifting of the reconstruction is related to anion adsorption[12], it appears that the presence of naphthalene molecules on the gold surface hinders sulfate adsorption. The presence of NPT on gold leads to a slightly lower double-layer capacity giving rise to a decrease of the current density between 0.16 – 0.66 V. The naphthalene adlayer appears to be more energetically stable on the unreconstructed Au (100) -(1x1) surface, and therefore the reconstruction is lifted at less positive potentials. The potential window labeled 3 in Figure 5a shows a reversible peak at ca. 0.81 V. This peak corresponds to sulfate adsorption, as it is absent in perchloric acid (see Fig. B4 in the Appendix B). In the absence of NPT, the peak at 0.68 V corresponds to a sulfate phase transition occurring concomitantly with lifting of the (hex) reconstruction[44]. The presence of NPT on the surface hinders the sulfate adsorption, shifting it to more positive potentials. In the potential window labeled 4, the Au (100) surface still shows a lower capacitive current density, which indicates the wide adsorption range of naphthalene molecules on the Au (100) surface. We conclude that naphthalene molecules are

_____

adsorbed on the gold surface over a wide potential window, essentially the entire double layer window, blocking sulfate anions from access to the surface.

The adsorption of NPTS exhibits a somewhat different behavior, as illustrated in Figure 5b. Two reversible couples are seen in the potential windows labeled 1 and 3, around 0.11 and 1.04 V, respectively. Most importantly, Figure 5b does not show the peak around 0.68 V, assigned to the lifting of the reconstruction on the Au (100) by the anion adsorption[12]. Also, the peak at 0.81 V that is observed in the presence of NPT, is missing in the presence of NPTS. Compared to the CV in the presence of NPT, this suggests that a more compact film is formed in the presence of NPTS, blocking the sulfate adsorption on the Au (100) surface better than NPT.

Figure 5c shows new features compared to the voltammetry with NPT and NPTS, largely in agreement with what is observed for polycrystalline gold: oxidative current without reductive counterpart, and a higher double-layer capacity. As mentioned, previous studies have shown polymerization of naphthol as a consequence of oxidation under acidic conditions[40, 41, 42, 43] which we suspect also happens with HNPTS. Figure 5d shows the effect of ENSA on the voltammetry of Au (100), which is again very different from Fig.5a and 5b, but qualitatively similar to Fig.5c: irreversible oxidation at high potential, and higher double-layer capacity.
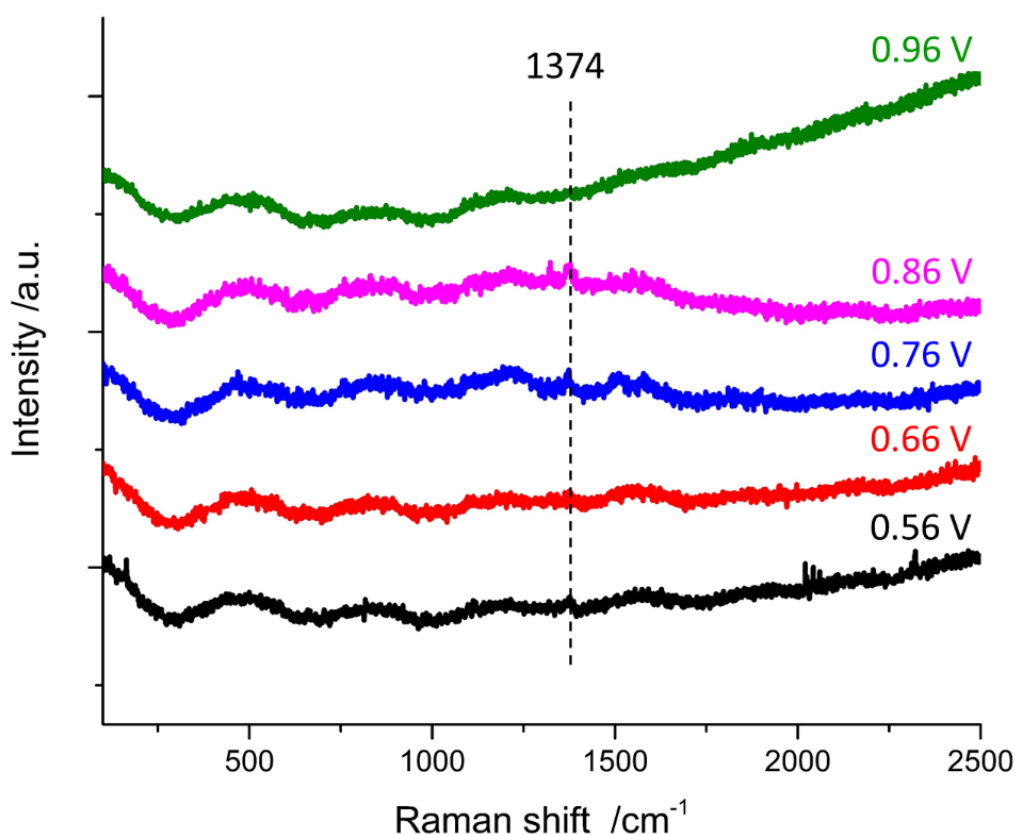

Figure 6. SER spectrum of 0.2 mM of NPT in 0.1 M H_2SO_4 on polycrystalline gold at different potentials from 0.56 to 0.96 V, see band at 1374 cm^{-1}; The full spectrum recorded between 0.01 to 1.06 V is shown in Fig. B8

Chapter 3. The effect of naphthalene-based additives on tin electrodeposition on a gold electrode

_____

Surface Enhanced Raman Spectroscopy (SERS) was used to obtain more information about NPT, NPTS, HNPTS and ENSA adsorption. Fig. 6 shows that NPT gives rise to a very low intensity band at ~1374 cm⁻¹ between 0.56 to 0.96 V, the band is ascribed to the characteristic C-C stretching of NPT ring planar oriented on Au. This observation is in agreement with previous studies of Busby and Creighton that showed the same band at 1376 cm⁻¹, and ascribed it to naphthalene ring mode on a planar orientation on Au and Ag electrodes [45]. Dahms and Green also showed evidence for the planar position of naphthalene on the gold surface by means of the shape of the adsorption isotherm using a ^{14}C-radio tracer technique [46], and Wan and Itaya demonstrated by electrochemical scanning tunneling microscopy (STM) that naphthalene molecules are flat oriented on the copper surface [47].
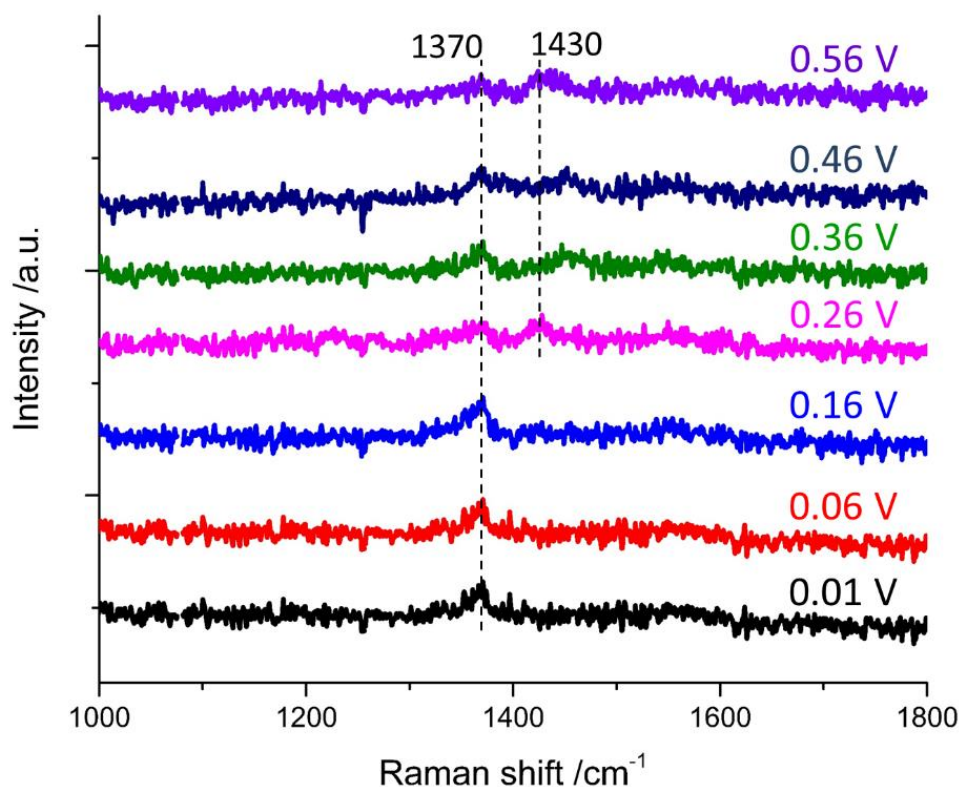

Figure 7. SER spectrum of 1 mM of NPTS in 0.1 M H₂SO₄ on polycrystalline gold at different potentials from 0.01 to 0.56 V, see bands at 1370 and 1430 cm⁻¹; The full spectrum recorded between 0.01 to 1.06 V is shown in Fig. B9

Figure 7 shows the evolution of SER spectrum of NPTS on gold recorded in a potential window from 0.01 to 1.06 V. Similar to NPT, the NPTS spectrum exhibits a band at ~1370 cm⁻¹ ascribed to C-C stretching of the NPT ring flat oriented on the Au surface. Interestingly, the SER spectra show that between 0.26 to 0.56 V a second band appears at ~1430 cm⁻¹ which is ascribed to symmetric stretching of v_s (C-C) [48][49][50][51] of the naphthalene ring, coinciding with the region of the lowest differential capacity in Fig. 2b. Based on these observations, in combination with

_____

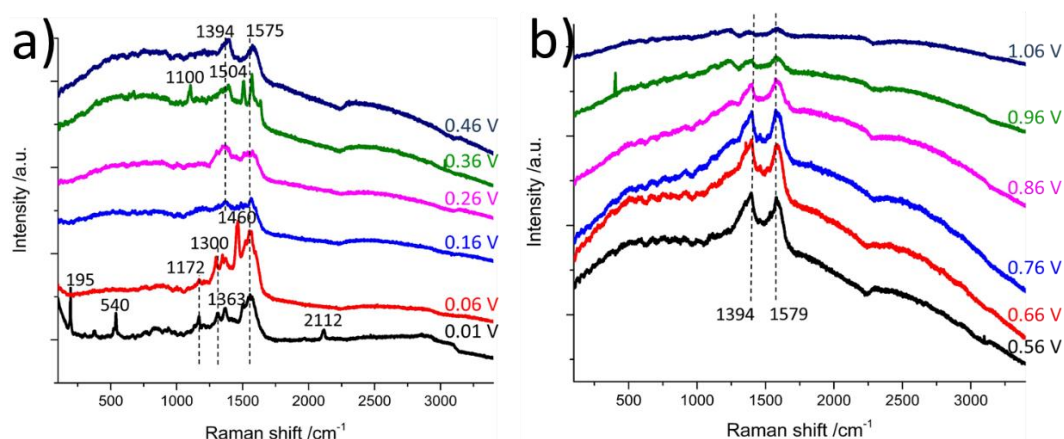the DFT calculations, we propose that a flat orientation is the most likely adsorption mode of NPT and NPTS.

Figure 8. SER spectra of 1 mM of HNPTS in 0.1 M H_2SO_4 on polycrystalline gold at different potentials: (a) detailed spectra from 0.01 to 0.46 V; (b) detailed spectra from 0.56 to 1.06 V. The full spectra are shown in Fig. B10

Figure 8a shows the evolution of SER spectrum of HNPTS on gold between 0.01 to 0.46 V. The spectra at 0.01 and 0.06 V exhibit a considerable number of bands presumably ascribed to vibrational modes of the naphthalene ring, sulfonate and hydroxyl groups. We ascribed bands at 1460, 1502 and ~1560 cm^{-1} to vibrational modes of the naphthalene ring such as symmetric stretching of v_s (C-C) and in plane bending of β(H-C-C) [48 49 50 51]. Bands at 540 cm^{-1} to scissoring of δ (-SO$_2$-)[48], at 1363 cm^{-1} to antisymmetric stretching v_{as} (-SO$_2$-) [48 49], and 2112 cm^{-1} to stretching of v(OH) from (C-SO$_3^-$H$_3$O$^+$) [49] of the sulfonate group. Additionally, the band at 1300 cm^{-1} is ascribed to in plane bending [β(H-O)][52] of OH group bound to the naphthalene ring. Between 0.16 and 0.46 V, the SER spectra exhibit remarkable changes; it roughly coincides with the adsorption peaks A and B in the voltammogram of Fig. 5c (see also Fig. B5c). From 0.46 to 0.86 V (see Fig 8b), the spectra mainly show two peaks, one at 1394 cm^{-1} ascribed to antisymmetric stretching v_{as} (-SO$_2$-) [48 49] of the sulfonate group and the other one at 1579 cm^{-1} ascribed to symmetric stretching v_s (C-C) [48] and in-plane bending β(H-C-C) [48 49 50 51] of the naphthalene ring. A slight shift of the peaks to a higher wavenumber is seen as a consequence of the Stark effect. Above 0.96 V, no strong features are noticeable in the spectra, which also agrees with the abrupt increase in the current due to peaks C, D, E (see Fig 5c).

The above observations suggest that HNPTS does not lie flat on the surface, in contrast to NPT and NPTS. Moreover, it is seen that above 0.96 V it undergoes a complex process that is not sensitive to the electrode surface, which we tentatively ascribe to oxidative polymerization of the naphthol group[40, 41, 42, 43].

Fig 9a shows the evolution of the ENSA spectra between 0.01 to 0.26 V. We ascribed band at 1363 cm^{-1} to antisymmetric stretching v_{as} (-SO$_2$-) of the sulfonate group [48] [49], the band at 1556 cm^{-1} to the symmetric stretching v_s (C-C) [48] and in-plane bending β(H-C-C) [48] [49] [50] [51] of the naphthalene ring and the band at 3150 cm^{-1} to stretching v (O-H)[48] of the hydroxyl group. We highlight the absence of bands correlated with the ethoxy group at v_s(C-O-C) [48, 49,] at ~900 cm^{-1}, v_s (Aryl-O) [48, 49,] 1200 – 1300 cm^{-1}. Instead, a band at 2264 cm^{-1} characteristic of C-N stretching is seen, which presumably comes from contamination. Fig 9b shows the spectra between 0.36 to 1.06 V: the spectra exhibit a band at 1326 cm^{-1} ascribed to antisymmetric stretching of sulfonate group v_{as} (-SO$_2$-) [48] [49] and 3150 cm^{-1} ascribed to stretching of v (O-H)[48, 49]. A strong increase of the background signal is also observed, implying the formation of a thick film on the electrode surface.

Evolution of SER spectra also suggests that naphthalene ring of ENSA does not lie flat on the electrode surface. Furthermore, the increase in the background upon 0.36 V coincides with the noticeable rise of anodic currents in the cyclic voltammogram, see Fig. 5d. Similarly, to HNPTS, oxidative polymerization of naphthol under acidic conditions is suggested to be responsible for this[40, 41, 42, 43].
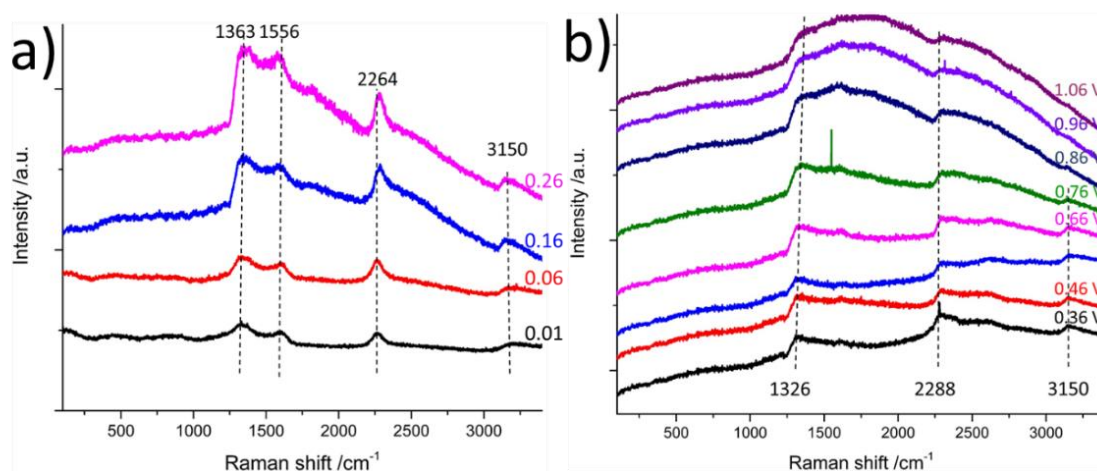
Figure 9. SER spectrum of 1 mM of ENSA in 0.1 M H$_2$SO$_4$ on polycrystalline gold at different potentials (8a) detailed spectra from 0.01 to 0.26 V (8b) detailed spectra from 0.36 to 1.06 V. The full spectrum is shown in Fig. B11

To provide a possible explanation for the difference between the NPT and NPTS films, density functional theory calculations were performed to estimate the lateral interaction of NPT and NPTS molecules (Fig. 10). These calculations show that for NPT the interaction between the molecules is weak or negligible, their lateral interaction energy is only -0.02eV, which was calculated by moving neighboring molecules closer together to neighboring adsorption sites at a constant coverage. On the other hand, for NPTS molecules the lateral interaction energy

_____

is -0.29 eV (the negative sign --indicates attractive interaction, see Figures B12 and B13 of the Appendix B). The difference in lateral interaction energy is caused by the favorable hydrogen bonding formation between NPTS adsorbates; as a consequence, a more compact film is formed between NPTS. This hydrogen bonding could be supported by studies of Ataka and Osawa showing water molecules bridging through hydrogen bonding in sulfate adlayers on Au (111)[53].

These DFT calculations neglect the effect of solvent near the surface and the fraction of protonated sulfonate groups was taken to be 50%. Given that sulfonate is a strong acid, future calculations should consider solvation and the effective pKa of the adsorbed molecules and hydrogen bonded pairs. Density functional theory studies were not performed for HNPTS, taking into account the complexity of its behavior due to the possible polymerization[41].

Similar DFT calculations of NPT and NPTS adsorption on metallic tin (α–Sn) were performed, see Figures 11a and 11b, respectively. A similar behavior in comparison to NPT and NPTS on gold surface is seen. Fig 11a shows that NPT molecules exhibit repulsive lateral interaction, and Fig. 11b shows NPTS molecules exhibit strongly attractive lateral interaction. The observed behavior is agreement with NPT and NPTS binding to gold and tin surfaces mainly through Van der Waals interactions, which are expected to be metal independent. Also, oxidative polymerization is a process which is generally not very sensitive to the nature of the electrode material[40, 41, 42, 43]. Therefore, we assume that adsorption structures formed on gold will likely also form on tin. See Figures B13 and B14.

a)

$\Delta E = -0.02 \ eV$
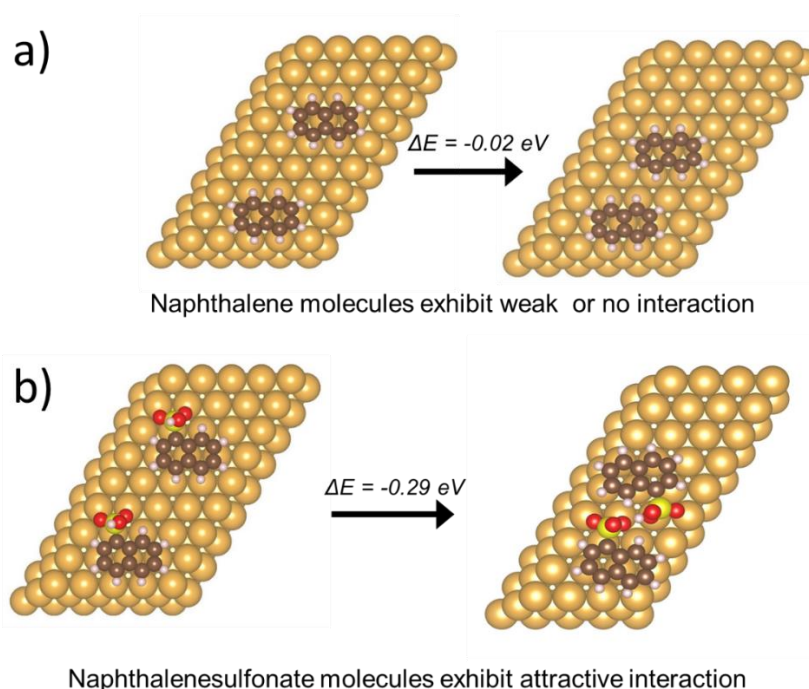
Naphthalene molecules exhibit weak or no interaction

b)

$\Delta E = -0.29 \ eV$

Naphthalenesulfonate molecules exhibit attractive interaction

Figure 10. Difference of lateral interaction energy for (a) NPT and (b) NPTS on Au (111)

Summarizing, the above electrochemical, spectroscopic and computational results show that NPT and NPTS do not strongly alter the gold CV profile in the sense that the onset potential for the gold (hydr-)oxide formation and HER activity are not affected significantly. However, noticeable changes in the double layer region are present; this region exhibits a decrease in differential capacity, which is characteristic for organic film formation. Studies with single crystal surfaces suggest both NPT and NPTS remain adsorbed over a wide potential range, but that NPTS forms a more compact film than NPT. SER spectroscopy and DFT calculations show that both naphthalene and naphthalenesulfonate bind flat onto the gold surface, and the NPTS exhibits lateral attractive interactions due to hydrogen bonding, which may explain why its film appears to be more compact. On the other hand, HNPTS and ENSA show very different behavior, suggesting oxidative polymerization and polymer film formation.
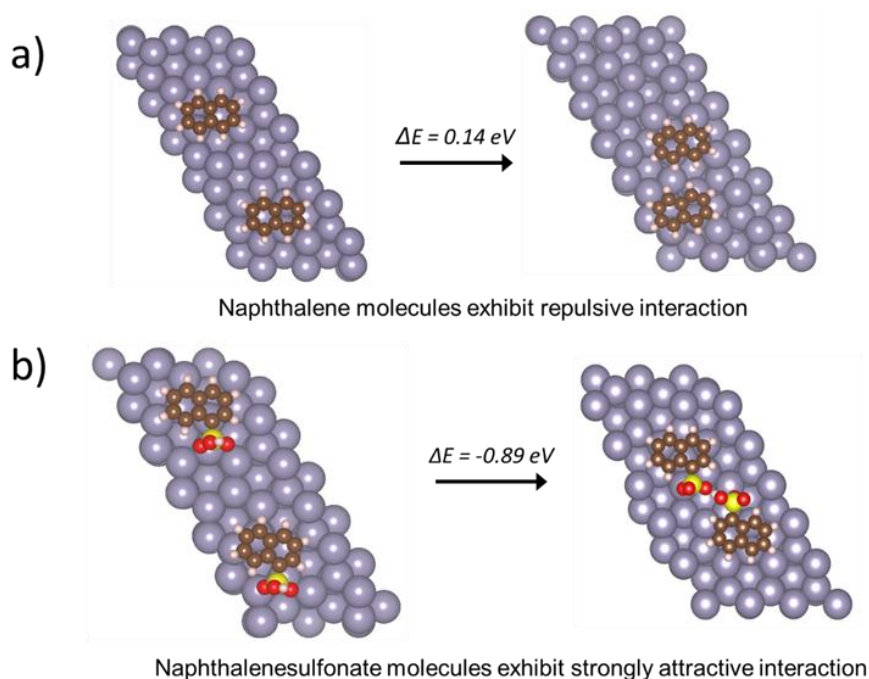
Figure 11. Difference of lateral interaction energy for (a) NPT and (b) NPTS on Sn (111)

3.3.1 Tin electrodeposition on polycrystalline gold in the presence of naphthalene, naphthalenesulfonate and hydroxynaphthalenesulfonate

Tin electrodeposition on polycrystalline gold takes place via at least three different deposition mechanisms (irreversible adsorption, underpotential deposition, and overpotential deposition). It has been shown that in the cyclic voltammogram, the deposition process exhibits five distinct peaks: two cathodic peaks associated with tin underpotential and

_____

overpotential deposition, and three main anodic peaks, corresponding to the oxidation of the bulk Sn, of the AuSn intermetallic layer, and of the adsorbed Sn(II) to Sn(IV)[54, 55]. These processes are summarized by the following equations:

$$C1: Sn\ (II)_{ads} + 2e \rightarrow Sn\ (0)_{UPD}\ (1)$$

$$C2: Sn\ (II)_{sol} + 2e \rightarrow Sn\ (0)_{OPD}\ (2)$$

$$A3: Sn\ (0)_{OPD} \rightarrow Sn\ (II)_{sol} + 2e\ (3)$$

$$A2: AuSn \rightarrow Au + Sn\ (II)_{sol} + 2e\ (4)$$

$$A1: Sn\ (II)_{ads} \rightarrow Sn\ (IV) + 2e\ (5)$$
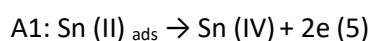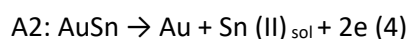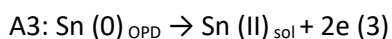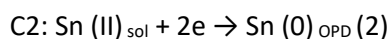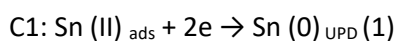
Figures 12a, 13a and 14a show the cyclic voltammograms at a gold rotating disk electrode (RDE) in an extended range of potential (-0.54 to 0.66 V) with and without NPT, NPTS and HNPTS at different concentrations.

It is observed in Figure 12a that the peak related to stripping of the bulk deposited tin (A3) decreases considerably in the presence of NPT, showing that a smaller amount of tin has been deposited. An increase in the cathodic current at the most negative potentials is also seen, which has been ascribed to the concurrent reaction of hydrogen evolution reaction (HER) on the remaining gold surface[55]. This higher HER current also suggests a decrease in the amount of tin deposited as this will lead to a higher surface area of gold available for HER, in agreement with the previous observation of island formation during tin deposition on gold[56, 55]. Furthermore, no changes are seen in the stripping of the alloy AuSn (A2, A2') and in the Sn(II) oxidation process (A1), neither in the current densities nor in the potential of the respective processes.

Since all the cyclic voltammetry measurements were performed at the same scan rate and rotation speed, peak A3 is a good marker to estimate the amount of tin bulk deposited. From the voltammetric information, naphthalene does not seem to affect strongly most of the reactions involved during the deposition and stripping processes, other than it generally seems to slow down the tin reduction.
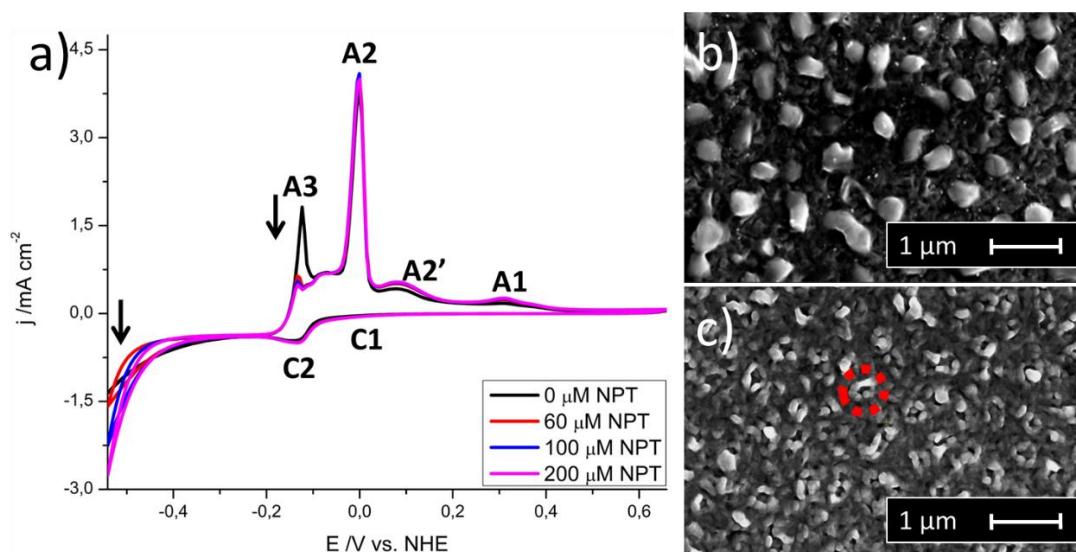
Figure 12. (a) Cyclic voltammograms of tin electrodeposition on a polycrystalline gold RDE, 0.1 M H_2SO_4, 0.6 mM $SnSO_4$ at different concentrations of NPT, recorded between -0.541 to 0.659 V and 30 mV s^{-1} and 1600 rpm. SEM micrographs of tin electrodeposited, on polycrystalline gold; potential was swept from 0.659 to -0.241 V at 30 mV s^{-1} and 1600 rpm, subsequently the potential was held at -0.241 V during 1 minute, 0.1 M H_2SO_4, 0.6 mM $SnSO_4$, in the presence of: (b) without NPT (c) with 200 μM NPT

Figures 12b and 12c show the SEM images of the morphology of the tin deposit in the absence and presence of naphthalene, respectively. The deposit in the absence of naphthalene exhibits a low density and large 3D nuclei, with features sizes between 300 – 900 nm. On the other hand, in the presence of naphthalene, the deposit exhibits a higher number of nuclei and smaller feature size (<100 nm) that appear coalesced. Moreover, the deposit seems to be be organized in a circular arrangement (see Fig 12c – doted red line).   The number of tin deposited monolayers shows almost not differences in the number of equivalent tin layers from $\theta_{Sn(0\ \mu M\ NPT)} = 50\ ML$ to $\theta_{Sn(0\ \mu M\ NPT)} = 49\ ML$. These observations suggests that NPT acts to slow down only the tin bulk electrodeposition process, yielding smaller features which are presumably primarily AuSn alloy particles

Figure 13a shows the effect of naphthalenesulfonate on tin electrodeposition process. In accordance with the effect of NPT, NPTS also gives rise to a decrease in the peak A3, related to the oxidation of bulk deposited tin, and an increase of the HER current on gold at the most negative potentials. SEM micrographs also show a decrease of the feature size with NPTS and production of circular shapes, the tin deposit also exhibits a higher number of nuclei (Fig. 13c), very similar to NPT. Furthermore, a slight (though perhaps not very significant) increase in the equivalent number of tin layers from $\theta_{Sn\ (0\ \mu M\ NPTS)} = 50\ ML$ to $\theta_{Sn\ (200\ \mu M\ NPTS)} = 54\ ML$ and a more condensed structure of the deposit are observed. Additionally, a shift in the peak A2, attributed to stripping of the Au-Sn alloys. Voltammograms at different scan rates show that this shift is not kinetic in nature (see Fig B15 in the Appendix B).

_____
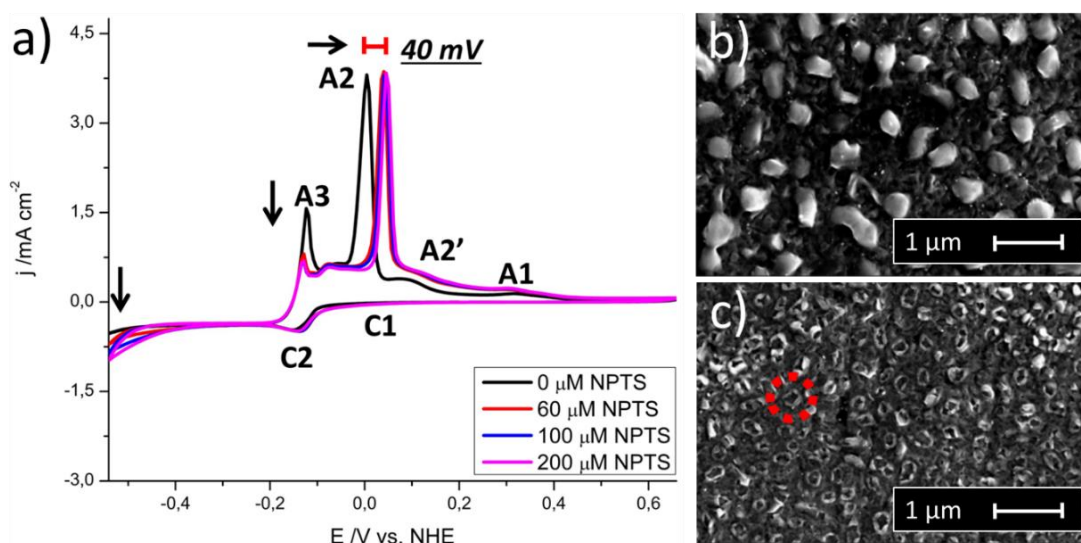
Figure 13. (a) Cyclic voltammograms of tin electrodeposition on RDE polycrystalline gold, 0.1 M H_2SO_4, 0.6 mM $SnSO_4$ at different concentrations of NPTS, recorded between -0.541 to 0.659 V and 30 mV s^{-1} and 1600 rpm. SEM micrographs of tin electrodeposited on polycrystalline gold, potential was swept from 0.659 to -0.241 V at 30 mV s^{-1} and 1600 rpm, subsequently potential was held at -0.241 V during 1 minute, 0.1 M H_2SO_4, 0.6 mM $SnSO_4$, in the presence of: (b) without NPTS (c) with 200 µM NPTS

Figure 14. (a) Cyclic voltammograms of tin electrodeposition on a polycrystalline gold RDE, 0.1 M H_2SO_4, 0.6 mM $SnSO_4$ at different concentrations of HNPTS, recorded between -0.541 to 0.659 V and 30 mV s^{-1} and 1600 rpm. SEM micrographs of tin electrodeposited, on polycrystalline gold; potential was swept from 0.659 to -0.241V at 30 mV s^{-1} and 1600 rpm, subsequently potential was held at -0,241 V during 1 minute, 0.1 M H_2SO_4, 0.6 mM $SnSO_4$, in the presence of: (b) without HNPTS (c) with 200 µM HNPTS

Chapter 3. The effect of naphthalene-based additives on tin electrodeposition on a gold electrode

_____

Figure 14a shows the cyclic voltammogram of tin electrodeposition in the presence of HNPTS. Unlike NPT and NPTS, HNPTS exhibits an increase in both peak A3 and A2, related to the oxidation of bulk electrodeposited tin and tin-gold alloys, resp. A small increase of the number of equivalent tin layers from $\theta_{Sn\,(0\,\mu M\,HNPTS)} = 50\,ML$ to $\theta_{Sn\,(200\,\mu MHNPTS)} = 55\,ML$ is observed, as well as of the intensities of the A2 and A3 peaks, suggest that a higher amount of tin bulk and AuSn alloy have been deposited. SEM micrographs in the absence and presence of HNPTS also show remarkable differences; the tin deposit exhibits a higher 3D nuclei density, with a smaller feature size (about 100 nm). Unlike tin deposits in the presence of NPT and NPTS, the features do not appear coalesced. The voltammogram also shows an increase in the HER and a shift in the peak A2, which is again not kinetic in nature.

We ascribe the shift in the potential of peak A2 for NTPS and HNPTS to the incorporation of some form of sulfur in the AuSn deposit. The incorporation of sulfur in nickel deposits due to reduction of allylsulfonates has been observed previously by Gotthard and Trivich[57], who proposed it to happen via an early desulfonation. Later, Kendrick[58] also mentioned the sulfur incorporation during nickel electrodeposition caused by reduction of naphthalene derivatives and proposed two mechanisms: via mercaptan formation and via an early desulfonation. Brook and Crossley also showed the presence of sulfur in nickel deposits and claimed that the process happens via an early desulfonation, with a thiosulfate as intermediate[59]. These reactions are described by the following equations:

$$R\text{-}SO_3H + 2e \rightarrow R\text{-}H + SO_3^{2-} \quad (6)$$

$$2SO_3^{2-} + 6H_3O^+ + 4e \rightarrow S_2O_3^{2-} + 9H_2O \quad (7)$$

$$S_2O_3^{2-} + 2Ni + 6H_3O^+ + 4e \rightarrow 2NiS + 9H_2O \quad (8)$$

In the case of nickel electroplating in the presence of naphthalenesulfonate, Brook and Crossley showed the presence of naphthalene via extraction with amyl acetate and subsequent identification via UV spectroscopy and chromatography. However, the presence of thiosulfate as an intermediate was not corroborated.

Figure 15 shows cyclic voltammograms of tin electrodeposition in the absence and presence of naphthalene and with different concentrations of sodium thiosulfate. Voltammograms in the absence of thiosulfate (black and red) exhibit the behavior of the tin deposition in the absence and presence of naphthalene. When thiosulfate is added in the electrolyte, a shift in the A2 peak (ca. 40 mV) is seen which perfectly agrees with the shift observed in the presence of NPTS and HNPTS. This observation agrees with the assertion of Brook and Crossley that thiosulfate may act as an intermediate in the sulfur incorporation in the metal deposit, though we are not claim it to be the intermediate for NPTS, HNPTS and ENSA. More importantly, it shows that the peak shift observed in the presence of NPTS and HNPTS is most likely due to some form of sulfur incorporation in the deposit.
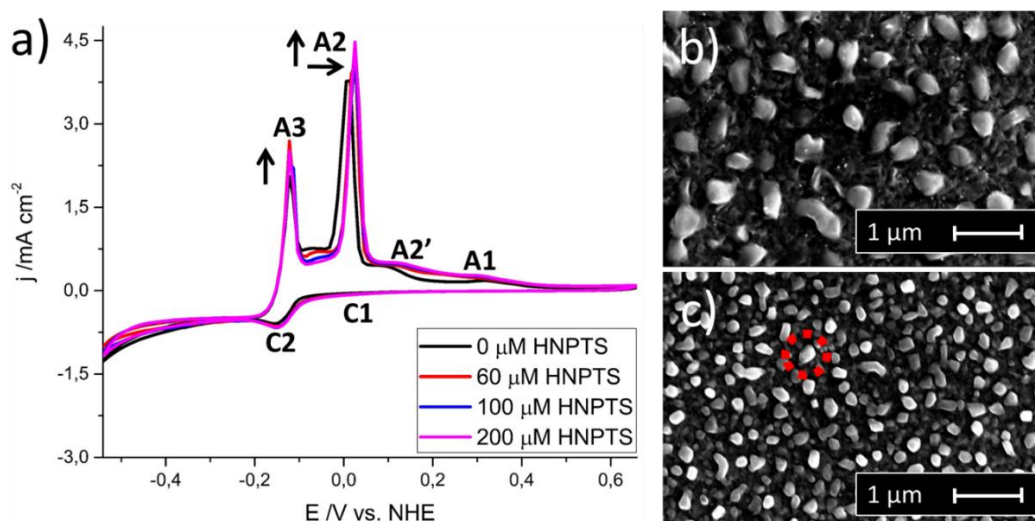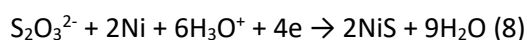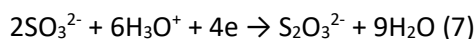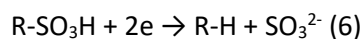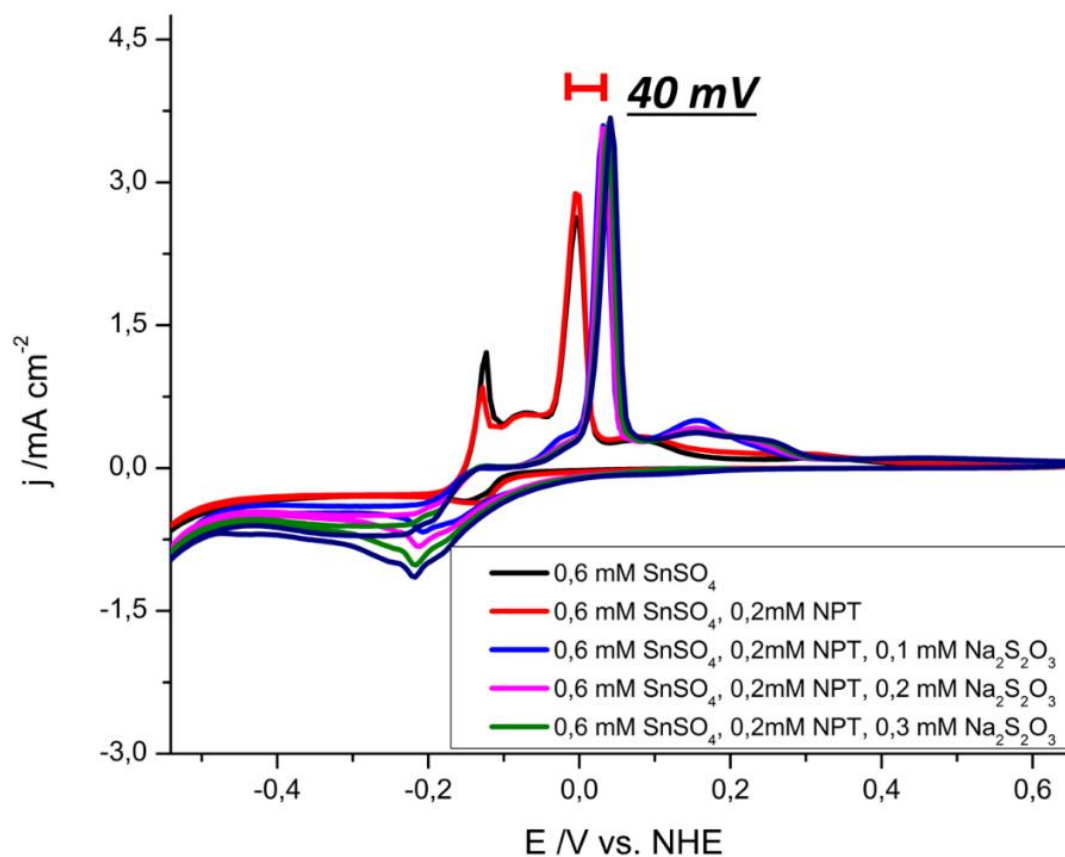
Figure 15. Cyclic voltammogram of tin electrodeposition on polycrystalline gold, 0.1 M H_2SO_4, 0.6 Mm $SnSO_4$, 0.2 mM NPT. 30 mV s^{-1} and 1600 rpm.

3.3.2 Tin electrodeposition on polycrystalline gold in the presence of ethoxylated naphthalenesulfonic acid (ENSA-6)

Figure 16 shows the cyclic voltammetry of tin electrodeposition in the absence and presence of ENSA–6. Compared to NPT, NPTS and HNPTS, in the presence of ENSA show there is a much stronger inhibition effect on tin bulk deposition, as evidenced by the decrease in the peak A3. Fig. 16a also shows a shift in the potential of the peak A2 ascribed to sulfur incorporation in the AuSn alloy.
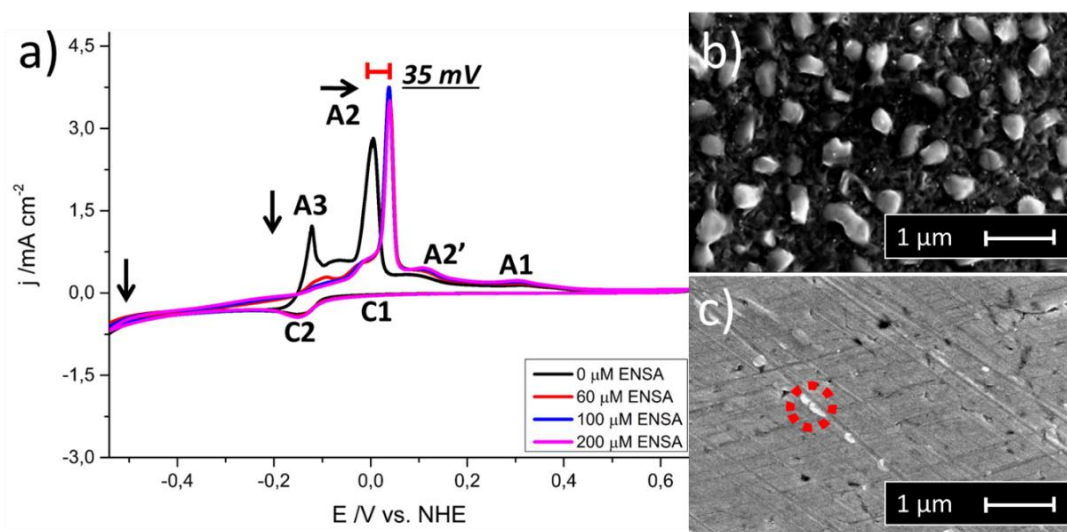
Figure 16. (a) Cyclic voltammograms of tin electrodeposition on RDE polycrystalline gold, 0.1 M H_2SO_4, 0.6 mM $SnSO_4$ at different concentrations of ENSA, recorded between -0.541 to 0.659 V at 30 mV s^{-1} and 1600 rpm. SEM micrographs of tin electrodeposited on polycrystalline gold, potential was swept from 0.659 to -0.241 V at 30 mV s^{-1}, subsequently potential was held at -0.241 V during 1 minute, (b) without ENSA (c) with 200 µM ENSA

The equivalent number of tin layers was calculated for the deposit shown in the SEM image, showing a decrease from $\theta_{Sn\,(0\,\mu M\,ENSA)} = 50\,ML$ to $\theta_{Sn\,(200\,\mu M\,ENSA)} = 29\,ML$. The scanning electron micrograph shows almost no tin features on the substrate, apart perhaps from a few tin features along the substrate defects. Fig. 17 shows the relative sulfur and tin abundance on the substrate for all the naphthalene-based additives. Tin deposited in the presence of NPTS, HNPTS and ENSA exhibit sulfur, although the values are very dispersed and hardly above the noise, so that further spectroscopic studies are required to unveil the nature and quantity of the sulfur compound(s) present in the deposit. Moreover, Figure 17 also shows that ENSA exhibits the lowest amount of tin. This agrees with the SEM image which basically shows an essentially featureless AuSn alloy surface. Previous studies of the effect of ENSA on tin electrodeposition on different substrates have ascribed the inhibition of the tin deposition to a decrease of the rate of electron transfer[19], and to Sn(II) mass transport limitations to the substrate surface caused by a compact stable layer of ENSA molecules on the surface[20]. Our work shows that ENSA does not remain stable on the Au surface, instead it may undergo an oxidative polymerization process. Furthermore, for Sn electrodeposition on gold, ENSA mainly seems to have an effect on tin bulk deposition process, and it shows little effect on the AuSn alloying process; except from sulfur incorporation into the alloy and a slight increase in the charge associated to the dealloying peak from 5.5 (0 mM ENSA) to 5.7 mC cm^{-2} (0.2 mM ENSA), similar values of the charge for AuSn dealloying process were previously reported by Petersson et al. [54]. Results show that ENSA strongly inhibits the 3D growth of the tin features, but promotes the Au-Sn alloying process. Moreover, ENSA exhibits almost no effect on the

_____

early stages of the tin deposition on gold, unlike previous studies[20] that suggested that ENSA molecules also have a strong influence on early stages of the tin deposition on iron electrodes.

Additionally, the above results show that tin deposits grown in the absence and presence of additives all show a very similar AuSn alloy stripping peak (apart from sulfur-related shift). This suggests that the alloying itself is hardly influenced by the presence of additives, and therefore more likely related to the very early stages of tin deposition (such as UPD), and not much related to the growth of bulk tin features.
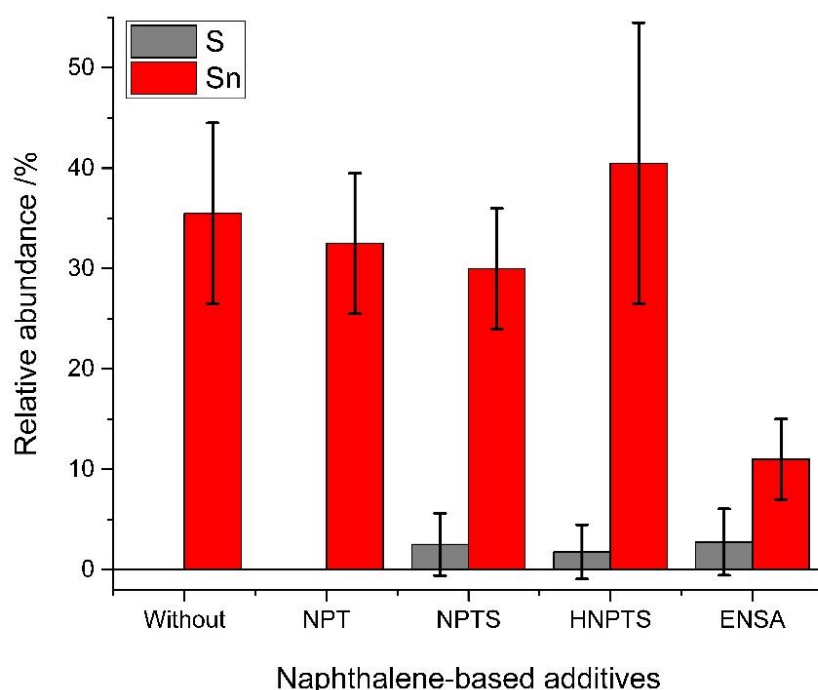
Figure 17. Comparison of the tin and sulfur relative abundance for each additive from the EDS measurements. Percentage was calculated from the average of the relative ratio of tin in a line scan measurement of about ~0.5 μm length, over the tin features.

Previous in situ STM studies by Mao et al.[56,60] have demonstrated the complex nature of Sn UPD on Au single crystal electrodes, with the UPD intimately linked to the surface alloying process. They showed that underpotential deposition of Sn on Au presents strikingly different features from usual UPD processes, such as distorted and size confined clustering, preferential nucleation, anisotropic growth, and the formation of an disordered adlayer on Au (111) surfaces[56]. Mao et al. show a strong correlation between surface alloying and the unusual UPD, in the sense that Sn forms clusters of about 2 nm size, which remain stable over time, and depending on the electrode potential and substrate surface structure, Sn diffuses into the gold lattice, as a result of which SnAu alloying would take place. Tin underpotential deposition and alloy formation also exhibit a slow kinetics[56].

Given the slow kinetics of the underpotential deposition and the associated alloy formation, the relatively small effect that ENSA but also NPT, NPTS and HNPTS exhibit on the alloying process seems reasonable. Our measurements suggest that a certain amount of tin adatoms on the gold surface go through UPD and subsequent surface alloying without being affected by the presence of naphthalene derivatives on the surface. The amount of alloying would only be affected by changes in the gold interdiffusion barrier, which is apparently not affected by the additive. In contrast, the kinetics of tin overpotential process is fast and as a consequence, Sn OPD deposition is affected by additive adsorption, due to a kinetic effect.

3.4 Conclusions

In this study, we have investigated the effect of naphthalene derivatives, NPT, NPTS, HNPTS, and ENSA, on the tin electrodeposition process on a gold electrode. From experiments and density functional theory calculations, we conclude the formation of films of NPT, NPTS, HNPTS and ENSA. NPT and NPTS lie flat on the gold surface. NPTS forms a denser film due to attractive interactions via hydrogen bonding between the adsorbed molecules, and HNPTS and ENSA forms surface films as a result of oxidative polymerization. Tin electrodeposition is strongly affected by the presence of the NPT, NPTS, HNPTS, and ENSA films. Tin bulk electrodeposition is inhibited in the presence of NPT and NPTS, but promoted in the presence of HNPTS. Tin deposits grown in the presence of NPT and NTPS seem to have the same morphology, but tin deposit grown in the presence of HNPTS exhibits markedly smaller features. Sulfonated additives lead to some form of sulfur incorporation in the SnAu alloys as a consequence of reductive desulfonation and subsequent sulfonate reduction; thiosulfate was identified as a possible intermediate in this reaction.

Ethoxylated napthalenesulfonic acid (ENSA), a commonly used additive in the tin electroplating industry, exhibits a similar behavior to NPT and NPTS during the tin deposition process in terms of the measured voltammetry: a suppression of the bulk Sn electrodeposition, but essentially no effect on the AuSn alloy formation, besides sulfur incorporation. Nonetheless, SEM shows that ENSA severely inhibits the tin bulk deposition to the extent that the surface shows no notable features in the SEM images. Finally, the lack of a strong effect of naphthalene derivatives and ENSA on the SnAu alloying process is ascribed to the slow nature of Sn UPD on gold and SnAu alloying process.

_____

3.5 References

(1)   Paunovic, M.; Schlesinger, M. *Fundamentals of Electrochemical Deposition Second Edition*, Sceond.; A JOHN WILEY & SONS: United States of America, 2006.

(2)   Franklin, T. C. Some Mechanisms of Action of Additives in Electrodeposition Processes. *Surf. Coatings Technol.* 1987, *30* (4), 415–428.

(3)   Oniciu, L.; Muresan, L. Some Fundamental Aspects of Levelling and Brightening in Metal Electrodeposition. *J. Appl. Electrochem.* 1991, *21* (7), 565–574.

(4)   Whelan, C. M.; Smyth, M. R.; Barnes, C. J. The Influence of Heterocyclic Thiols on the Electrodeposition of Cu on Au(111). *J. Electroanal. Chem.* 1998, *441* (1–2), 109–129.

(5)   Petri, M.; Kolb, D. M.; Memmert, U.; Meyer, H. Adsorption of PEG on Au(111) Single-Crystal Electrodes and Its Influence on Copper Deposition. *J. Electrochem. Soc.* 2004, *151* (12), C793.

(6)   Yanson, Y.; Frenken, J. W. M.; Rost, M. J. A General Model of Metal Underpotential Deposition in the Presence of Thiol-Based Additives Based on an in Situ STM Study. *Phys. Chem. Chem. Phys.* 2011, *13* (35), 16095–16103.

(7)   Hoizle, M. H.; Apsel, C. W.; Will, T.; Kolb, D. M. Copper Deposition onto Au(l 11) in the Presence of Thiourea. *J. Electrochem. Soc.* 1995, *142* (11), 3741–3749.

(8)   Shi, Z.; Wu, S.; Lipkowski, J. Investigations of Cl– Adsorption at the Au(111) Electrode in the Presence of Underpotentially Deposited Copper Atoms. *J. Electroanal. Chem.* 1995, *384* (1–2), 171–177.

(9)   Wu, S.; Shi, Z.; Lipkowski, J.; Hitchcock, A. P.; Tyliszczak, T. Early Stages of Copper Electrocrystallization: Electrochemical and in Situ x-Ray Absorption Fine Structure Studies of Coadsorption of Copper and Chloride at the Au(111) Electrode Surface. *J. Phys. Chem. B* 1997, *101* (49), 10310–10322.

(10)   Herrero, E.; Buller, L. J.; Abruña, H. D. Underpotential Deposition at Single Crystal Surfaces of Au, Pt, Ag and Other Materials. *Chem. Rev.* 2001, *101* (7), 1897–1930.

(11)   Magnussen, O. M. Atomic Structure of Ordered Copper Adlayers on Single-Crystalline Gold Electrodes. *J. Vac. Sci. Technol. B Microelectron. Nanom. Struct.* 1991, *9* (2), 969.

(12)   Kolb, D. M. Reconstruction Phenomena at Metal-Electrolyte Interfaces. *Prog. Surf. Sci.* 1996, *51* (2), 109–173.

(13)   Walsh, F. C.; Low, C. T. J. A Review of Developments in the Electrodeposition of Tin. *Surf. Coatings Technol.* 2016, *288*, 79–94.

(14)   Sekar, R.; Eagammai, C.; Jayakrishnan, S. Effect of Additives on Electrodeposition of Tin and Its Structural and Corrosion Behaviour. *J. Appl. Electrochem.* 2010, *40* (1), 49–57.

(15)   Nakamura, Y.; Kaneko, N.; Nezu, H. Surface Morphology and Crystal Orientation of Electrodeposited Tin from Acid Stannous Sulfate Solutions Containing Various Additives. *J. Appl. Electrochem.* 1994, *24* (6), 569–574.

Chapter 3. The effect of naphthalene-based additives on tin electrodeposition on a gold electrode

_____

16)   Kaneko, N.; Shinohara, N.; Nezu, H. Effects of Aromatic Carbonyl Compounds on the Surface Morphology and Crystal Orientation of Electrodeposited Tin from Acid Stannous Sulfate Solutions. *Electrochim. Acta* 1992, *37* (13), 2403–2409.

(17)   Martyak, N. M.; Seefeldt, R. Additive-Effects during Plating in Acid Tin Methanesulfonate Electrolytes. *Electrochim. Acta* 2004, *49* (25), 4303–4311.

(18)   Barry, F. J.; Cunnane, V. J. Synergistic Effects of Organic Additives on the Discharge, Nucleation and Growth Mechanisms of Tin at Polycrystalline Copper Electrodes. *J. Electroanal. Chem.* 2002, *537* (1–2), 151–163.

(19)   Van Velzen, C.J; Sluyters-Rehbach, M; Sluysters, J. H. The Electrochemical Reduction of Sn (II) at the Dropping Mercury Electrode from Aqueous 1 M Sulfuric Acid and from 0.3 M Phenolsulfonic Acid and Its Inhibition by ENSA -6. *Electrochim. Acta* 1987, *32* (5), 815–821.

(20)   Lee, J.-Y.; Kim, J.-W.; Chang, B.-Y.; Tae Kim, H.; Park, S.-M. Effects of Ethoxylated α-Naphtholsulfonic Acid on Tin Electroplating at Iron Electrodes. *J. Electrochem. Soc.* 2004, *151* (5), C333.

(21)   Stuart Tobias, R. Studies of the Hydrolysis of Metal Ions: The Hydrolysis of the Tin (II) Ion, Sn(II). *Acta Chem. Scand.* 1958, *12*, 198–223.

(22)   Pettine, M.; Millero, F. J.; Macchi, G. Hydrolysis of Tin(II) in Aqueous Solutions. *Anal. Chem.* 1981, *53* (7), 1039–1043.

(23)   Cigala, R. M.; Crea, F.; De Stefano, C.; Lando, G.; Milea, D.; Sammartano, S. The Inorganic Speciation of Tin(II) in Aqueous Solution. *Geochim. Cosmochim. Acta* 2012, *87*, 1–20.

(24)   Lothenbach, B.; Ochs, M.; Wanner, H.; Yui, M. Thermodynamic Data for the Speciation and Solubility of Pd, Pb, Sn, Sb, Nb and Bi in Aqueous Solution. *Japan Nucl. Cycle Dev. Inst.* 2004, 1–356.

(25)   Trasatti, S.; Petrii, O. A. Real Surface Area Measurements. *J. Electroanal. Chem* 1992, *327* (1–2), 353–376.

(26)   Kresse, G.; Furthmüller, J. Efficient Iterative Schemes for Ab Initio Total-Energy Calculations Using a Plane-Wave Basis Set. *Phys. Rev. B* 1996, *54* (16), 11169–11186.

(27)   Kresse, G.; Furthmüller, J. Efficiency of Ab-Initio Total Energy Calculations for Metals and Semiconductors Using a Plane-Wave Basis Set. *Comput. Mater. Sci.* 1996.

(28)   Kresse, G.; Hafner, J. Ab Initio Molecular Dynamics for Liquid Metals. *Phys. Rev. B* 1993, *47* (1), 558–561.

(29)   Blöchl, P. E. Projector Augmented-Wave Method. *Phys. Rev. B* 1994, *50* (24), 17953–17979.

(30)   Kresse, G.; Joubert, D. From Ultrasoft Pseudopotentials to the Projector Augmented-Wave Method. *Phys. Rev. B* 1999, *59* (3), 1758–1775.

(31)   Perdew, J. P.; Burke, K.; Ernzerhof, M. Generalized Gradient Approximation Made Simple. *Phys. Rev. Lett.* 1996, *77* (18), 3865–3868.

(32)   Perdew, J. P.; Burke, K.; Ernzerhof, M. Perdew, Burke, and Ernzerhof Reply: *Phys. Rev. Lett.* 1998, *80* (4), 891.

(33)   Wyckoff, R. W. G. *Crystal Structures*, Vol. 1.; Interscience, Ed.; Wiley: New York, 1963.

(34)   Tran, R.; Xu, Z.; Radhakrishnan, B.; Winston, D.; Sun, W.; Persson, K. A.; Ong, S. P. Surface Energies of Elemental Crystals. *Sci. Data* 2016, *3* (1), 160080.

(35)   Grimme, S.; Antony, J.; Ehrlich, S.; Krieg, H. A Consistent and Accurate Ab Initio Parametrization of Density Functional Dispersion Correction (DFT-D) for the 94 Elements H-Pu. *J. Chem. Phys.* 2010, *132* (15), 154104.

(36)   Grimme, S.; Ehrlich, S.; Goerigk, L. Effect of the Damping Function in Dispersion Corrected Density Functional Theory. *J. Comput. Chem.* 2011, *32* (7), 1456–1465.

(37)   Wan, L.-J.; Itaya, K. In Situ Scanning Tunneling Microscopy of Benzene, Naphthalene, and Anthracene Adsorbed on Cu(111) in Solution. *Langmuir* 1997, *13* (26), 7173–7179.

(38)   Jarząbek, G.; Borkowska, Z. Adsorption of Dimethylsulfoxide on the Polycrystalline Gold Electrode from Aqueous Solutions. *J. Electroanal. Chem.* 1988, *248* (2), 399–410.

(39)   Retter, U.; Lohse, H. On the Temperature Dependence of the Two-Dimensional Condensation of Adenosine at the Mercury/Electrolyte Interface. *J. Electroanal. Chem. Interfacial Electrochem.* 1982, *134* (2), 243–250.

(40)   Pham, M. C.; Moslih, J.; Barbero, C.; Haas, O. Influence of the Cation Size on the Charge Compensation Process in Poly(1-Naphthol) Coated Electrodes. Multiple Internal Reflection FTIR Spectroscopy (MIRFTIRS) and Probe Beam Deflection (PBD) Study. *J. Electroanal. Chem.* 1991, *316* (1–2), 143–154.

(41)   Laser, D. Ariel, M. Electro-Optical Study of the Oxidative Adsorption of 1-Naphthol on Platinum and Gold Film Electrodes. *Electroanal. Chem. interfacial Electrochem.* 1972, *35*, 405–414.

(42)   Kirk, M. G. D. W. The Electrochemical Oxidation of Aqueous Phenol at a Glassy Carbon Electrode. *Can. J. Chem. Eng.* 1990, *68* (1981), 997–1003.

(43)   Panizza, M.; Cerisola, G. Influence of Anode Material on the Electrochemical Oxidation of 2-Naphthol: Part 1. Cyclic Voltammetry and Potential Step Experiments. *Electrochim. Acta* 2003, *48* (23), 3491–3497.

(44)   Kleinert, M. Cuesta, A. Kibler, L. A. Kolb, D. M. In Situ Observation of an Ordered Sulfate Adlayer on Au (100) Electrodes. *Surf. Sci.* 1999, *430* (1), 521–526.

(45)   Busy, C. C. Creighton, J. A. Efficient Gold and Silver Electrodes for Surface Enhanced Raman Spectral Studies of Electrochemical Systems: The Behaviour of Pridine and Naphthalene Adsorbed on Roughened Gold Electrodes. *J. Electroanal. Chem* 1982, *140*, 379–390.

(46)   Dahms, H. Green, M. The Adsorption of Aromatic Hydrocarbons at the Gold Electrolyte Interface. *J. Electrochem. Soc.* 1963, *110* (10), 1075–1080.

(47)   Wan, L. Itaya, K. In Situ Scanning Tunneling Microscopy of Benzene, Naphthalene, and Anthracene Adsorbed on Cu(111) in Solution. *Langmuir* 1997, *13* (26), 7173–7179.

(48)   Daimay Lin-Vien, Norman B. Colthup, William G. Fateley, J. G. G. *The Handbook of Infrared and Raman Characteristic Frequencies of Organic*; 191AD.

(49)   Larkin, P. IR and Raman Spectra-Structure Correlations. *Infrared Raman Spectrosc.* 2011, 73–115.

(50)   Sebastian, S.; Sylvestre, S.; Sundaraganesan, N.; Amalanathan, M.; Ayyapan, S.; Oudayakumar, K.; Karthikeyan, B. Vibrational Spectra, Molecular Structure, Natural Bond Orbital, First Order Hyperpolarizability, TD-DFT and Thermodynamic Analysis of 4-Amino-3-Hydroxy-1- aphthalenesulfonic Acid by DFT Approach. *Spectrochim. Acta - Part A Mol. Biomol. Spectrosc.* 2013, *107*, 167–178.

Chapter 3. The effect of naphthalene-based additives on tin electrodeposition on a gold electrode

_____

(51)   Sellers, H.; Pulay, P.; Boggs, J. E. Theoretical Prediction of Vibrational Spectra. 2. Force Field, Spectroscopically Refined Geometry, and Reassignment of the Vibrational Spectrum of Naphthalene1. *J. Am. Chem. Soc.* 1985, *107* (23), 6487–6494.

(52)   Nogueira, H. I. S.; Quintal, S. M. O. Surface-Enhanced Raman Scattering (SERS) Studies on 1,1'-Bi-2-Naphthol. *Spectrochim. Acta - Part A Mol. Biomol. Spectrosc.* 2000, *56* (5), 959–964.

(53)   Ataka, K.; Osawa, M. In Situ Infrared Study of Water–sulfate Coadsorption on Gold(111) in Sulfuric Acid Solutions. *Langmuir* 1998, *14* (4), 951–959.

(54)   Petersson, I.; Ahlberg, E. Kinetics of the Electrodeposition of Pb-Sn Alloys: Part II. At Polycrystalline Gold Electrodes. *J. Electroanal. Chem.* 2000, *485*, 178–187.

(55)   Aranzales, D.; Wijenberg, J. H. O. J.; Koper, M. T. M. Voltammetric Study of Tin Electrodeposition on Polycrystalline Gold from Sulfuric and Methanesulfonic Acid. *J. Electrochem. Soc.* 2019, *166* (8), D283–D289.

(56)   Mao, B. W.; Tang, J.; Randler, R. Clustering and Anisotropy in Monolayer Formation under Potential Control: Sn on Au(111). *Langmuir* 2002, *18* (14), 5329–5332.

(57)   Gotthard, H.; Trivich, D. Studien Zur Elektrolytischen Reduktion von Natrium-Allylsulfonat an Nickelkathoden. *Electrochim. Acta* 1962, *7* (3), 369–383.

(58)   Kendrick, R. J. The Effects of Some Aromatic Sulfonic Acids on the Stress, Structure, and Composition of Electrodeposited Nickel. *Trans. IMF* 1963, *40* (1), 19–27.

(59)   Brook, P. A.; Crossley, J. A. The Reduction of Some Naphthalene Derivatives during the Electro-Deposition of Nickel. *Electrochim. Acta* 1966, *11* (9), 1189–1196.

(60)   Yan, J. W.; Tang, J.; Yang, Y. Y.; Wu, J. M.; Xie, Z. X.; Sun, S. G.; Mao, B. W. In Situ STM Studies on Underpotential Deposition of Sn on Au(100). *Surf. Interface Anal.* 2001, *32* (1), 49–52.

The effect of naphthalene-based additives on the kinetics of tin electrodeposition on a boron doped diamond electrode

Chapter 4. The effect of naphthalene-based additives on the kinetics of tin electrodeposition on a boron doped diamond electrode

_____
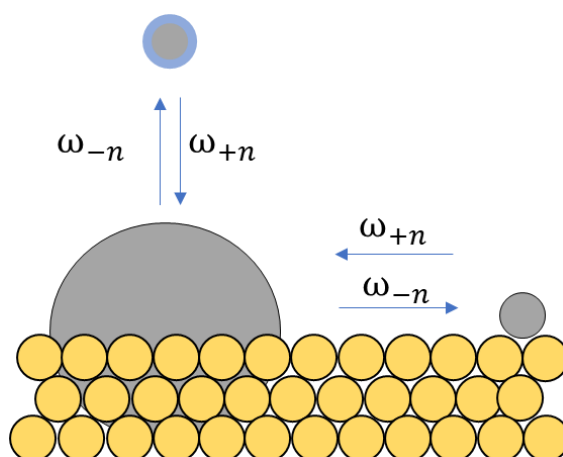
Abstract

The effect of naphthalene-based additives: naphthalene (NPT), naphthalenesulfonate (NPTS) and hydroxynaphthalenesulfonate (HNPTS) on the kinetics of tin electrodeposition on a boron doped diamond (BDD) electrode has been studied by means of chronoamperometry and scanning electron microscopy (SEM). Potentiostatic current transients in the absence and the presence of naphthalene-based additives are analyzed by using the Scharifker-Hills model. A strong decrease of the kinetics of tin nucleation on BDD was observed in the presence of naphthalene-based additives, NPT showing the smallest effect and HNPTS showing the largest effect. From the long-term Cottrell behavior of the transients, similar values of tin (II) diffusion coefficients were obtained for all additives, suggesting that there is no complexation of Sn (II) by the additives and that the charge-transfer kinetics itself is not influenced by the presence of the additives. In the absence of additives, tin deposition on BDD displays a progressive nucleation and growth mechanism at less negative potential, switching to instantaneous nucleation and growth at more negative potential. In the presence of NPTS and HNPTS, progressive nucleation and growth transients are observed. The growth mode results are confirmed by the tin features observed in the scanning electron micrographs. In conclusion, NPT, NPTS and HNPTS mainly decrease the rate of the nucleation of tin deposition. In comparison, ethoxylated α-napthalenesulfonic acid (ENSA, a commonly used additive in the tin plating industry) inhibits tin deposition process on BDD even more strongly. These observations show a striking similarity to our previous study of tin deposition on gold electrodes.

4.1 Introduction

Tin electrodeposition is a low-cost and versatile process, widely used in corrosion protection and in the packaging industry. During the last years, new applications for tin plating in electronics and manufacturing have been developed[1] and since then, new challenges in the micro- and nanotechnology of the process have emerged. The production of high-quality tin coatings requires the addition of organic compounds in the electroplating baths, in order to obtain the desired chemical and physical properties of the metal deposits. Determining the role of these additives allows the optimization and enhancement of the tin deposition, and the extension of its applications.

Earlier studies of tin electrodeposition[2–4] have mainly focused on the use of metal[3,4] and glassy carbon substrates[5]. Following our previous work on tin electrodeposition on a gold substrate[6], we study here the effect of naphthalene-based derivatives, naphthalene (NPT), naphthalenesulfonate (NPTS) and hydroxynaphthalenesulfonate (HNPTS), on the kinetics of the nucleation and growth of tin electrodeposition on a boron doped diamond surface (BDD). This substrate has been considered as highly suitable to study metal deposition [7], [8], [9], [10] due to its high stability, reproducibility, and flat surface with height variation of ~5 nm over 5x5 μm areas. The relatively low defect density is expected to lead to a low nucleation rate. This facilitates nucleation and growth measurements by electrochemical transient experiments and in-situ microscopic techniques[7] .

4.2 Experimental details

Before each measurement all glassware was stored overnight in a solution of 1g L^{-1} KMnO$_4$ in 0.5 M H$_2$SO$_4$. Before use, it was rinsed with water and 30% hydrogen peroxide solution in order to remove permanganate anions and trace impurities. Glassware was boiled in water five times before starting the experiments. The water used to clean glassware and to prepare solutions was demineralized and ultra-filtrated by a Millipore MilliQ system (18.2 MΩ cm). A gold wire was chosen as a counter electrode and a reversible hydrogen electrode (RHE) was used as a reference, but all the potentials are referred to the normal hydrogen electrode (NHE).

Chronoamperometric experiments were performed using a potentiostat VSP-300 (Bio-logic). The electrode potential was corrected for Ohmic drop during the measurements, by using 85% of the Ohmic resistance measured by electrochemical impedance spectroscopy.

Chapter 4. The effect of naphthalene-based additives on the kinetics of tin electrodeposition on a boron doped diamond electrode

_____

The working electrode was a boron doped diamond disk (BDD) (1 cm diameter, 1 mm thick). It was prepared before each experiment by mechanical and electrochemical methods. Firstly, it was polished during 5 minutes with diamond powder (0.05 μm particle size), and subsequently it was transferred to an ultrasound bath, and treated during 10 min in acetone and another 10 min in water. After mechanical polishing, the BDD electrode was electropolished by cycling 10 times between -0.74 to 1.56 V vs. NHE in 0.1 M H_2SO_4 solution at 50 mV s^{-1}. A cyclic voltammogram of the BDD surface was recorded in 0.1 M H_2SO_4 solution at potentials between -0.74 to 1.56 V at 50 mV s^{-1} before starting the measurements in order to check the cleanliness of the electrode surface.

The morphology of tin deposit was observed ex situ by scanning electron microscopy SEM. Micrographs were taken using the model JEOL 820 SEM at 2 - 10 kV. Low voltages were chosen due to the semiconductor nature of BDD electrode.

All solutions were prepared from chemicals with the highest purity commercially available: H_2SO_4 (96% ultrapure, Merck), $SnSO_4$ (≥ 95%, Sigma Aldrich), naphthalene (≥ 99%, Sigma Aldrich), 2-napthalenesulfonic acid sodium salt (99.6%, Sigma Aldrich), sodium thiosulfate (≥ 99.99%, Sigma Aldrich), 4-hydroxy-1-naphthalenesulfonic acid sodium salt (≥ 95 %, Santa Cruz Biotechnology) and ethoxylated α-napthalenesulfonic acid (73.6%, Pulcra chemicals). In the case of ENSA the main impurities are sulfuric acid with 8.7 %, and water with 2.4 %, other impurities were not provided by the supplier.

4.3 Results and discussion

4.3.1 Chronoamperometric transients

Figure 1 shows the cyclic voltammogram for tin electrodeposition and electro-dissolution on a BDD electrode (under static conditions, i.e., no rotation). The voltammogram exhibits a broad cathodic wave with a peak at -0.266 V, and a sharp anodic peak at -0.156 V, characteristic of Sn (II) reduction and Sn (0) oxidation, respectively. The cyclic voltammogram was used as a reference to choose the potential region to record the current transients, as indicated by the red lines, from -0.220 to -0.460 V.

Figure 2 presents the recorded current transients for tin electrodeposition without additives; transients show rising currents related with the nucleation and growth processes, followed by a current decay caused by the overlap of the growing nuclei and at longer times by mass transport limitations. The recorded current transients exhibit shorter peak times and higher current maxima with increasingly negative potential[7]. This behavior is usual for nucleation and growth processes, provided the substrate is not being strongly modified over the range of applied potentials[11].
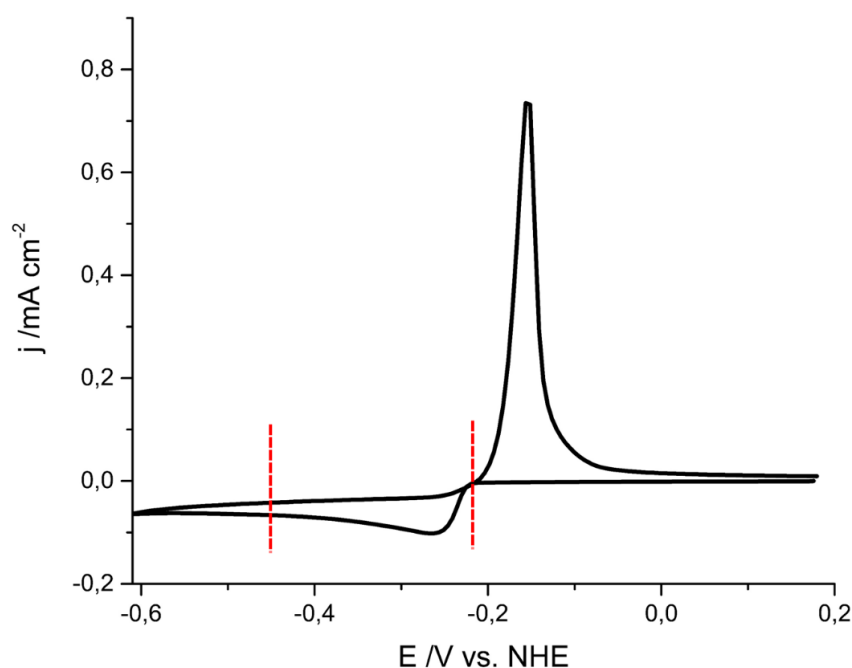
_____

Figure 1. Cyclic voltammogram of tin electrodeposition on a boron doped diamond surface in 0.1 M H_2SO_4 and 0.5 mM $SnSO_4$. CV recorded between -0.61 to 0.19 V at 30 mV s^{-1}. Red-dashed lines indicate the potential region used for measuring the current transients
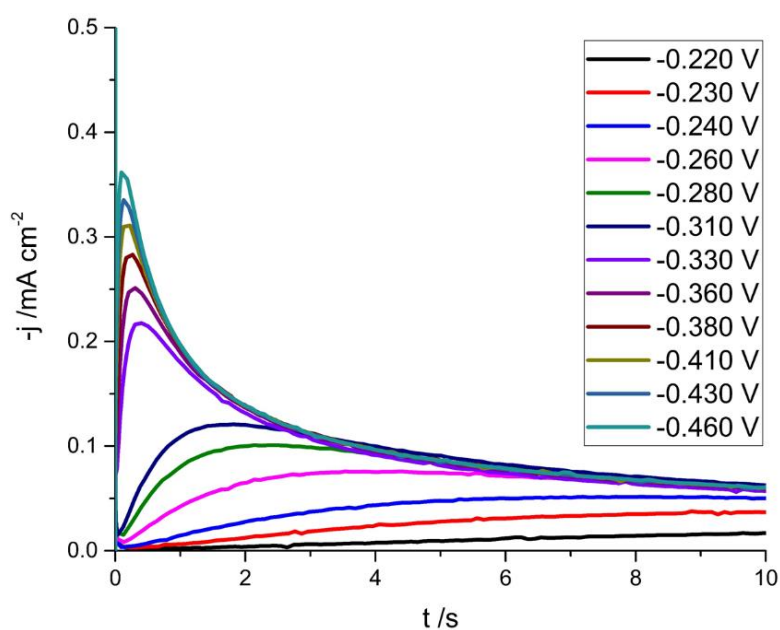

Figure 2. Current transients of tin electrodeposition on a boron doped diamond surface in 0.1 M H_2SO_4 and 0.5 mM $SnSO_4$. Transients were recorded between -0.220 to -0.460 V. For each transient, the respective potential was applied during 1 min, and it was followed by applying 0.14 V during 3 minutes to dissolve the deposit. Dissolution of the tin deposit was carried out before applying each respective potential.

Chapter 4. The effect of naphthalene-based additives on the kinetics of tin electrodeposition on a boron doped diamond electrode

_____

The current transients are analyzed by comparison to the well-established Scharifker-Hills (SH) model[12]. The SH model considers nuclei of hemispherical shape, whose growth is controlled by three-dimensional diffusion. Two limiting cases of nucleation and growth are described by the model: instantaneous and progressive.

The nucleation rate is described by:

$$N(t) = N_o(1 - e^{-At}) \quad (1)$$

where N is the number of nuclei, N_0 the number of nucleation sites, and A the nucleation rate constant. For instantaneous nucleation, all nuclei are formed at once when applying the step potential, so that $At \gg 1$ and therefore $N(t) = N_o$. The current–time transient for instantaneous nucleation and growth is given by:

$$j(t) = \frac{zFD^{1/2}c}{\pi^{1/2}t^{1/2}}[1 - \exp(-N_o\pi\kappa Dt)] \quad (2)$$

where $\kappa = (8\pi cM/\rho)^{1/2}$, with c the concentration (of Sn^{2+}), M the molar mass, and ρ the molar density.

For progressive nucleation and growth, nuclei are gradually formed after applying the step potential, so that $At \ll 1$ and therefore $N(t) = AN_ot$. The current-time transient for progressive nucleation and growth is given by:

$$j(t) = \frac{zFD^{1/2}c}{\pi^{1/2}t^{1/2}}\left[1 - \exp\left(-\frac{2}{3}AN_o\pi\kappa Dt^2\right)\right] \quad (3)$$

By plotting current transients in normalized coordinates, $(\frac{j}{j_{max}})^2$ vs $\frac{t}{t_{max}}$, we avoid the use of the system-specific parameters (c, M, ρ, AN_0, N_0) in comparing the experimental transients with the two limiting cases[13]. The associated expressions for instantaneous and progressive nucleation are described by equations (4) and (5)[13, 14] respectively:

$$\frac{j^2}{j^2_{max}} = 1.9542 \left(\frac{t}{t_{max}}\right)^{-1}\left[1 - \exp\left(-1.2564\frac{t}{t_{max}}\right)\right]^2 \quad (4)$$

with $j_{max} = 0.6382zFDc(kN)^{1/2}$ and $t_{max} = 1.2564/N\pi kD$ for instantaneous nucleation

$$\frac{j^2}{j^2_{max}} = 1.2254 \left(\frac{t}{t_{max}}\right)^{-1}\left[1 - \exp\left(-2.3367\frac{t^2}{t^2_{max}}\right)\right]^2 \quad (5)$$

with $j_{max} = 0.4959zFD^{3/4}c(kaN_0)^{1/4}$ and $t_{max} = (3.505/aN_0\pi kD)^{1/2}$ for progressive nucleation.
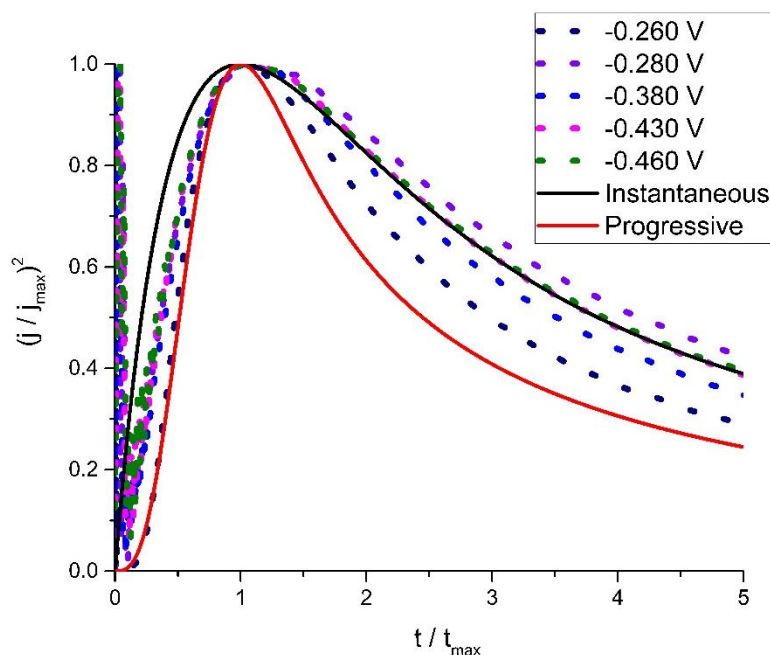
Figure 3. Normalized current transients calculated with SH model for the limiting cases (solid lines) compared with the normalized experimental transients (dotted lines). Experimental transients were recorded in 0.1 M H_2SO_4 and 0.5 mM $SnSO_4$.

Figure 3 shows the comparison of normalized current transients for tin deposition on boron doped diamond from low to high overpotentials compared to the instantaneous and progressive nucleation limiting cases. For a potential of -0.260 V, it is seen that at short times the experimental transient curve satisfactorily overlaps with the progressive nucleation mechanism. However, at longer times the experimental curve deviates from the progressive nucleation mechanism. Furthermore, at higher overpotentials and shorter times, the experimental current transients do not satisfactorily fit with neither the progressive nor the instantaneous nucleation mechanisms. But at longer times, the experimental curves fit better with the instantaneous mechanism. Figure 3 also shows the transition from progressive to instantaneous nucleation with increasingly negative potential. This behavior is also indicative that the electrode surface (and the number of nucleation sites) is not changing considerably with potential. In order to confirm the transition from progressive to instantaneous nucleation when increasing the negative potential, the first and second derivatives of the current transients at less and more negative potentials were calculated. For a progressive nucleation and growth mechanism, one expects a positive second derivative at short times, whereas for instantaneous nucleation, the second derivative should be negative at short times. Figure 4 shows the second derivative (blue dotted line) for the onset of the transient (short times) for various potentials, showing that the transition to instantaneous nucleation and growth happens at a potential of ca. -0.33 V. Figures 4c and 4d exhibit high noise level at short times (i.e. < 0.2 s) as a consequence of the charge-discharge double layer process. The noise level also increases during the derivation process.
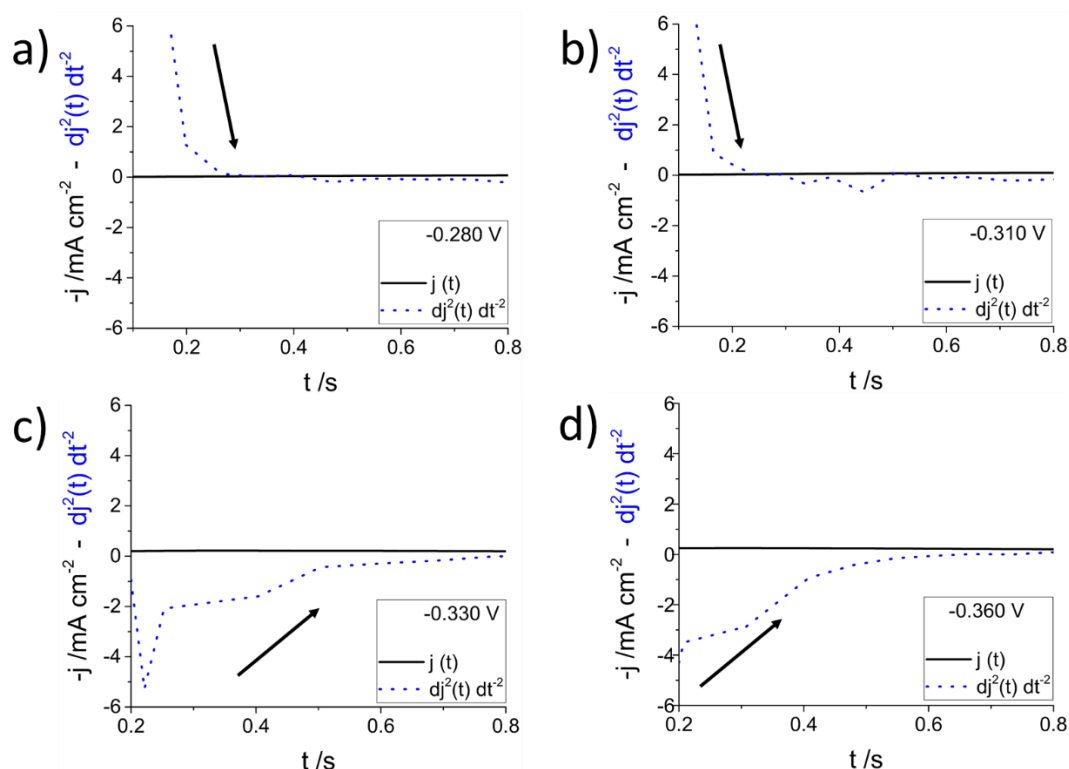
67

Chapter 4. The effect of naphthalene-based additives on the kinetics of tin electrodeposition on a boron doped diamond electrode

_____

Figure 4. Current transient j(t) and second derivative $\frac{d^2 j(t)}{dt^2}$ for current transients recorded in 0.1 M H$_2$SO$_4$ and 0.5 mM SnSO$_4$ at (a) -0.280 V (b) -0.310 V (c) -0.330 V and (d) -0.360 V

Although the SH model equations do not perfectly fit the recorded current transients, a reasonable fitting is reached at high overpotentials and long times. The recorded transients were fitted by hand to the expressions for instantaneous and progressive nucleation and growth, equations 2 and 3, respectively. Current transients recorded at potentials > -0.3 V were fitted to the progressive nucleation, and at potentials < -0.3 V to the instantaneous. No attempt was made to perform a least-squares fit because the fit is never perfect, as can be seen from Figure 3. Instead, the steady state nucleation rate[15] (AN_0) and the number density of nuclei (N_0) were estimated from the corresponding expressions of t_{max}, see equations 4 and 5 .

Figure 5 presents the SH model curves for progressive nucleation and growth fitted to the measured current transients. At -0.230 V (low negative potential) and short times the theoretically predicted curve adequately fits the recorded transient, but at longer times the overlap is less good. Furthermore, with increasing the negative potentials, it is seen that the theoretically predicted transients adjust better to the experimental transients, from -0.360 V to higher overpotentials, curves tend to merge at higher times (i.e., >1s)
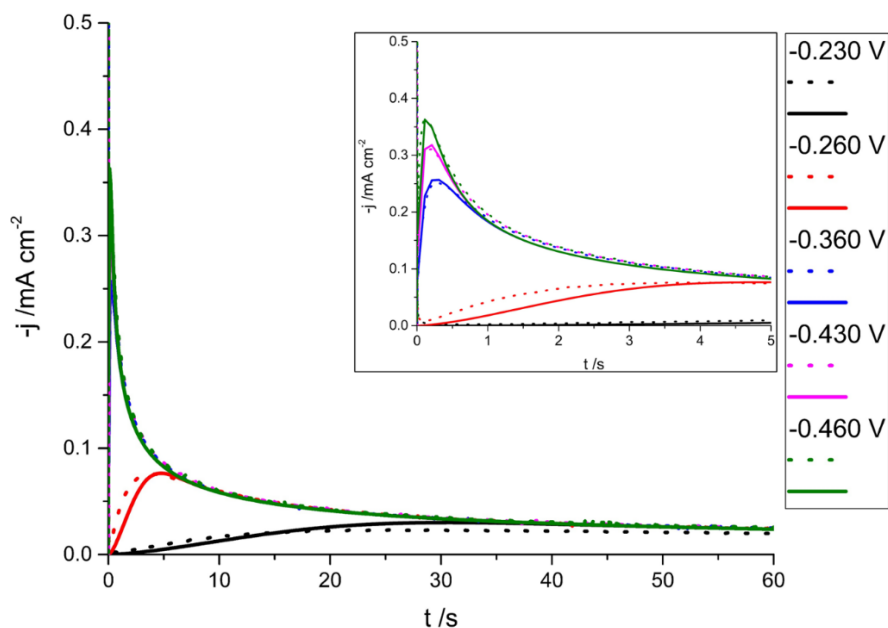
_____

Figure 5. SH expression for progressive nucleation and growth (solid lines) fitted to recorded current transients (dotted lines) for tin electrodeposition on a boron doped diamond surface in 0.1 M H_2SO_4 and 0.5 mM $SnSO_4$. Given that there is never a very good excellent fit (Fig.3), these fits were performed "by hand", transients recorded at E > -0.3 V were fitted to progressive and at E < -0.3 V to instantaneous nucleation mode. The parameters N_0 and AN_0 shown in Figure 6 were, however, not obtained from the fit, but from the corresponding expressions for t_{max} (see main text).
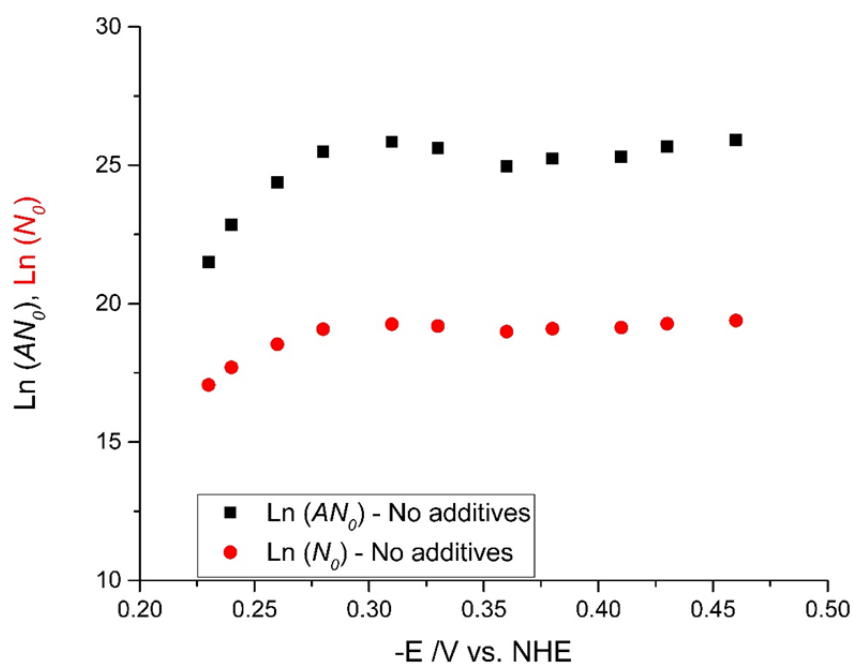

Figure 6. Logarithm of steady state nucleation rate (AN_0) versus applied potential and the Logarithm of number density of nuclei (N_0) versus applied potential of tin electrodeposition on a boron doped diamond surface in 0.1 M H_2SO_4 and 0.5 mM $SnSO_4$

Chapter 4. The effect of naphthalene-based additives on the kinetics of tin electrodeposition on a boron doped diamond electrode

_____

Figure 6 shows the logarithm of the steady state nucleation rate (AN_0) and number density of nuclei (N_0) plotted versus the applied potential. The parameters AN_0 and N_0 were obtained from the corresponding expressions for t_{max} (see equations 4 and 5). It is observed that both AN_0 and N_0 exhibit an approximately linear increase at potentials below -0.28 V, and remain essentially constant at potentials more negative than -0.30 V. This transition potential corresponds reasonably well to the transition from progressive to instantaneous nucleation evaluated in Figure 4c. Therefore, we consider the AN_0 data more meaningful for potentials > -0.3 V and the N_0 data for potentials < -0.3 V. The atomistic theory of nucleation predicts a linear dependence of the logarithm of the steady state nucleation rate (AN_0) on the overpotential at high supersaturation[16]. Figure 6 indeed exhibits a linear dependence of the steady state nucleation rate on the applied potential in the window where the AN_0 data are meaningful. The data for E < -0.3 V, where the data for N_0 is more meaningful, show that N_0 is essentially constant over a wide potential window.

An alternative way to determine these parameters is to fit the initial part of the transient to a general nucleation equation. Sluyters-Rehbach et al.[17] described a general equation of nucleation and diffusion-controlled hemispherical growth, and employed a graphical analysis of the current transients: ($j^{2/3}$ vs t) and (j^2 vs t) to check the consistency between the model and the experimental transients and also to determine whether one of the two nucleation limiting cases, vis. instantaneous or progressive, predominates. This offers a more accurate way of determining parameters such as A and N_0. However, given the high double-layer current at short times, the values of the parameters A and N_0 were difficult to extract, and since we were primarily interested in the qualitative behavior of A and N_0, deriving them from t_{max} served our purposes well.

4.3.2 Effect of naphthalene-based additives on kinetics of tin electrodeposition on BDD

In order to study the effect of naphthalene-based additives on the kinetics of tin electrodeposition on a boron doped diamond electrode, current transients of tin electrodeposition were recorded in the presence of three different additives: NPT, NPTS and HNPTS. Figure 7a, 7b and 7c show current transients recorded at highly negative potential (-0.460 V) in the presence of different concentrations of NPT, NPTS and HNPTS, respectively, and Figure 7d shows the comparison of the different naphthalene-based additives.

Figure 7a shows transients in the absence and presence of NPT at different concentrations. Transients exhibit an increase of t_{max} and decrease of i_{max}, ascribed to a decrease in the nucleation rate of tin deposition on BDD. The transients do not show a remarkable dependence on the NPT concentration which we attribute to the low solubility of NPT molecules in the aqueous electrolyte, leading to the same bulk concentration and thereby limiting the amount of NPT available that can be adsorbed on BDD surface. Furthermore,

current transients in the absence and in the presence of different NPT concentrations overlap after about 1.5 seconds.
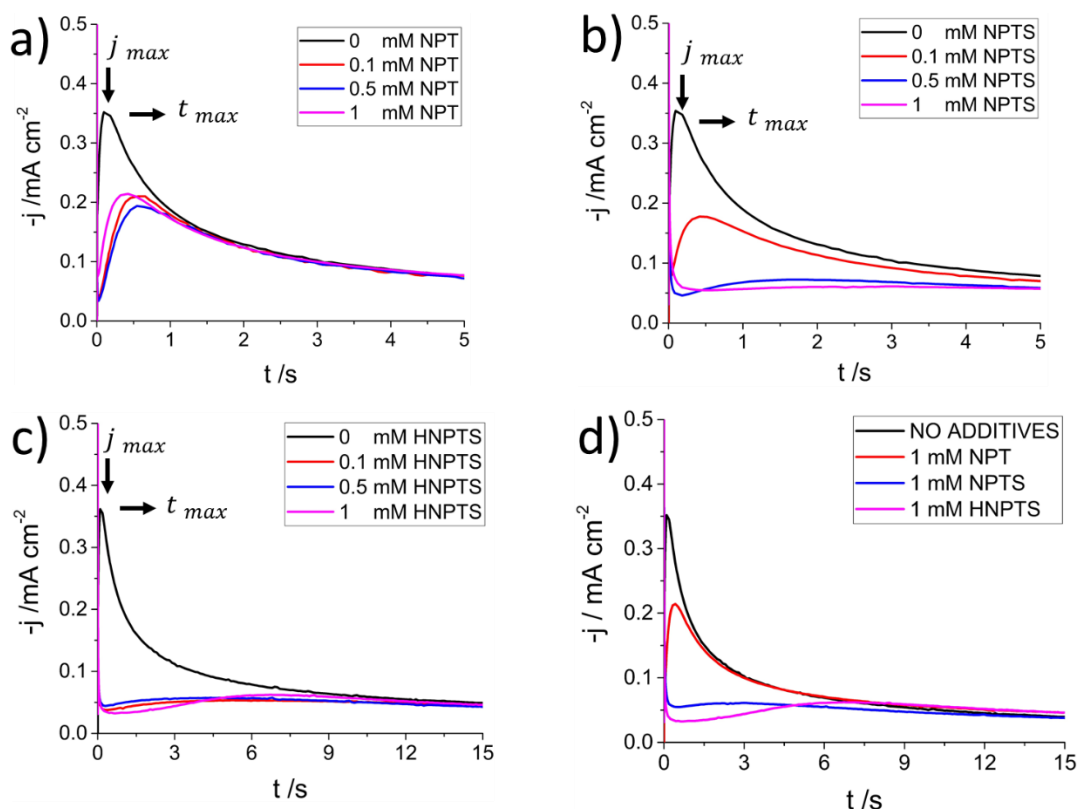

Figure 7. Current transients recorded at highly negative potential (-0.460 V) of tin electrodeposition on a boron doped diamond surface in 0.1 M H₂SO₄, 0.5 mM SnSO₄ and different naphthalene-based concentrations: (a) NPT, (b) NPTS and (c) HNPTS (d) Comparison of transients in the absence and presence of 1 mM naphthalene-based additives

Figure 7b shows transients in the absence and presence of NPTS. Parameters t_{max} and i_{max} increase and decrease, respectively, with increasing NPTS concentration. This change is also ascribed to a decrease in the nucleation kinetics of tin deposition. The transient in the presence of 1 mM of NPTS looks almost flat in comparison to the other transients. Figure 7c presents the transients in the absence and presence of HNPTS; transients exhibit a much stronger decrease in i_{max} and increase in t_{max} compared to the transients in the presence of NPT and NPTS. Additionally, Fig. 7d compares the different additives in a single figure, clearly illustrating the evolution of the transient as a function of the additive.

For long deposition times, the SH model assumes the growth of the deposit to be completely diffusion limited. Therefore, tin (II) diffusion coefficients ($D_{Sn^{2+}}$) can be calculated in the presence of different concentrations of naphthalene-based additives by fitting the transient to the Cottrell equation. The results are summarized in Table C1 in the Appendix C.

Chapter 4. The effect of naphthalene-based additives on the kinetics of tin electrodeposition on a boron doped diamond electrode

_____

The equation was applied for the transients at -0.460 V, and at times longer than 15 s to avoid contributions from nucleation kinetics. A plot of j vs. $t^{-1/2}$ yields a straight line in all cases. The calculated value of tin (II) diffusion coefficient ($D_{Sn^{2+}}$) in the absence of naphthalene-based additives is 7.7 ± 0.2 X 10^{-6} cm^2 s^{-1}, which is in accordance with previously determined values[3][1], and the values in the presence of 1mM of NPT, NPTS and HNPTS are 6.8 X 10^{-6}, 7.0 X 10^{-6} and 7.3 X 10^{-6} cm^2 s^{-1} respectively, all in reasonable agreement. In the presence of different concentrations of HNPTS, the calculated tin (II) diffusion coefficient ($D_{Sn^{2+}}$) also does not change considerably. Furthermore, when tin (II) diffusion coefficients ($D_{Sn^{2+}}$) are calculated from transients obtained at less negative potentials in the presence of the naphthalene-based additives, no significant differences were observed, see Table C2. These results suggest that naphthalene-based additives do not affect the diffusion coefficient nor the kinetics of tin deposition on BDD electrode; they only affect the nucleation rate.
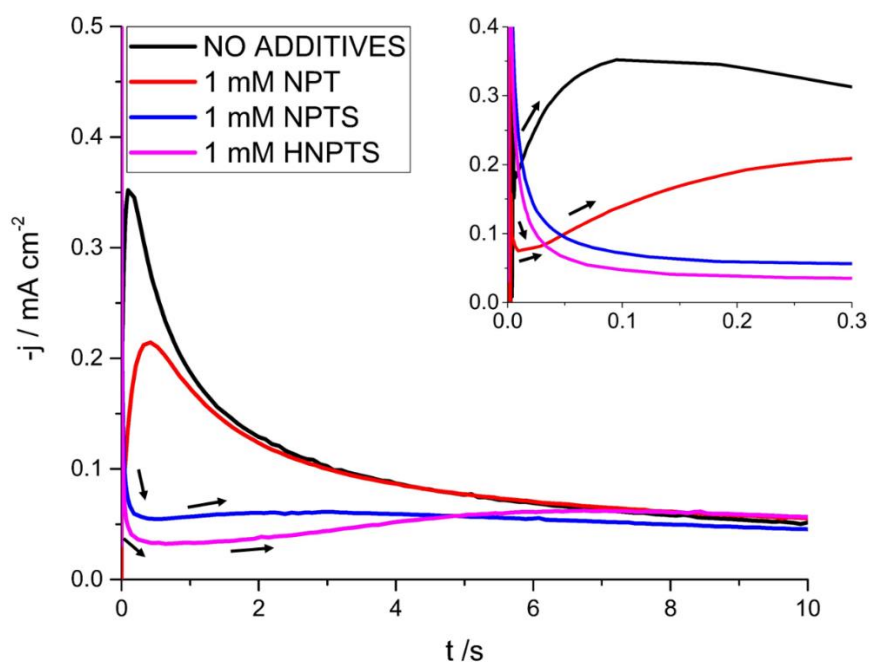

Figure 8. Onset of the current transients recorded in 0.1 M H₂SO₄, 0.5 mM SnSO₄ at high negative potentials E=-0.460 V, in the absence and presence of 1 mM of NPT, NPTS, and HNPTS at -0.460 V.

Figure 8 shows the onset of the current transients recorded in the absence and presence of naphthalene-based additives. The onset of the current transients in the presence of NPTS and HNPTS clearly show the progressive nucleation behavior, where current gradually increases when new nuclei originate. The black arrows indicate the increasing growth of the current typical for progressive nucleation. On the other hand, the onset of the transient in the presence of NPT (Inset of Fig. 8) is more characteristic of instantaneous nucleation. See analysis of the second derivative for NPT, NPTS and HNPTS in the Figure S1.
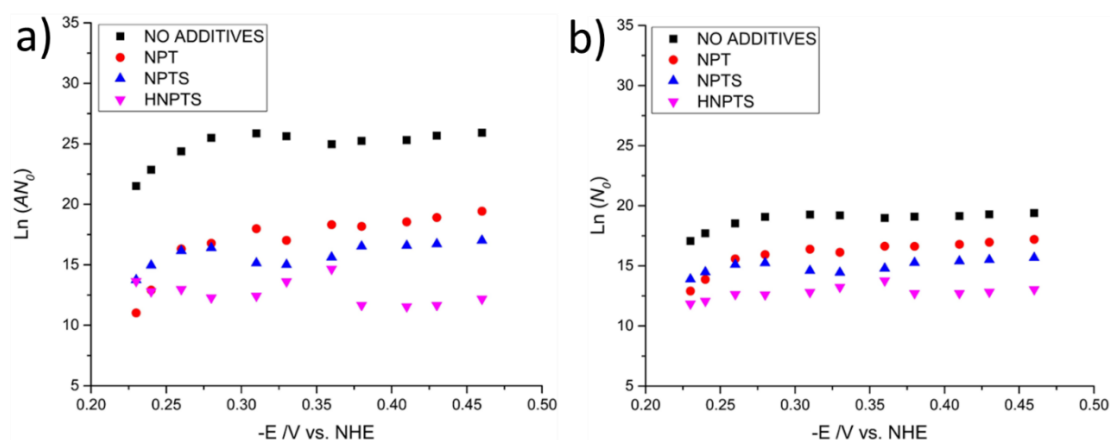
Figure 9. Dependence of logarithm of (a) steady state nucleation rate (AN_0) and (b) number density of nuclei (N_0) on the applied potential for tin electrodeposition on a boron doped diamond surface in 0.1 M H_2SO_4 and 0.5 mM $SnSO_4$ in the absence and presence of 1 mM of: NPT, NPTS and HNPTS. The steady state nucleation rate (AN_o) and the number density of nuclei (N_0) were obtained from times of the maximum of the current transients by using Eqs. 4 and 5.

Figure 9 shows the relationship between the logarithm of (AN_o) and (N_0) and the applied potential in the presence of the different naphthalene-based additives NPT, NPTS and HNPTS, as determined from the expressions for t_{max}, Eqs. 4 and 5. As expected, a considerable decrease of the steady state nucleation rate (AN_0) or the number density of nuclei (N_0) is observed in the order NPT > NPTS > HNPTS.

Although the fit with the SH nucleation and growth expressions is never perfect, the analysis above shows that the naphthalene-based additives act primarily on the nucleation probability, and that the diffusion limited growth of formed nuclei is not affected by the additive.

4.3.3 Scanning electron microscopy

Scanning electron micrographs were recorded to image the morphology of the tin deposits on BDD in the absence and presence of naphthalene-based additives.

Figure 10a and 10b shows the BDD surface before the tin deposition. Surface defects such as cracks, holes and grain boundaries are visible. Large flat areas of about ~ 1 X 1 μm are also seen. The BDD surface in general exhibits lighter and darker zones which correlated with zones of lower and higher conductivity[7]. By scanning large enough areas, both types of surfaces can be observed in a single image[7]. Images reported here are representative of several images taken over the BBD electrode surface.

Chapter 4. The effect of naphthalene-based additives on the kinetics of tin electrodeposition on a boron doped diamond electrode
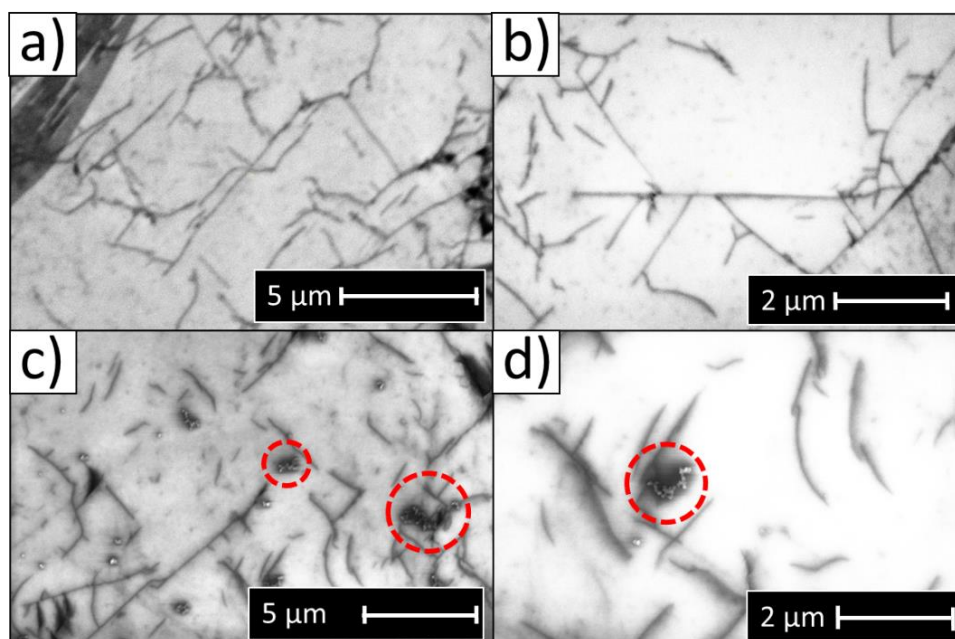
_____

Figure 10. Scanning electron micrographs of BDD surface before tin deposition (a, b) and after tin deposition (c, d). Deposition was performed in 0.1 M H_2SO_4 and 0.5 mM $SnSO_4$. Potential was held at -0.266 V for 10 s where nucleation and early growth happened, subsequently the potential was held at -0.230 V during 60 s where the nuclei were grown.

Figure 10c and 10d show tin crystallites on BDD surface, obtained in the absence of surfactants by holding the potential at -0.266 V for 10 s at which nucleation and early growth happened, after which the potential was stepped back to -0.230 V during 60 s, at which potential the nuclei were grown further. Figs. 10c and d show how crystallites cluster together at or near the darker defect areas of higher conductivity. The size of the crystallites is approximately ~50 nm diameter and does not change substantially over the electrode surface.

Figure 11a presents the tin deposits on BDD in the absence of naphthalene-based additives. Unlike tin deposits grown in the absence of additives, tin electrodeposited in the presence of NPT on BDD (Fig. 11b) exhibits crystallites over the entire surface, not only near the surface defects but also on the large flat areas. Nonetheless, tin deposition is still preferred around the defects, where clusters of crystallites are seen mainly on the cracks and holes. Furthermore, a larger distribution of crystallite shapes is noticeable. Figure 11c shows the tin deposit grown in the presence of NPTS, tin crystallites are visible near the surface defects and on the large flat areas; crystallites seem to have a specific shape and exhibit a higher distribution and bigger sizes (~100 nm) than in the absence and presence of NPT.

Tin deposits grown in the presence of HNPTS are shown in Figure 11d. Tin crystallites grow mainly near the defects; crystallites exhibit a larger size distribution (~100 to ~500 nm) which indicates that they were not formed at the same time, i.e., the progressive nucleation mode is operative.
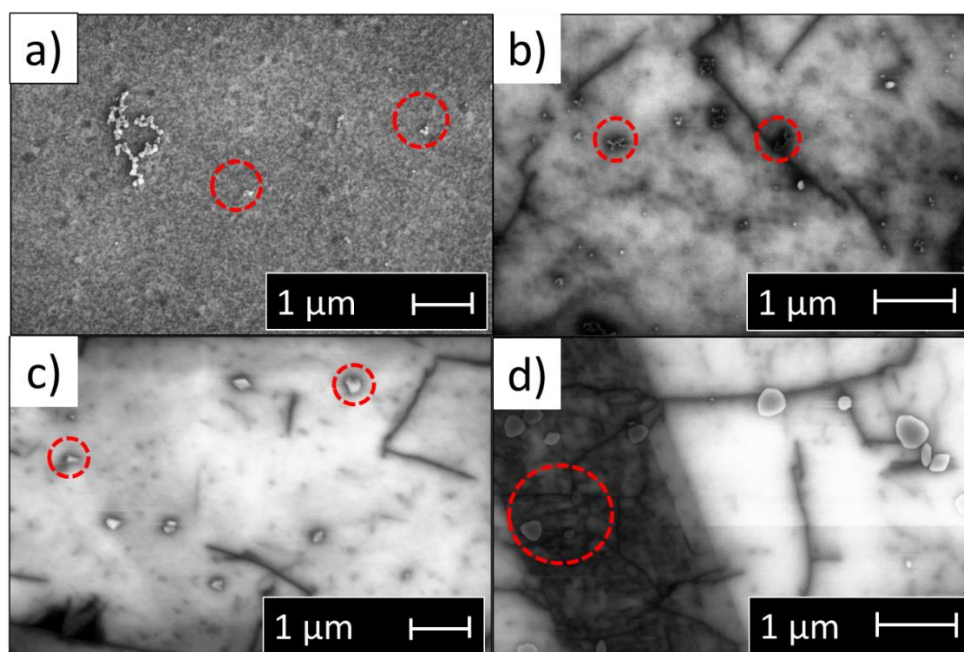
Figure 11. Scanning electron micrographs of tin electrodeposited on a boron doped diamond surface in 0.1 M H_2SO_4 and 0.5 mM $SnSO_4$: (a) in the absence of naphthalene-based additives (b) in the presence of 1 mM of NPT, (c) 1 mM NPTS, (d) 1 mM HNPTS. Potential was held at -0.266 V for 10 s where nucleation and early growth happened, subsequently the potential was held at -0.230 V during 60 s where the nuclei were grown.

Finally, the effect of ethoxylated α-napthalenesulfonic acid (ENSA), a commonly used additive in the tin electroplating industry, was also studied during tin electrodeposition on a boron doped diamond electrode. Figure 12a shows the current transient of tin electrodeposition recorded in the presence of ENSA; an almost complete inhibition of the tin deposition is seen (note that the currents are much lower than in Fig.7). Transients are essentially flat, the absence of t_{max} and i_{max} does not allow to compare these results to the standard nucleation and growth model of SH. Furthermore, the SEM image in Figure 12b confirms the inhibition of the tin electrodeposition on Boron doped diamond electrode in the presence of ENSA. Hardly any tin crystallites (in fact only one) are seen in the micrograph.

4.3.4 Comparison to tin electrodeposition on gold

The above results are in partial agreement with our previous work on the effect of naphthalene-based additives on tin electrodeposition on gold[6]. In our previous study, we showed that on gold surfaces, NPT and NPTS lie flat on the surface and interact mainly via van der Waals forces, with NPTS molecules, forming a more compact structure due to intermolecular lateral interactions. Thus, one can expect that on BDD, NPT and NPTS might

Chapter 4. The effect of naphthalene-based additives on the kinetics of tin electrodeposition on a boron doped diamond electrode

_____

also lie flat, since van der Waals interactions are not very sensitive to the electrode surface. Also, the intermolecular lateral interactions between NPTS molecules are not expected to change significantly on BDD. The results on BDD show that a more compact film formed in the presence of NPTS decreases the nucleation kinetics more than NPT.
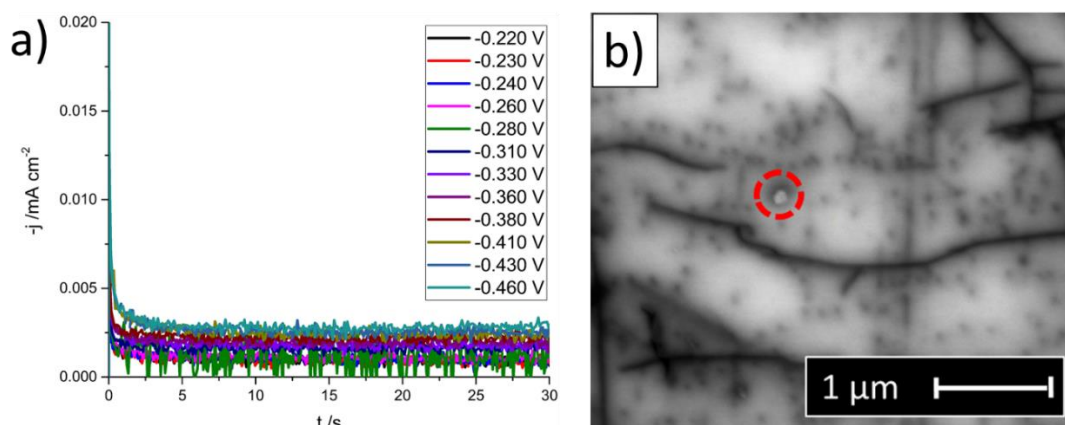

Figure 12. (a) Current transients of tin electrodeposition on a boron doped diamond surface in the presence of 1 mM ENSA, 0.1 M H_2SO_4, 0.5 mM $SnSO_4$, recorded between -0.220 to -0.460 V. (b) Scanning electron micrograph of tin electrodeposited on a boron doped diamond surface in 0.1 M H_2SO_4 and 0.5 mM $SnSO_4$ and in the presence 1 mM of ENSA. The potential was held at -0.266 V for 10 s, subsequently the potential was held at -0.230 V during 60 s.

With respect to HNPTS, our work on gold showed[6] it does not lie flat on the surface, but rather that the naphthol group undergoes reductive desulfonation and subsequent polymerization via crosslinked reactions. Since polymerization processes are not highly sensitive to the electrode surface, a polymeric film is likely to form in the presence of HNPTS on BDD. Furthermore, ethoxylated α-napthalenesulfonic acid (ENSA) shows equivalent polymer film formation, and indeed tin electrodeposition on BDD is highly inhibited in its presence.

The effect of naphthalene-based additives on the kinetics of tin electrodeposition on boron doped diamond is complementary to our previous work on gold electrodes[6], giving insights on the way naphthalene-based additives affect the kinetics of tin electrodeposition process. On gold, the nucleation process appeared to be too fast to obtain meaningful transients. In this study, we were able to show that NPT, NPTS and HNPTS mainly have an effect on the nucleation process. Moreover, although the transients in the presence of ethoxylated α-napthalenesulfonic acid (ENSA) could not be compared to the standard nucleation and growth model of Scharifker and Hills, ENSA exhibits a very similar behavior to that on gold, i.e., a strong inhibition of the tin electrodeposition process.

_____

4.4 Conclusions

The effect of naphthalene (NPT), naphthalenesulfonate (NPTS) and hydroxynaphthalenesulfonate (HNPTS) on the kinetics of tin electrodeposition on a boron doped diamond electrode has been studied by using chronoamperometry and scanning electron microscopy (SEM). The potentiostatic current transients were analyzed with the standard Scharifker-Hills model, giving the steady state nucleation rate (AN_0) and the number density of nucleation sites (N_0) at different applied potentials. In the absence of additives, the nucleation and growth process is shown to transition from progressive to instantaneous with increasingly negative potential. A decrease in the nucleation kinetics of tin deposition on BDD was observed in the presence of naphthalene-based additives: NPT showed the smallest effect on the reduction of the kinetics, followed by NPTS, and the strongest effect was observed in the presence of HNPTS. Analysis with the Scharifker-Hills model, shows that the steady-state nucleation rate and the number density of nucleation sites exhibit the expected decrease in the presence of the different naphthalene-based additives over the entire studied potential range. Additionally, tin (II) diffusion coefficients were determined by fitting the current transients at longer times to the Cottrell equation, the calculated values of tin (II) diffusion coefficient ($D_{Sn^{2+}}$) giving similar values in the absence and presence of the additives. This observation indicates that tin (II) is not complexed by the additives. Moreover, similar values of tin (II) diffusion coefficients were obtained at low negative potentials, suggesting that also the charge-transfer kinetics itself is not influenced by the presence of the additives. The additives only affect the nucleation process. Ethoxylated α-napthalenesulfonic acid (ENSA) strongly inhibits the tin electrodeposition process, similar to deposition on gold, yielding transients that cannot be analyzed with the Scharifker-Hills model.

4.5 References

(1)   Walsh, F. C.; Low, C. T. J. A Review of Developments in the Electrodeposition of Tin. _Surf. Coatings Technol._ **2016**, _288_, 79–94.

(2)   Tzeng, G. S.; Lin, S. H.; Wang, Y. Y.; Wan, C. C. Effects of Additives on the Electrodeposition of Tin from an Acidic Sn(II) Bath. _J. Appl. Electrochem._ **1996**, _26_ (4), 419–423.

(3)   Barry, F. J.; Cunnane, V. J. Synergistic Effects of Organic Additives on the Discharge, Nucleation and Growth Mechanisms of Tin at Polycrystalline Copper Electrodes. _J. Electroanal. Chem._ **2002**, _537_ (1–2), 151–163.

(4)   Wen, S.; Szpunar, J. A. Nucleation and Growth of Tin on Low Carbon Steel. _Electrochim. Acta_ **2005**, _50_ (12), 2393–2399.

Chapter 4. The effect of naphthalene-based additives on the kinetics of tin electrodeposition on a boron doped diamond electrode

_____

(5)   Wijenberg, J. H. O. J. Initial Stages of Electrochemical Phase Formation, Utrech, 1991.

(6)   Aranzales, D.; Briliani, I.; McCrum, I. T.; Wijenberg, J. H. O. J.; de Vooys, A. C. A.; Koper, M. T. M. The Effect of Naphthalene-Based Additives on Tin Electrodeposition on a Gold Electrode. *Electrochim. Acta* **2021**, *368*, 137606.

(7)   Hyde, M. E.; Jacobs, R.; Compton, R. G. In Situ AFM Studies of Metal Deposition. *J. Phys. Chem. B* **2002**, *106* (43), 11075–11080.

(8)   Enea, O.; Riedo, B.; Dietler, G. AFM Study of Pt Clusters Electrochemically Deposited onto Boron-Doped Diamond Films. *Nano Lett.* **2002**, *2* (3), 241–244.

(9)   Simm, A. O.; Ji, X.; Banks, C. E.; Hyde, M. E.; Compton, R. G. AFM Studies of Metal Deposition: Instantaneous Nucleation and the Growth of Cobalt Nanoparticles on Boron-Doped Diamond Electrodes. *ChemPhysChem* **2006**, *7* (3), 704–709.

(10)   Zak, J.; Kolodziej-Sadlok, M. AFM Imaging of Copper Stripping/Deposition Processes in Selected Electrolytes on Boron-Doped Diamond Thin-Film Electrodes. *Electrochim. Acta* **2000**, *45* (17), 2803–2813.

(11)   Milchev, A. *ELECTROCRYSTALLIZATION Fundamentals of Nucleation and Growth*; Kluwer Academic Publishers: New York, Boston, Dordrecht, London, Moscow, 2002.

(12)   Scharifker, B. R.; Mostany, J. Three-Dimensional Nucleation with Diffusion Controlled Growth: Part I Three-Dimensional Nucleation and Nucleation Rates per Site. *J. Electroanal. Chem.* **1984**, *177*, 13–23.

(13)   Scharifker, B. Theoretical and Experimental Studies of Multiple Nucleation. *Electrochim. Acta* **1982**, *28* (2), 879–889.

(14)   Scherb, G.; Kolb, D. M. Cu Deposition onto N-GaAs(100): Optical and Current Transient Studies. *J. Electroanal. Chem.* **1995**, *396* (1–2), 151–159.

(15)   Milchev, A. Electrochemical Nucleation on Active Sites - What Do We Measure in Reality? Part I. *J. Electroanal. Chem.* **1998**, *457* (1–2), 35–46.

(16)   Milchev, A.; Stoyanov, S.; Kaischev, R. Atomistic Theory of Electrolytic Nucleation: I. *Thin Solid Films* **1974**, *22* (3), 255–265.

(17)   Sluyters-Rehbach, M.; Wijenberg, J. H. O. J.; Bosco, E.; Sluyters, J. H. The Theory of Chronoamperometry for the Investigation of Electrocrystallization. Mathematical Description and Analysis in the Case of Diffusion-Controlled Growth. *J. Electroanal. Chem.* **1987**, *236* (1–2), 1–20.

The effect of naphthalene-based additives on tin electrodeposition on an iron electrode: an industrial approach

Chapter 5. The effect of naphthalene-based additives on tin deposition on an iron electrode: an industrial approach

_____
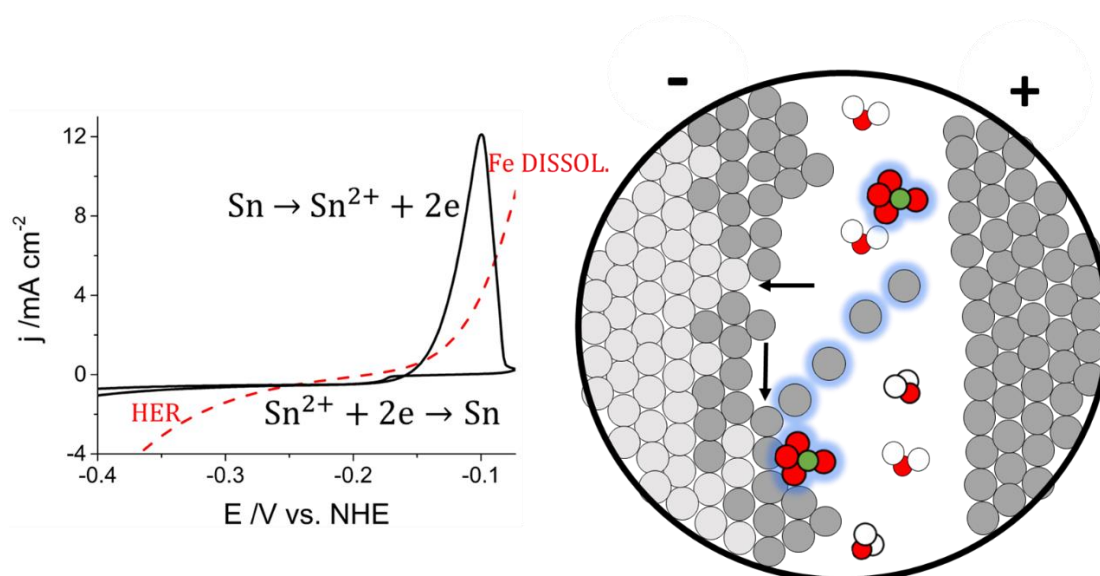
Abstract

In this chapter, we describe preliminary measurements of the effect of naphthalene-based additives on tin electrodeposition on an iron electrode in sulfuric acid media. Considering the highly reactive and complex nature of the iron electrode surface, these measurements aim to compare and use the gathered knowledge of our previous studies of the effect of naphthalene-based additives on tin electrodeposition on more stable substrates, i.e., gold and boron doped diamond electrodes, to provide insights of the interaction of the additives with iron and their effect on the overall tin deposition process on an iron electrode.

Naphthalene-based additives showed to strongly affect tin electrodeposition on iron under acidic media. In the case of NPT and NPTS, tin electrodeposition remains mainly independent of the substrate, NPT and NPTS molecules presumably arrange in a similar way as on a gold surface, since they interact with the substrate mainly via Van der Waals forces. A more compact film of NPTS molecules is formed on the iron substrate since a strong decrease of tin electrodeposition is observed in comparison to NPT. HNPTS stronger decreases the tin deposition, which is in agreement with our observations of its effect on tin deposition on a BDD electrode. Furthermore, we showed that Sn (II) ions transport from the bulk to the electrode surface is not affected by NPT, NPTS and HNPTS but ENSA-6, which exhibits a strong decrease of Sn (II) ions on the surface, presumably due to a slow mass transport of the ions through the ENSA film formed on the electrode surface. Furthermore, ENSA-6 also highly inhibits tin deposition process.

_____

5.1 Introduction

Tin electroplating process finds application as an alloy or coating, and therefore tin plays an important role in daily life, being used in food packaging, jewellery, and also in modern technology [1]. One of the most traditional and important applications of tin electroplating is the protection of iron or steel from air oxidation and the enhancement of their corrosion resistance [12]. Few studies have aimed to understand the effect of industrial additives on the tin deposition process on iron [3]. The main purpose of the present chapter is to use the gathered knowledge of the effect of naphthalene-based additives on tin electrodeposition process on more stable substrates such as gold [4] and boron doped diamond [5] and compare it to the phenomena observed on the tin electrodeposition on an iron electrode, a highly reactive surface.

5.2 Experimental details

Before each measurement all glassware was stored overnight in a solution of 1g L^{-1} $KMnO_4$ in 0.5 M H_2SO_4. Before use, it was rinsed with water and 30% hydrogen peroxide solution in order to remove permanganate anions and trace impurities. Glassware was boiled in water five times before starting the experiments. The water used to clean glassware and to prepare solutions was demineralized and ultra-filtrated by a Millipore MilliQ system (18.2 MΩ cm). The voltammetric experiments were performed in a three-electrode cell configuration at room temperature using an iron disk as a working electrode (5.0 mm diameter, 4.0 mm thickness purchased from Pine-research) used in the rotating-disk electrode (RDE) setup under hydrodynamic conditions, a gold wire as a counter electrode and RHE as a reference electrode, but all the potentials are reported on the normal hydrogen electrode (NHE) scale. The reference electrode was in contact with the electrolyte via a Luggin capillary and connected to an additional gold wire through a capacitor of 10 μF to filter small currents produced in the RHE electrode and to reduce the noise in measurements at low currents.

The iron working electrode was successively polished with 1.0, 0.3 and 0.05 μm of diamond powder suspension, rinsed and transferred to an ultrasound bath with water during 10 minutes before the measurements. The gold counter electrode was electrochemically etched before each experiment firstly by oxidizing it by applying 10 V during 20 s in 0.1M sulfuric acid, a graphite bar was used as a counter electrode, and subsequently by dissolving the gold hydr(oxides) formed on the counter electrode surface by dipping it in a 6 M HCl solution for 30 s. The experiments were performed using a potentiostat VSP-300 (Bio-logic) and the RDE experiments were performed with an MSR rotating electrode (Pine Research) at a rotation

rate of 1600 rpm. The electrode potential was corrected for Ohmic drop during the measurements by using 85% of the Ohmic resistance measured by electrochemical impedance spectroscopy. Finally, the morphology of the tin deposits on the iron electrode were observed ex situ by scanning electron microscopy SEM. Micrographs were taken using the model JEOL 820 SEM at 15 kV and 0.1 nA. Energy Dispersive X-Ray Spectroscopy (EDS) measurements were taken at 15 kV, the reported percentage of tin was calculated from the average of relative ratio of tin from a line scan measurement of 0.5 μm length, over the tin features.

All solutions were prepared from chemicals with the highest purity commercially available: H_2SO_4 (96% ultrapure, Merck), $SnSO_4$ (≥ 95%, Sigma Aldrich), naphthalene (≥ 99%, Sigma Aldrich), 2-napthalenesulfonic acid sodium salt (99.6%, Sigma Aldrich), sodium thiosulfate (≥ 99.99%, Sigma Aldrich), 4-hydroxy-1-naphthalenesulfonic acid sodium salt (≥ 95 %, Santa Cruz Biotechnology) and ethoxylated α-napthalenesulfonic acid (73.6%, Pulcra chemicals). In the case of ENSA the main impurities are sulfuric acid with 8.7 %, and water with 2.4 %, other impurities were not provided by the supplier. The solutions were deaerated with Argon for 20 min before each experiment and a constant flow of Argon above the solution was kept during all the experiments.

5.3 Results and discussion

Figure 1 shows the scanning electron micrographs of the "bare" iron surface just after the mechanical polishing and ultrasound treatment. Fig. 1a exhibits fissures as a consequence of the mechanical polishing procedure. Fig. 1b shows the surface zoom-in, it exhibits 3D flake-like structures almost over the entire flat surface. EDS measurements show the presence of oxygen in the 3D flake-like structures and also over the iron flat electrode surface with a relative ratio of O: Fe (5.4 ± 0.8 % : 94.6 ± 1.3 %). Furthermore, iron oxides are also visible on the electrode surface since the scanning electron micrographs exhibit brighter zones along the defects and edges of the electrode surface (lower conductivity), in which EDS measurements reveal higher contents of oxygen.
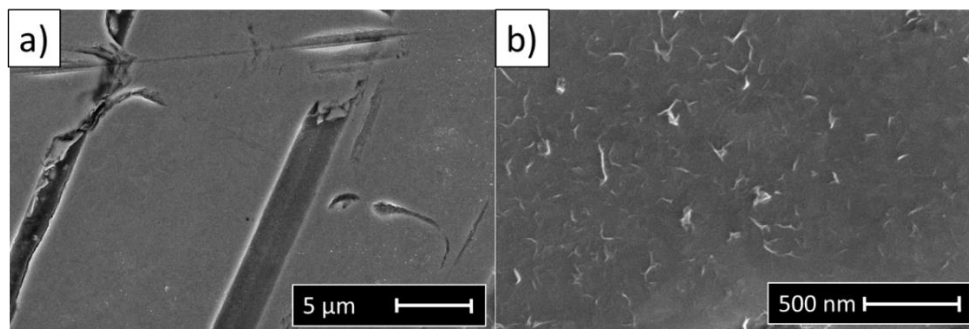

Figure 1. Scanning electron micrographs of the iron substrate 10 minutes after mechanical polishing

_____

Figure 2 shows the cyclic voltammetry of the iron electrode surface in sulfuric acid. Voltammetry recorded shows two different processes: iron dissolution and the hydrogen evolution reaction on the iron surface. From the recorded voltammetry one could say that between -0.15 to -0.35 V the iron surface does not seem very reactive. Nonetheless, the inset of Fig. 1a shows the presence of anodic and/or cathodic currents correlated with iron dissolution and (presumably) hydrogen evolution reaction over the entire potential window. Due to the highly reactive nature of iron substrate under acidic media, no polarizable double layer region is present. Figure 2b shows the Tafel plot of the two processes: hydrogen evolution reaction and iron dissolution. The junction between the anodic and cathodic branches of the Log |j| vs. E is known as the corrosion potential, and its value is -0.274 V. Moreover, Tafel slopes for hydrogen evolution and iron dissolution were obtained, 134 and 48 mV dec^{-1}, respectively, which are mostly in agreement with previously reported values for static conditions [6–9]. Moreover, Figure 3 shows the cyclic voltammetry for iron dissolution and hydrogen evolution reaction on iron electrode under hydrodynamic conditions, a strong increase in the anodic current is observed as a consequence of a strong mass transport effect during iron dissolution process. The values for the Tafel slope for HER is almost identical (137 mV decade^{-1}) to the one without rotation, but the Tafel slope changes in the case of iron dissolution (60 mV decade^{-1}). Moreover, a shift of the corrosion potential to less negative potentials is also observed (-0.19 V).
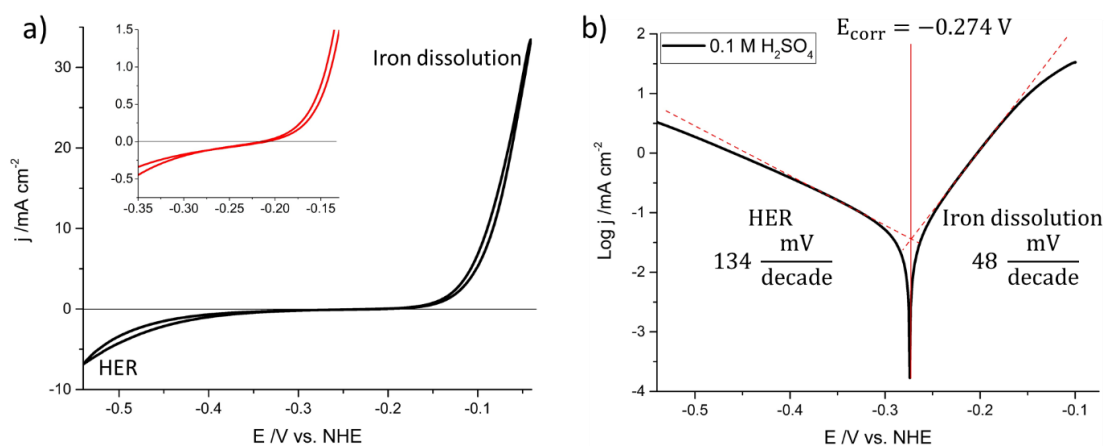

Figure 2. a) Cyclic voltammetry of the iron substrate in 0.1 M H$_2$SO$_4$. CV recorded between -0.56 to -0.05 V at 30 mV s^{-1}, static conditions b) Tafel plot for iron electrode in 0.1 M H$_2$SO$_4$
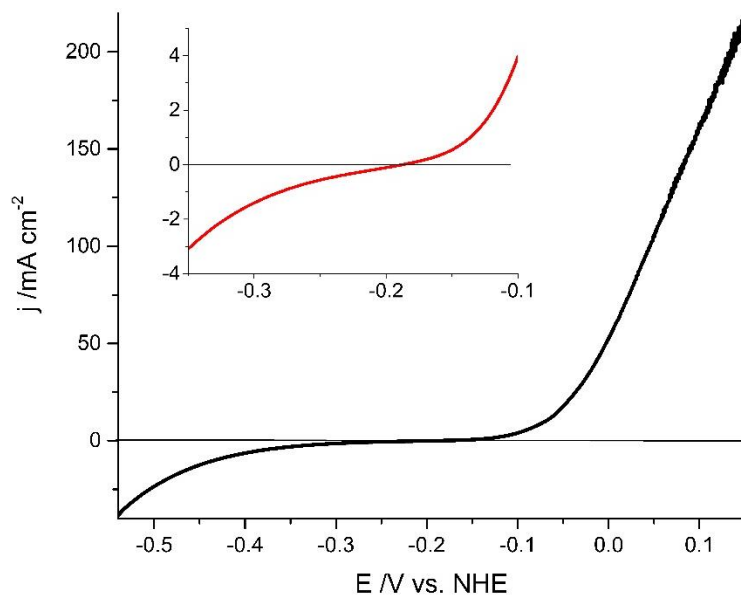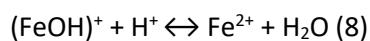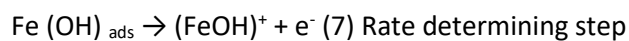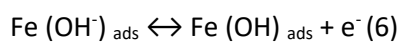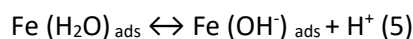
Figure 3. a) Cyclic voltammetry of the iron substrate in 0.1 M H_2SO_4. CV recorded between -0.56 to -0.05 V at 30 mV s^{-1}, under hydrodynamic rotating-disk conditions: 1600 rpm

Hydrogen evolution reaction on iron and iron dissolution processes have been described by the following equations[9]:

Hydrogen evolution reaction steps:

$$H^+ + e^- \leftrightarrow H_{ads} \text{ (1) Rate determining step}$$

$$H_{ads} + H^+ + e^- \leftrightarrow H_2 \text{ (2)}$$

$$2H_{ads} \leftrightarrow H_2 \text{ (3)}$$
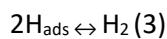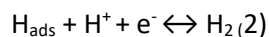
Iron dissolution reaction steps:

$$Fe + H_2O \leftrightarrow Fe(H_2O)_{ads} \text{ (4)}$$

$$Fe(H_2O)_{ads} \leftrightarrow Fe(OH^-)_{ads} + H^+ \text{ (5)}$$

$$Fe(OH^-)_{ads} \leftrightarrow Fe(OH)_{ads} + e^- \text{ (6)}$$

$$Fe(OH)_{ads} \rightarrow (FeOH)^+ + e^- \text{ (7) Rate determining step}$$

$$(FeOH)^+ + H^+ \leftrightarrow Fe^{2+} + H_2O \text{ (8)}$$

_____

5.3.1 Tin electrodeposition on an iron electrode

Following our previous studies about the effect of naphthalene-based additives on tin electrodeposition process on gold and boron-doped diamond electrodes[45], we study here the effect of naphthalene-based additives on tin electrodeposition on an iron electrode by means of cyclic voltammetry and ex-situ scanning electron microscopy.
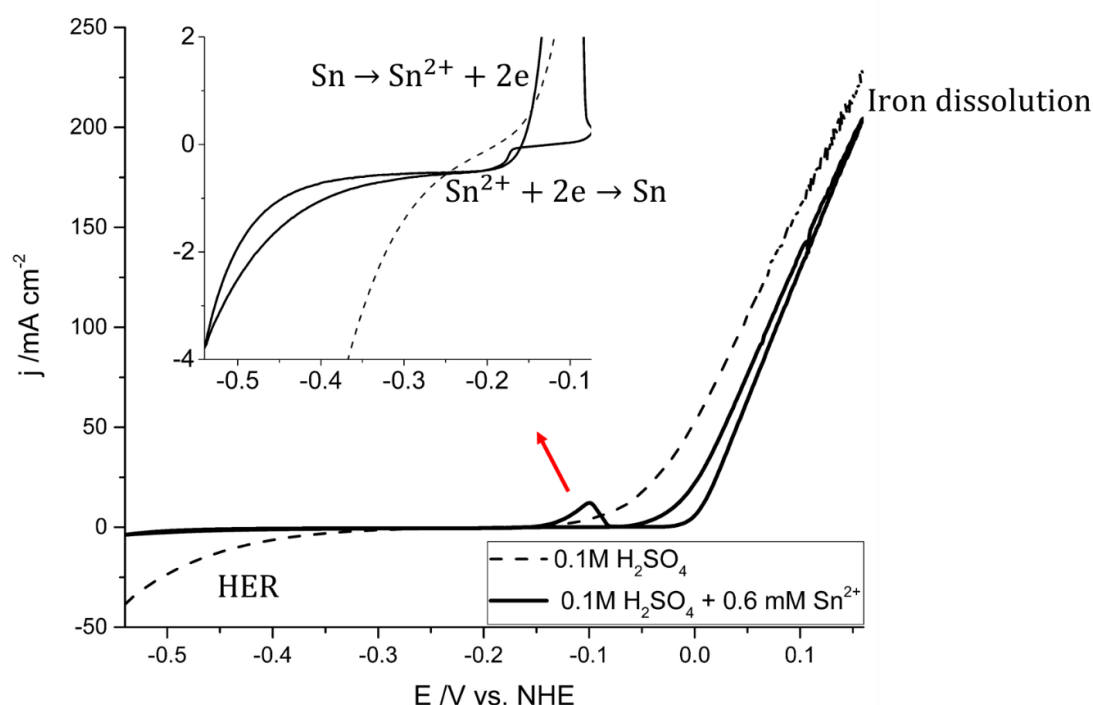

Figure 4. Cyclic voltammetry of tin deposition-dissolution on iron, recorded between -0.54 to -0.16 V at 30 mV s^{-1} and 1600 rpm (Bold line). Cyclic voltammetry of iron dissolution and HER on iron, recorded between -0.54 to -0.16 V at 30 mV s^{-1} and 1600 rpm (Dashed line). Inset of tin bulk deposition and dissolution.

Figure 4 shows the cyclic voltammogram for tin deposition and dissolution on an iron electrode under acidic conditions. In a narrow potential window (~-0.075 to -0.35 V), a cathodic wave at -0.17 V followed by a plateau related with tin bulk deposition under mass transport control at -0.19 V are observed, besides, an anodic peak related with tin dissolution is observed at -0.10 V. Furthermore, from ~-0.35 V to more negative potentials, hydrogen evolution is observed. Since the onset potential is more negative than the HER onset in the blank (see Figure 3), we ascribed it to HER on the tin surface, tin being a bad catalyst for HER. At positive potentials, a shift of the onset potential for iron dissolution to less negative

potentials is observed as a consequence of the tin presence on the iron surface. Furthermore, a decrease in the current density of iron dissolution is also observed.

5.3.2 The effect of naphthalene-based additives on tin electrodeposition on an iron electrode

Figure 5a, 6a and 7a show the cyclic voltammograms for tin electrodeposition and dissolution on an iron electrode in the presence and absence of different concentrations of naphthalene (NPT), naphthalenesulfonate (NPTS) and hydroxynaphthalenesulfonate (HNPTS).
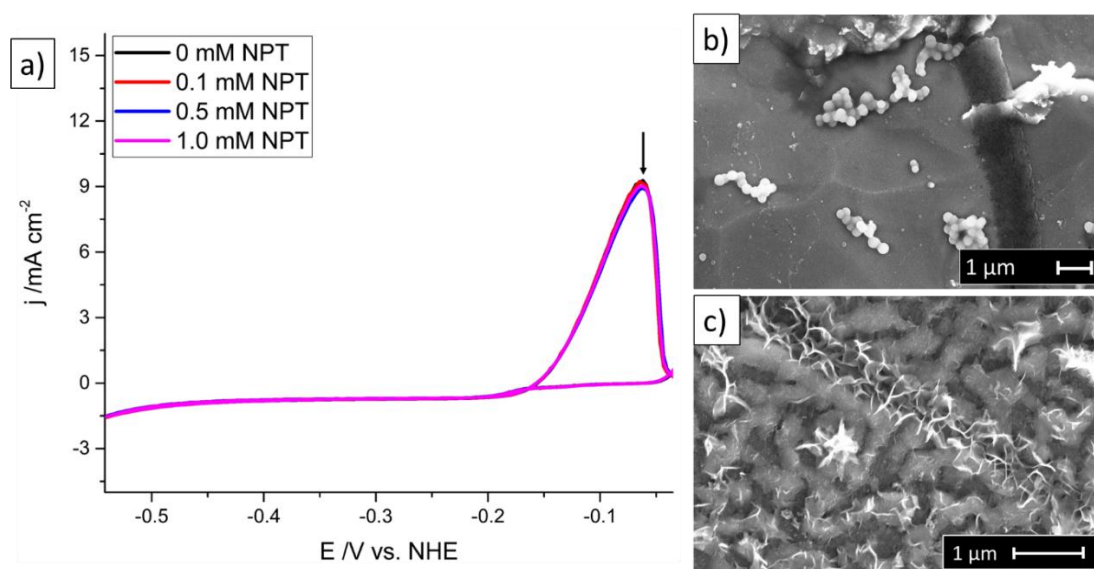
Figure 5. (a) Cyclic voltammograms of tin electrodeposition on a polycrystalline iron RDE, 0.1 M H_2SO_4 at different concentrations of NPT, recorded between -0.541 to 0.1 V and 30 mV s^{-1} and 1600 rpm. SEM micrographs of tin electrodeposited on polycrystalline iron; potential was swept from 0.1 to -0.241 V at 30 mV s^{-1} and 1600 rpm, subsequently the potential was held at -0.241 V during 1 minute, 0.1 M H_2SO_4, 0.6 mM SnSO$_4$ (b) without NPT (c) with 200 µM NPT

Figure 5a shows almost no effect of NPT on tin electrodeposition – dissolution on an iron electrode in terms of the voltammetric profile, only a very small decrease (if any) in the peak related to the stripping of tin bulk deposited is visible. No remarkable dependence on NPT concentration is observed. Figures 5b and 5c show the scanning electron micrographs of the tin deposits in the absence and presence of NPT, respectively. Unlike Figure 5a, Figures 5b and 5c reveal remarkable differences in the morphology of the tin deposits in the absence and presence of NPT. In the absence of NPT, tin deposits exhibit clusters of spherical tin crystallites almost over the entire surface. The tin crystallites sizes are about 300 nm. In the presence of

_____

NPT, the tin deposit does not show separate tin crystallites, instead a coalesced tin deposit is observed and merges with the 3D – needles of iron oxides.
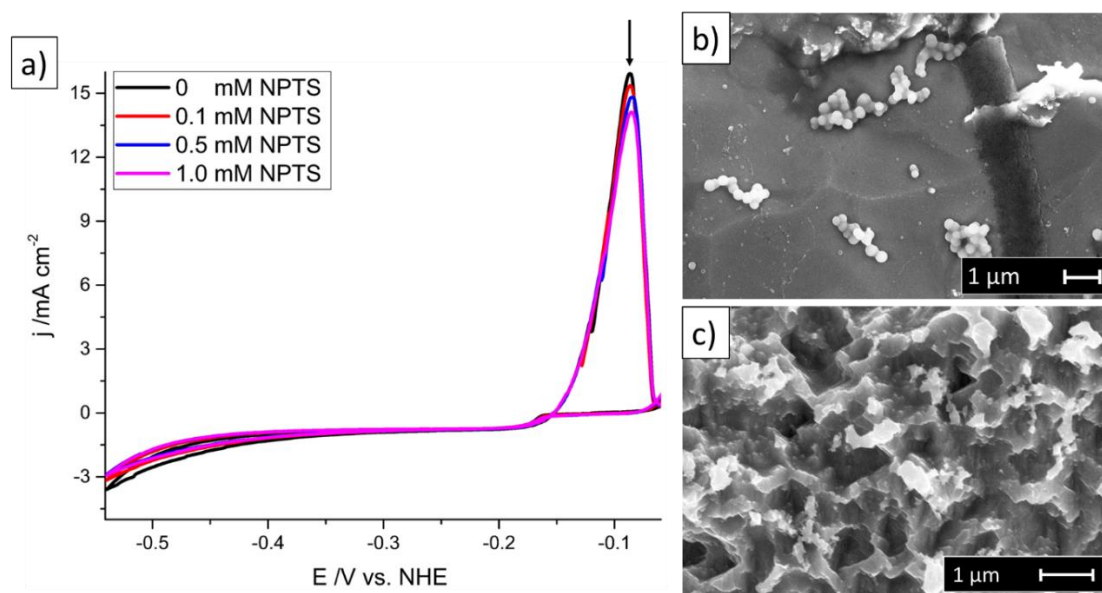

Figure 6. (a) Cyclic voltammograms of tin electrodeposition on a polycrystalline iron RDE, 0.1 M H_2SO_4 at different concentrations of NPTS, recorded between -0.541 to 0.1 V and 30 mV s^{-1} and 1600 rpm. SEM micrographs of tin electrodeposited, on polycrystalline iron; potential was swept from 0.1 to -0.241 V at 30 mV s^{-1} and 1600 rpm, subsequently the potential was held at -0.241 V during 1 minute, 0.1 M H_2SO_4 , 0.6 mM $SnSO_4$, in the presence of: (b) without NPTS (c) with 200 µM NPTS

Figure 6a shows the cyclic voltammogram of tin electrodeposition and dissolution on an iron electrode in the presence of different NPTS concentrations. A small but remarkable decrease of the peak correlated to the stripping of tin bulk deposited is seen in the presence of NPTS, and its decrease seems to be proportional to the increase of NPTS concentration, additionally a slight decrease of hydrogen evolution current is also observed as a consequence of the presence of NPTS. Figures 6b and 6c show that in the presence of NPTS tin deposits do not show well defined crystallites or clusters of crystallites, instead shapeless tin features are concentrated in specific regions of the electrode surface. Figure 6c also shows the presence of 3D layer - network structures on the iron substrate ascribed to iron oxides. Scanning electron micrographs reveal that the substrate morphology is not stable between different measurements, as it is expected due to the highly reactive nature of iron under acidic conditions and oxygen exposure.
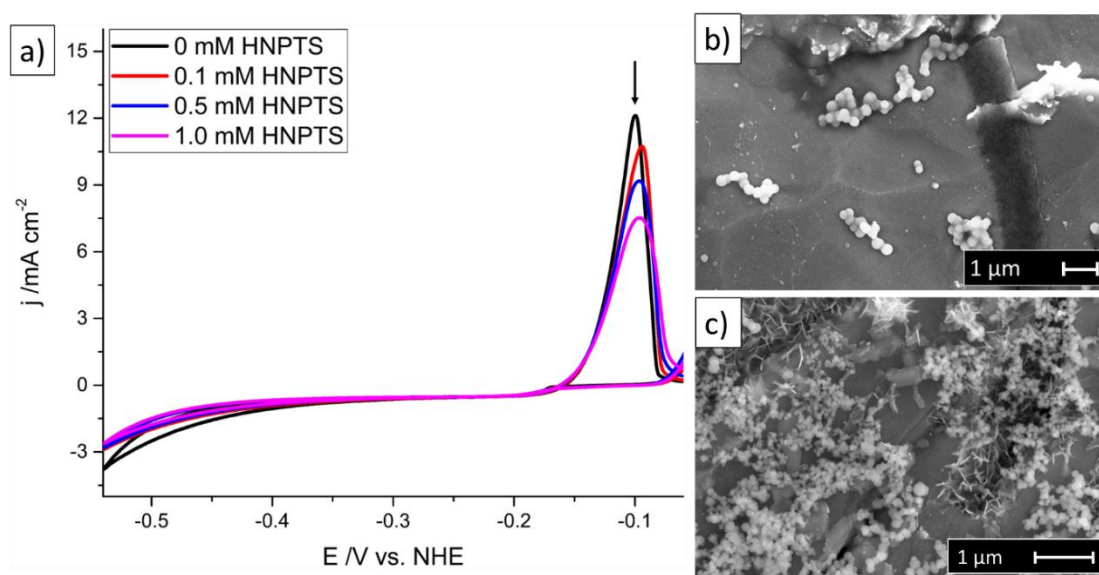
Figure 7. (a) Cyclic voltammograms of tin electrodeposition on a polycrystalline iron RDE, 0.1 M H_2SO_4 at different concentrations of HNPTS, recorded between -0.541 to 0.1 V and 30 mV s^{-1} and 1600 rpm. SEM micrographs of tin electrodeposited, on polycrystalline iron; potential was swept from 0.1 to -0.241 V at 30 mV s^{-1} and 1600 rpm, subsequently the potential was held at -0.241 V during 1 minute, 0.1 M H_2SO_4 , 0.6 mM SnSO$_4$, in the presence of: (b) without HNPTS (c) with 200 µM HNPTS

Figure 7a shows the cyclic voltammogram for tin deposition and dissolution in the presence of HNPTS. A larger decrease in the peak correlated to the oxidation of bulk deposited tin and a slight shift to less negative potentials are observed compared to NPTS. Moreover, a decrease of the hydrogen evolution is also observed. Figures 7b and 7d show the scanning electron micrographs of tin deposits in the absence and presence of HNPTS, respectively. In contrast to the effect of NPT and NPTS on the morphology of tin deposits, tin deposits in the presence of HNPTS do not seem to coalesce, instead spherical tin crystallites are visible, which arrange in clusters similar to the observed morphology of tin deposits in the absence of naphthalene-based additives. A decrease in the size of tin crystallites is seen: crystallites of about 100 nm are present in the clusters. Moreover, Fig. 7c also shows the 3D-flake-like iron oxides merged with and underneath the tin features.

The above results are correlated with our previous work on the effect of naphthalene-based additives on tin electrodeposition on gold [10] and boron-doped diamond electrodes[5]. From our previous study using a gold substrate, we demonstrated that NPT and NPTS lie flat on the gold surface and interact mainly via van der Waals forces with the substrate. Furthermore, we showed that NPTS molecules form a more compact structure due to intermolecular lateral interactions. Voltammetric profiles in the presence of NPT and NPTS revealed that NPTS decreases to a higher degree the tin bulk deposition on an iron electrode than NPT, as expected, considering the formation of a more compact film due to intermolecular interactions. Moreover, in spite of the remarkable differences between gold, BDD and iron

_____

substrates, since NPT and NPTS interact mainly via van der Waals forces with the substrate, interactions with the iron electrode surface might not drastically change, neither the intermolecular interactions.

Furthermore, we previously showed that HNPTS molecules do not lie flat on the gold surface, but rather the naphthol group undergoes oxidative polymerization, and such film formation is likely to be formed on other substrates as well since polymerization is not highly sensitive to the electrode surface. Our results of tin electrodeposition on an iron electrode show that HNPTS exhibits a stronger effect on the reduction of tin electrodeposition than NPTS and NPT, similarly to the effect observed on tin electrodeposition on BDD electrode. Additionally, we can see in Figures 5a, 6a and 7a that the cathodic limiting currents in the mass transport control region do not change in the presence of the different concentrations of NPT, NPTS and HNPTS suggesting that Sn (II) ions transport from the bulk to the electrode surface is not affected.

5.3.3 The effect of α-ethoxylated naphthalenesulfonic acid (ENSA -6) on tin electrodeposition on an iron electrode

Figure 8a shows the cyclic voltammograms of tin deposition and dissolution in the presence of ENSA-6. Voltammograms exhibit a strong decrease in the cathodic wave and the plateau correlated to tin deposition. This decrease in the cathodic currents is ascribed to the reduction in the transport of tin (II) ions to the electrode surface, previous studies suggested the complex formation between tin (II)-ENSA [11, 2], but no direct evidence of the complex formation has been confirmed. A decrease of Sn (II) reduction as a consequence of slow mass transport of Sn (II) ions through an ENSA film on the electrode surface is likely. Moreover, a strong decrease and shift to more positive potentials of the peak correlated to the stripping of the tin bulk deposited are observed. The decrease in the anodic peak is a consequence of a lower amount of tin deposited and the shift in the Sn stripping peak is not strongly affected by the rotation rate. However, the reason for this phenomenon requires further study.

Figure 8c and 8d show clear differences of the tin deposits in the absence and presence of ENSA. In the presence of ENSA-6, the electrode exhibits almost no-tin features over the entire surface and the surface shows the characteristic 3D-needle of iron-oxide structures. Nonetheless, Figure 8c shows that the 3D-needles of iron oxides are covered by a blurry structure.
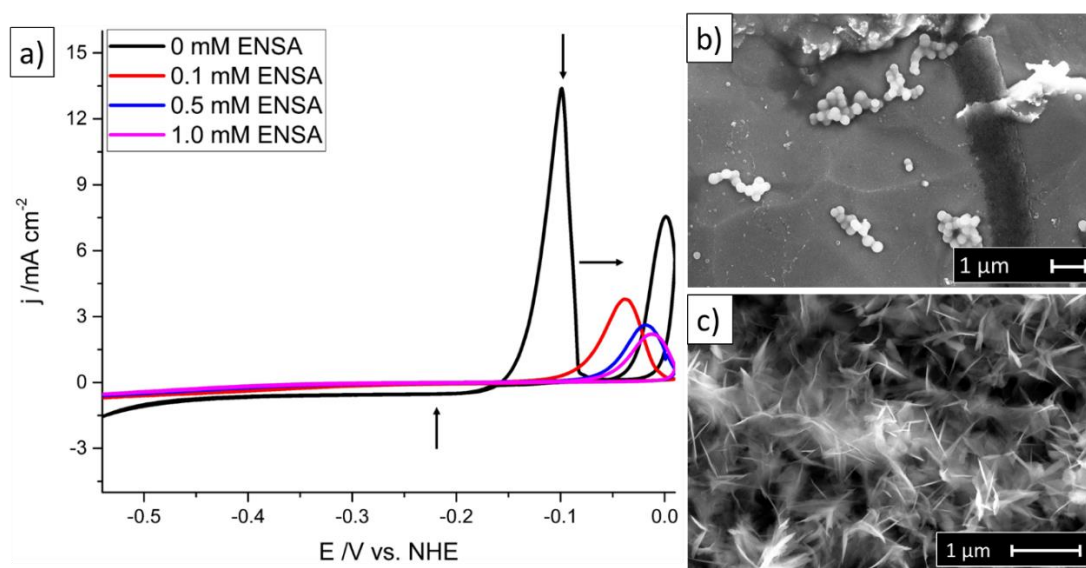
Figure 8. (a) Cyclic voltammograms of tin electrodeposition on a polycrystalline iron RDE, 0.1 M H_2SO_4 at different concentrations of ENSA, recorded between -0.541 to 0.1 V and 30 mV s^{-1} and 1600 rpm. SEM micrographs of tin electrodeposited, on polycrystalline iron; potential was swept from 0.1 to -0.241 V at 30 mV s^{-1} and 1600 rpm, subsequently the potential was held at -0.241 V during 1 minute, 0.1 M H_2SO_4, 0.6 mM SnSO$_4$: (b) without ENSA (c) with 200 µM ENSA
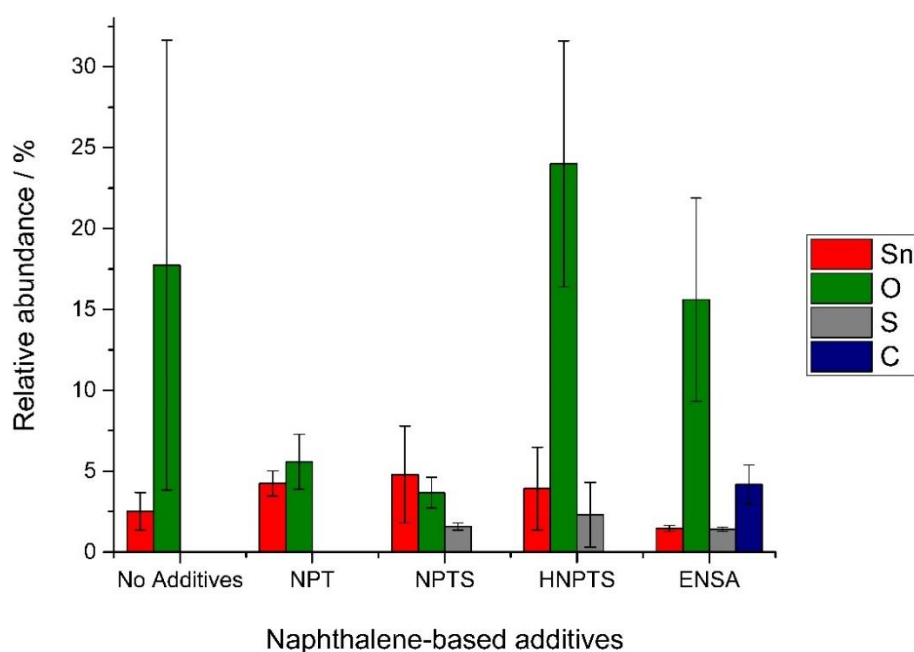

Figure 9. Comparison of relative abundance of the elemental composition for each additive from the EDS measurements. Percentage was calculated from the average of the relative ratio of the different elements in a line scan measurement of about ~0.5 µm length, over the tin features.

_____

Energy dispersive X-ray spectroscopy (EDS) measurements were taken in order to know the elemental composition of the tin deposits grown on the iron electrode in the absence and presence of the different additives. Figure 9 shows that every tin deposit exhibits at least 4% of oxygen content. Additionally, tin deposits in the presence of NPT and NPTS exhibit the lowest amount of oxygen on the surface. Further, tin deposit grown in the presence of ENSA-6 exhibits the lowest amount of tin content (~1.5 %) in accordance with the voltammetric profile (Fig.8a). Besides, a noticeable percentage of carbon and oxygen over the surface is present, which agrees with the ENSA-6 film formation over the tin-iron surface that is observed as a blurry structure on the scanning electron micrographs.

5.4 Conclusions

In this chapter, tin electrodeposition on iron electrodes has been shown to be highly affected by the presence of naphthalene-based additives. We showed the effect of NPT and NPTS on tin electrodeposition remains mainly independent of the substrate. HNPTS shows a stronger decrease of tin deposition, in agreement with has been previously observed on tin deposition on a BDD electrode. Furthermore, we showed that transport of Sn (II) ions from the bulk to the electrode surface is not affected by NPT, NPTS and HNPTS. Lastly, ENSA-6 exhibited the strongest inhibition of tin deposition on iron, an identical observed behavior on gold and BDD. Furthermore, in the presence of ENSA-6 a reduction in the transport of tin (II) ions to the electrode surface was observed; a slow mass transport of Sn (II) ions through an ENSA film on the electrode surface is likely.

5.5 References

(1)   Walsh, F. C.; Low, C. T. J. A Review of Developments in the Electrodeposition of Tin. *Surf. Coatings Technol.* 2016, *288*, 79–94. https://doi.org/10.1016/j.surfcoat.2015.12.081.

(2)   Van Velzen, C.J; Sluyters-Rehbach, M; Sluysters, J. H. The Electrochemical Reduction of Sn (II) at the Dropping Mercury Electrode from Aqueous 1 M Sulfuric Acid and from 0.3 M Phenolsulphonic Acid and Its Inhibition by ENSA -6. *Electrochim. Acta* 1987, *32* (5), 815–821.

(3)   Lee, J.-Y.; Kim, J.-W.; Chang, B.-Y.; Tae Kim, H.; Park, S.-M. Effects of Ethoxylated α-Naphtholsulfonic Acid on Tin Electroplating at Iron Electrodes. *J. Electrochem. Soc.* 2004, *151* (5), C333–C341. https://doi.org/10.1149/1.1690289.

(4)   Aranzales, D.; Briliani, I.; McCrum, I. T.; Wijenberg, J. H. O. J.; de Vooys, A. C. A.; Koper, M. T. M. The Effect of Naphthalene-Based Additives on Tin Electrodeposition on a Gold Electrode. *Electrochim. Acta* 2021, *368*, 137606. https://doi.org/10.1016/j.electacta.2020.137606.

(5)   Aranzales, D.; Wijenberg, J. H. O. J.; Koper, M. T. M. The Effect of Naphthalene-Based Additives on the Kinetics of Tin Electrodeposition on a Boron Doped Diamond Electrode.

(6)   Bockris, J. O. M.; Drazic, D.; Despic, A. R. The Electrode Kinetics of the Deposition and Dissolution of Iron. *Electrochim. Acta* 1961, *4* (2–4), 325–361. https://doi.org/10.1016/0013-4686(61)80026-1.

(7)   Bockris, J. O.; Kita, H. Analysis of Galvanostatic Transients and Application to the Iron Electrode Reaction. *J. Electrochem. Soc.* 1961, *108* (7), 676. https://doi.org/10.1149/1.2428188.

(8)   Bockris, J. O. M.; Drazic, D. The Kinetics of Deposition and Dissolution of Iron: Effect of Alloying Impurities. *Electrochim. Acta* 1962, *7* (3), 293–313. https://doi.org/10.1016/0013-4686(62)87007-8.

(9)   Kelly, E. J. The Active Iron Electrode, I. Iron Discussion and Hydrogen Evolution Reactions in Acidic Sulfate Solutions. *J. Electrochem. Soc.* 1960, *112* (12), 1256. https://doi.org/10.1149/1.2423430.

(10)   Aranzales, D.; Briliani, I.; McCrum, I. .; Wijenberg, J. H. O. .; Vooys, De, A. C. A.; Koper, M. T. M. The Effect of Naphthalene-Based Additives on Tin Electrodeposition on a Gold Electrode. *Electrochim. Acta* 2020.

(11)   Lee, J.-Y.; Kim, J.-W.; Chang, B.-Y.; Tae Kim, H.; Park, S.-M. Effects of Ethoxylated α-Naphtholsulfonic Acid on Tin Electroplating at Iron Electrodes. *J. Electrochem. Soc.* 2004, *151* (5), C333. https://doi.org/10.1149/1.1690289.

Appendices

Supporting information to Chapter 2:

Voltammetric study of tin
electrodeposition on polycrystalline gold
from sulfuric and methanesulfonic acid

A.1 Cluster formation during underpotential (UPD) and overpotential (OPD) tin deposition

Fig. A1 shows SEM images of nano-clusters formed in the early stages of the deposition (UPD), their growth and subsequent coalescence in the following stages (OPD).
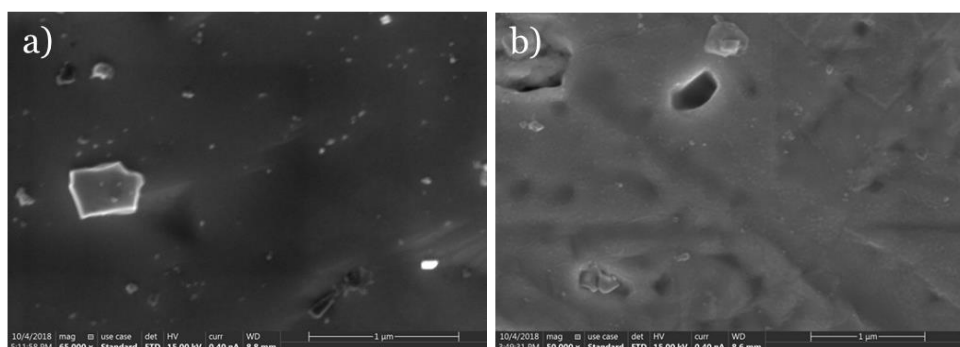

Figure A1. SEM images potentiostatic deposition of tin on polycrystalline gold electrodes in SA. a) Underpotential deposition (-0.1 V vs. RHE during 1 min). b) Overpotential deposition (-0.2 V vs. RHE during 1 min)

A.2 Concurrent HER during overpotential tin deposition

Figures A2 and A3 show that at 30 mV s^{-1} the current-voltage curves are not completely sigmoidal, and the plateau current does not vary linearly with the square root of the rotation rate in the Koutecky-Levich plots (inset), which indicates that under the present conditions no fully diffusion-limited current values are reached, neither in SA nor in MSA. This unusual behavior is related to a concurrent HER on the gold surface during the deposition process, which is likely to be present due to cluster formation, where a partial coverage of the surface is exhibited.
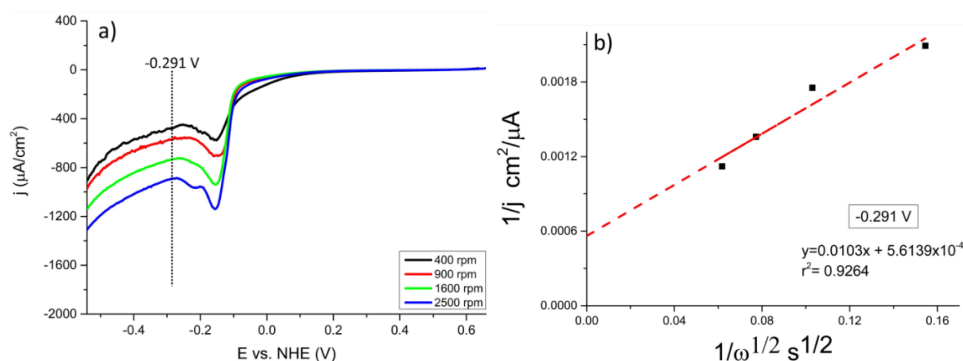
Figure A2. a) Linear sweep voltammograms of tin deposition from sulfuric acid on a gold rotating disc electrode. Concentration of solution Sn^{2+} 0.6 mM. Scan rate 30 mV s^{-1}; rotation rate 400, 900, 1600 and 2500 rpm. b) Koutecky-Levich plot.
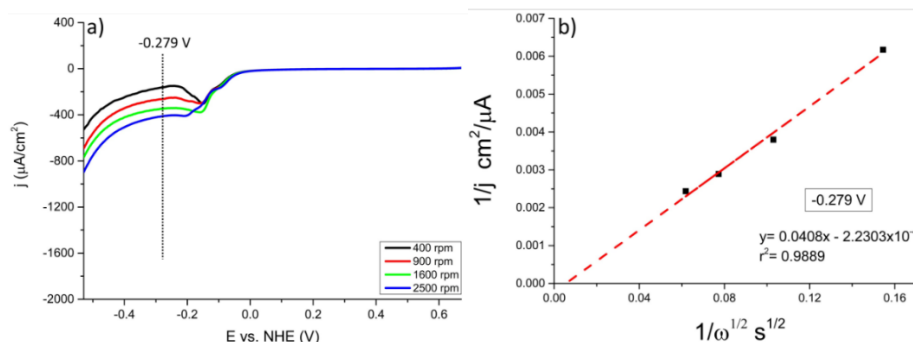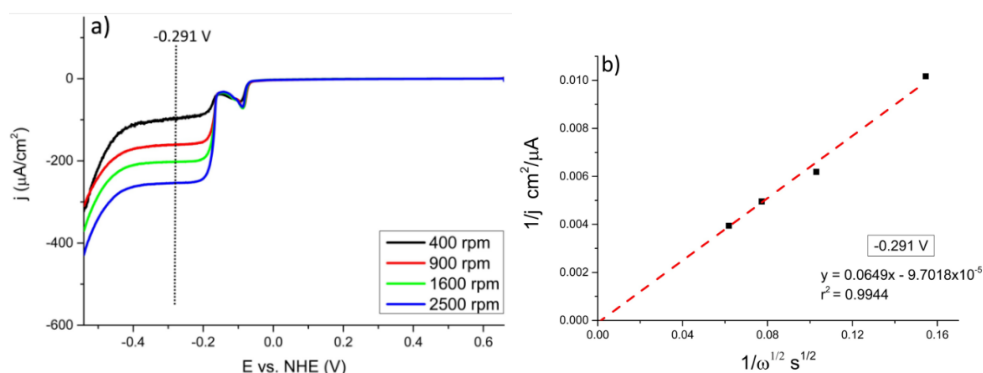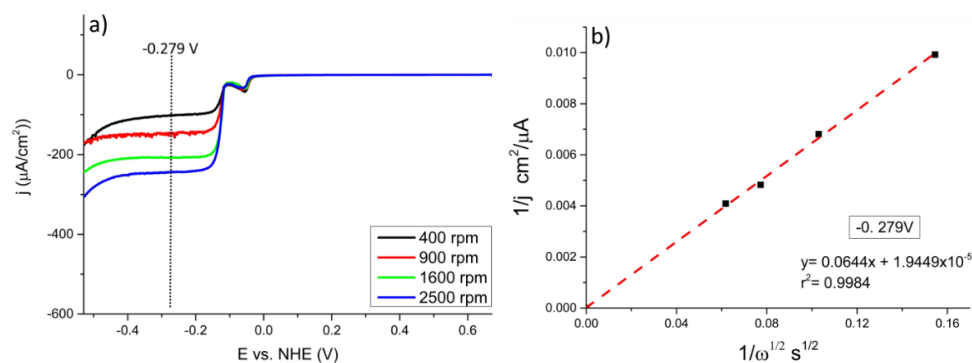

Figure A3. a) Linear sweep voltammograms of tin deposition from methanesulfonic acid on a gold rotating disc electrode. Concentration of solution Sn^{2+} 0.6 mM. Scan rate 30 mV s^{-1}; rotation rate 400, 900, 1600 and 2500 rpm. b) Koutecky-Levich plot.

A.3 Limiting diffusion control reached at low scan rates

Figure A4. a) Linear sweep voltammograms of tin deposition from sulfuric acid on a gold rotating disc electrode. Concentration of solution Sn^{2+} 0.6 mM. Scan rate 2 mV s^{-1}; rotation rate 400, 900, 1600 and 2500 rpm. b) Koutecky-Levich plot.

Figure A5. a) Linear sweep voltammograms of tin deposition from methanesulfonic acid on a gold rotating disc electrode. Concentration of solution Sn^{2+} 0.6 mM. Scan rate 2 mV s^{-1}; rotation rate 400, 900, 1600 and 2500 rpm. b) Koutecky-Levich plot.

As it has been already mentioned in the chapter, low scan rate leads to more tin deposition and subsequently a complete coverage of the gold surface, avoiding any concurrent non-desirable side reaction, such as HER on gold.   A full mass transport control region is seen in SA and MSA, following the Koutecky-Levich behavior.

B

Supporting information to Chapter 3:

The effect of naphthalene-based additives on tin electrodeposition on a gold electrode

B.1 Concentration effect of NPT, NPTS, HNPTS and ENSA on the gold surface

Figures B1, B2 and B3 show the cyclic voltammograms of NPT, NPTS, HNPTS and ENSA at different concentrations on gold single crystal surfaces.
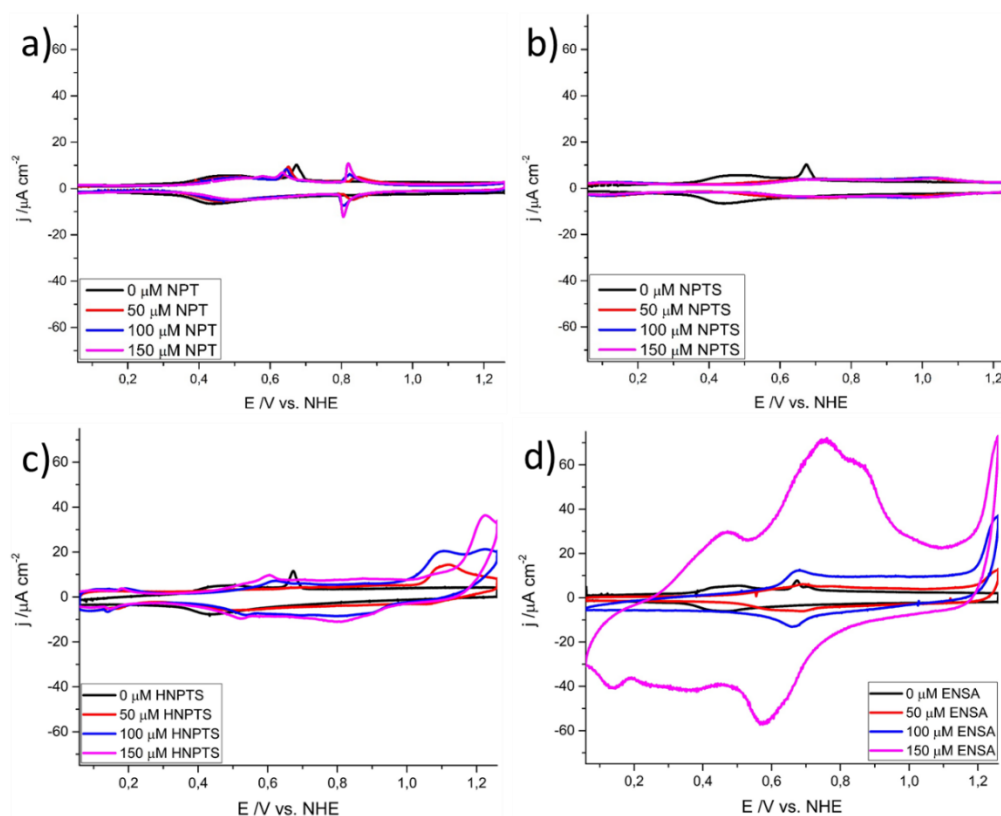

Fig B1. Cyclic voltammograms of Au (100), 0.1 M H_2SO_4 at different concentrations of (a) NPT (b) NPTS (c) HNPTS (d) ENSA recorded between 0,06 to 1.26 V DL- region, at 50 mV s^{-1}.
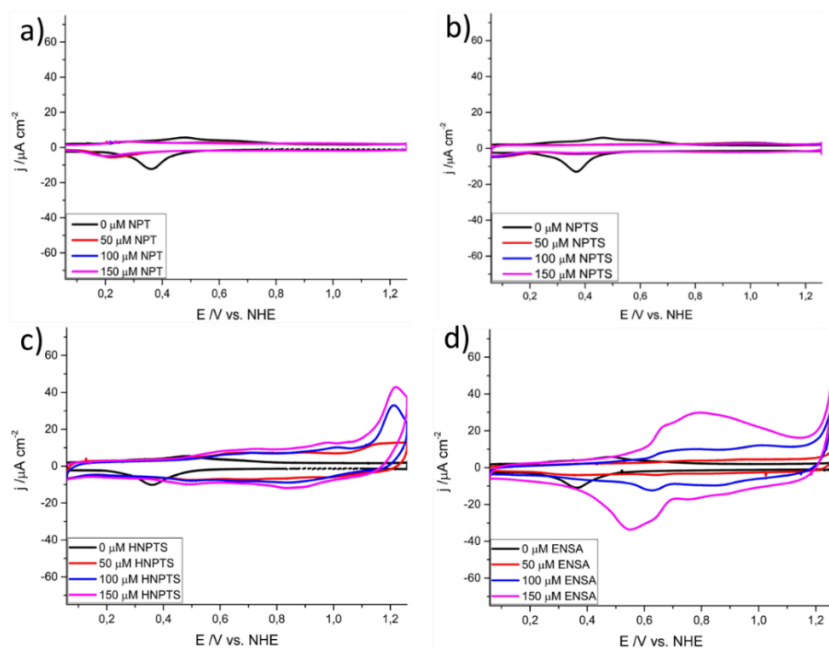
Fig B2. Cyclic voltammograms of Au (110), 0.1 M H_2SO_4 at different concentrations (a) NPT (b) NPTS (c) HNPTS (d) ENSA recorded between 0,06 to 1.26 V DL- region, at 50 mV s^{-1}.
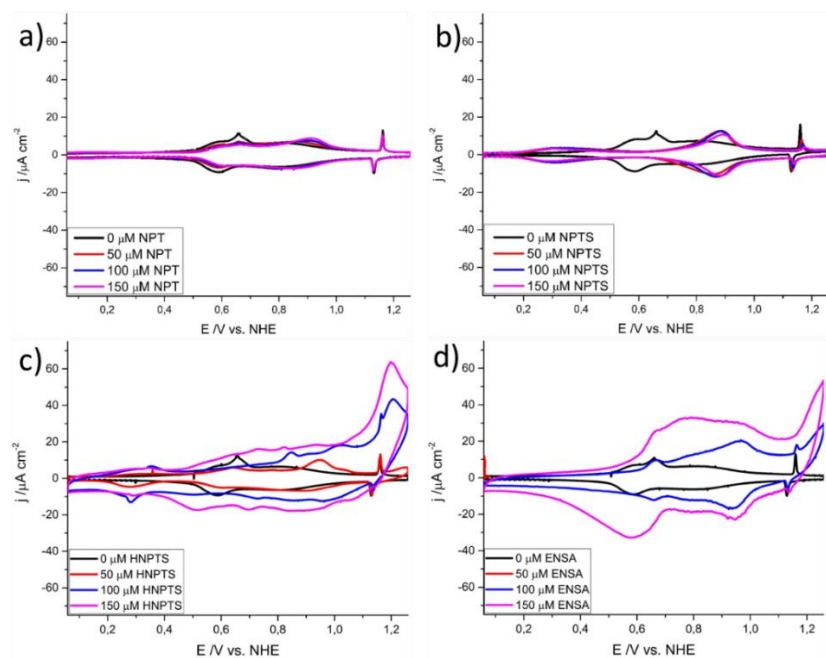

Fig B3. Cyclic voltammograms of Au (111), 0.1 M H_2SO_4 at different concentrations of ((a) NPT (b) NPTS (c) HNPTS (d) ENSA recorded between 0,06 to 1.26 V DL- region, at 50 mV s^{-}

B.2 Delay in the phase transition of sulfate adlayer as a consequence of NPT adsorption

Fig B4. shows the characteristic voltammogram of the double layer region of Au (100) in HClO$_4$ electrolyte[1, 2] (black line). When NPT is added (red line) a decrease in the capacitive current is observed, which is characteristic of 2D film formation. However, no sharp peak at about 0.81 V is seen, in contrast to what is observed in H$_2$SO$_4$ (Fig. B1 a). After the sulfate addition two reversible couples of peaks appear. The first couple at about 0.75 V is ascribed to sulfate specific adsorption and the second at 1.05 V to disorder – order transition in the sulfate adlayer. The peaks also shift slightly towards lower potentials with the higher sulfate concentration, as expected.
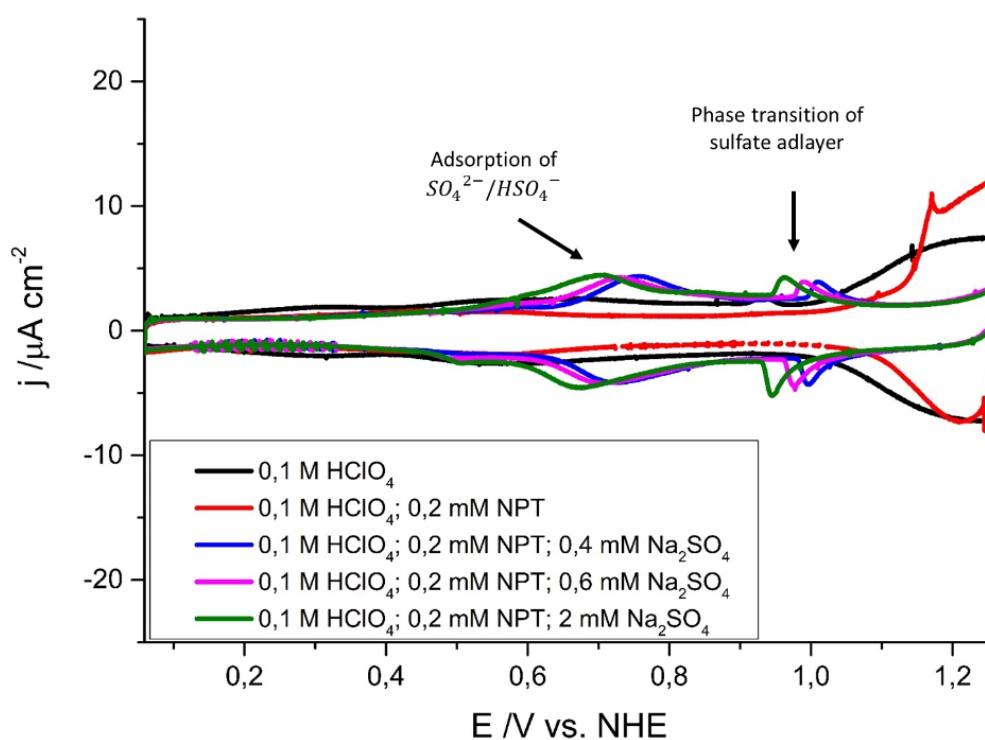

Fig B4. Cyclic voltammograms of Au (100), 0.1 M HClO$_4$, 0.2 mM NPT at different Na$_2$SO$_4$ concentrations. Recorded between 0.06 to 1.26 V DL- region

B.3 Naphthalene (NPT), naphthalenesulfonate (NPTS), hydroxynaphthalene sulfonic acid (HNPTS) and α-ethoxylated naphthalene sulfonic acid (ENSA) adsorption on the gold surface

The linear relationship between the peak current (I_p) and the scan rate (υ) is used as an argument to assign the peaks to processes related to adsorbed species. Figures B5, B6, and B7 show the mentioned linear relationship for some of the peaks of NPT, NPTS and HNPTS, but not for ENSA on the Au single crystals surfaces, which agrees with the oxidative polymerization process.
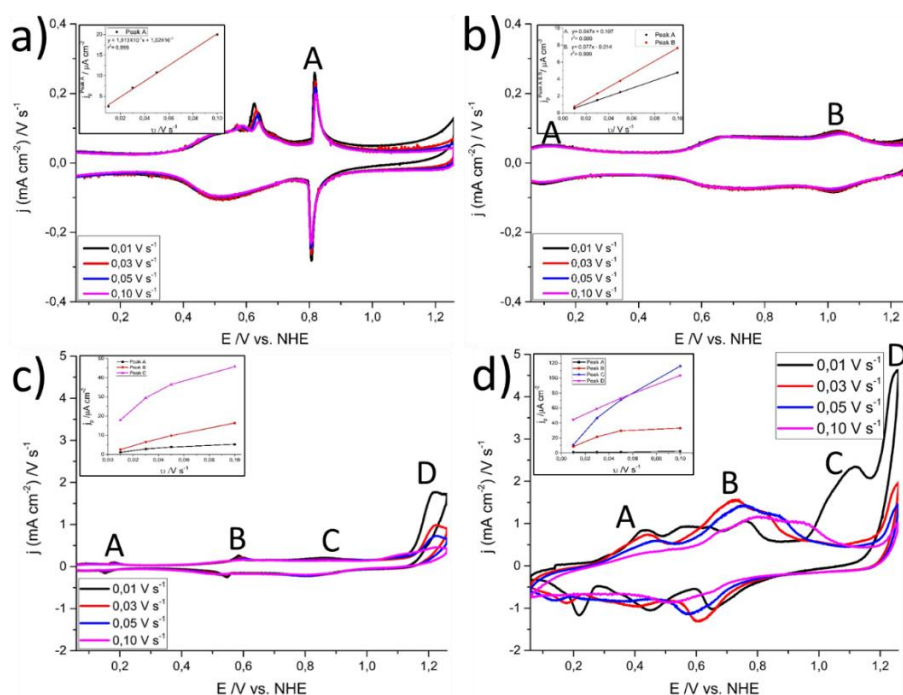

Fig B5. Cyclic voltammograms of Au (100), 0.1 M H_2SO_4 (a) 150 µM NPT and (b) 150 µM NPTS (c) 150 µM HNPTS (d) 150 µM ENSA recorded between 0,06 to 1.26 V DL- region, at different scan rates.

Fig B6. Cyclic voltammograms of Au (110), 0.1 M H_2SO_4 (a) 150 µM NPT and (b) 150 µM NPTS (c) 150 µM HNPTS (d) 150 µM ENSA recorded between 0,06 to 1.26 V DL- region, at different scan rates.
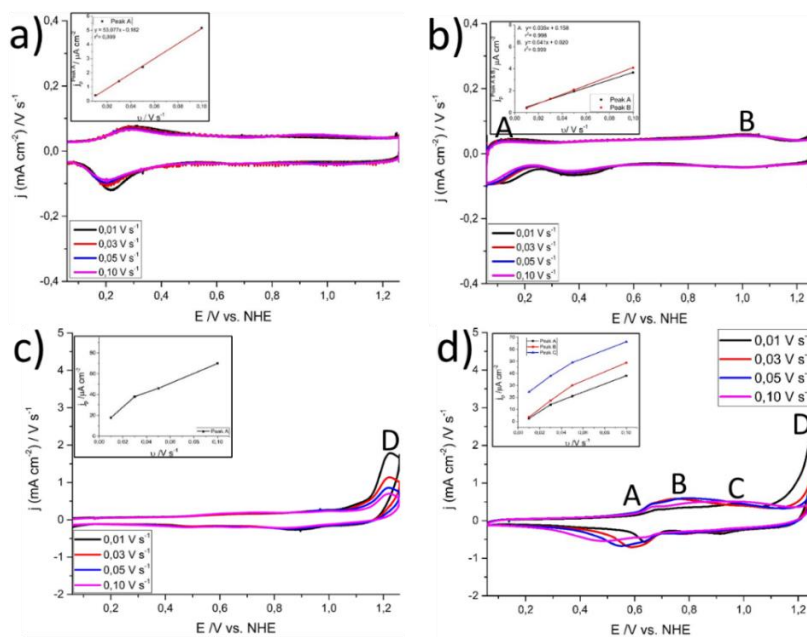

Fig B7. Cyclic voltammograms of Au (111), 0.1 M H_2SO_4 (a) 150 µM NPT and (b) 150 µM NPTS (c) 150 µM HNPTS (d) 150 µM ENSA recorded between 0,06 to 1.26 V DL- region, at different scan rates.
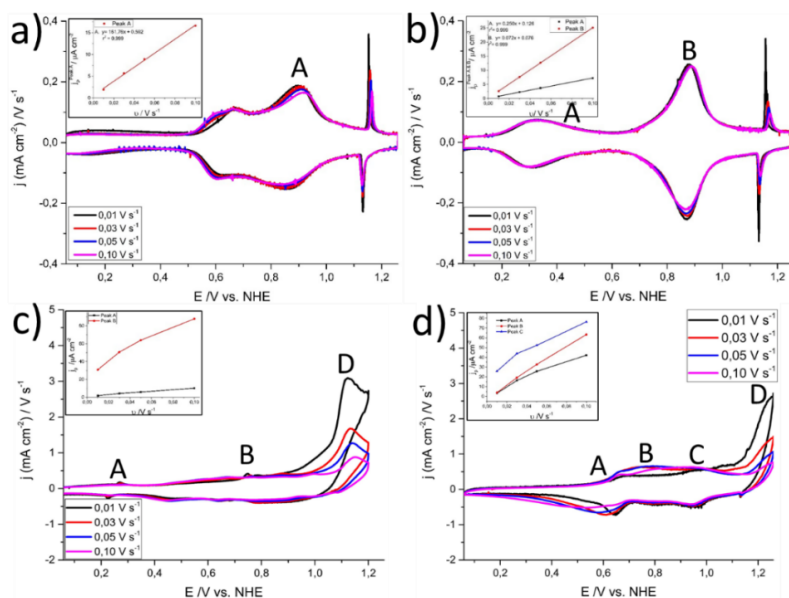
B.4 Surface enhanced Raman spectroscopy of NPT, NPTS, HNPTS and ENSA on the gold surface

Fig. B8, B9, B10 and B11 show the evolution of SER spectra of NPT, NPTS, HNPTS and ENSA on roughened gold electrode, recorded between 0.01 to 1.06 V.

Figure B8. SER spectrum of 0.2 mM of NPT in 0.1 M H_2SO_4 on polycrystalline gold at different potentials from 0.01 to 1.06 V

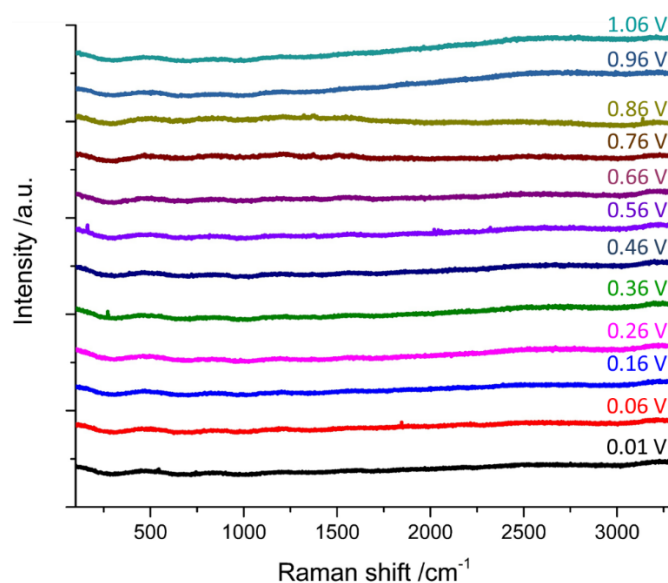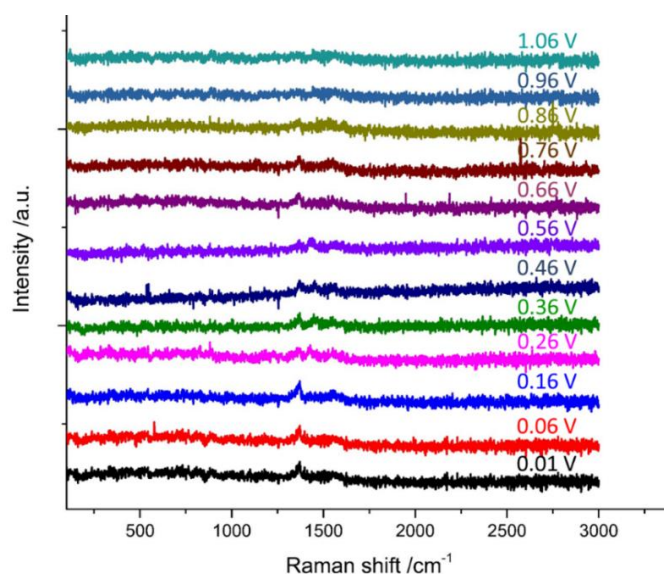**Figure B9.** SER spectrum of 1 mM of NPTS in 0.1 M H_2SO_4 on polycrystalline gold at different potentials from 0.01 to 1.06 V
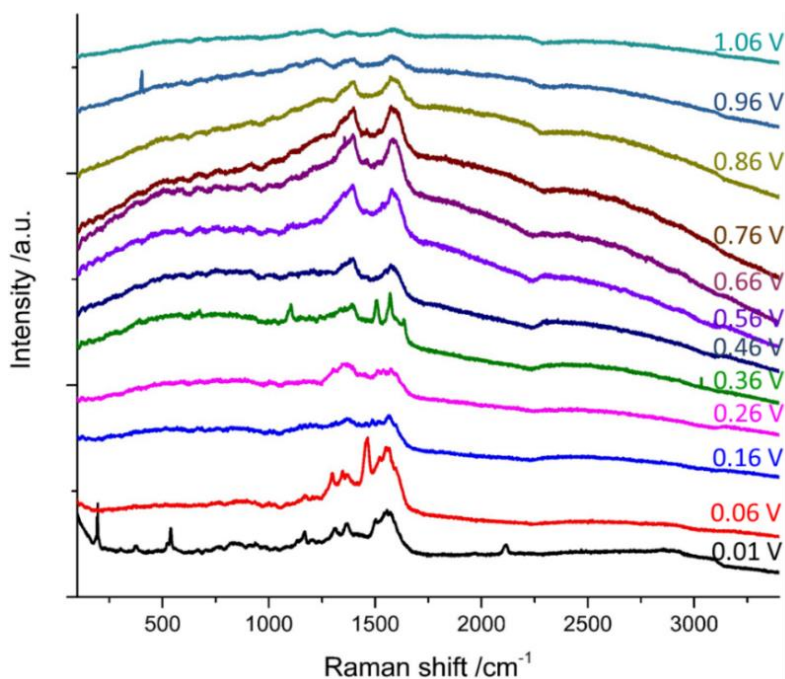
Figure B10. SER spectrum of 1 mM of HNPTS in 0.1 M H_2SO_4 on polycrystalline gold at different potentials from 0.01 to 1.06 V
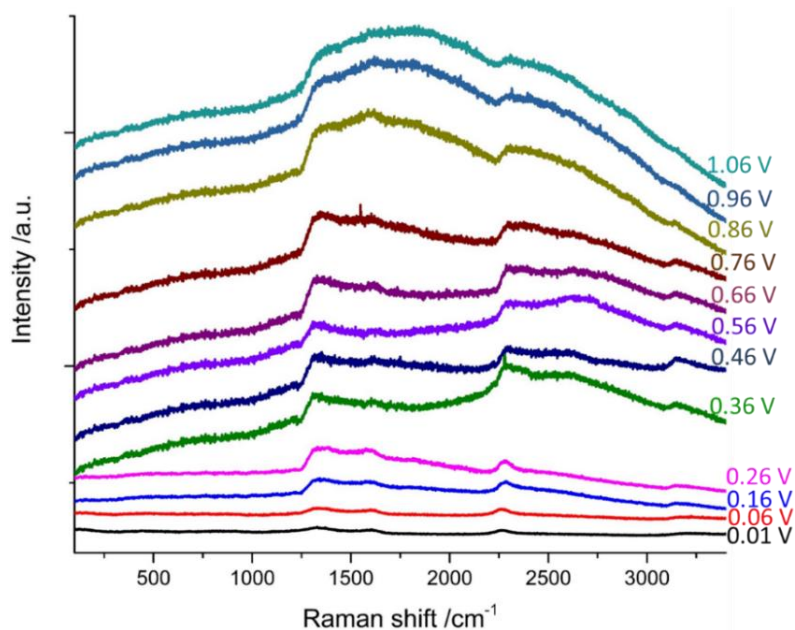
Figure B11. SER spectrum of 1 mM of ENSA in 0.1 M H_2SO_4 on polycrystalline gold at different potentials from 0.01 to 1.06 V

_____

B.5 Density functional theory study

Figure B12 shows the calculation of the lateral interaction energy between NPT and NPTS molecules, with the configuration which exhibits the highest possible attractive interaction on Au (111).

Fig B12. Difference of lateral interaction energy between (a) naphthalene and (b) naphthalenesulfonate

Figures B13 and B14 show the calculation of the lateral interaction energy between NPT and NPTS molecules, with the configuration which exhibits the highest possible attractive interaction on Sn (111).
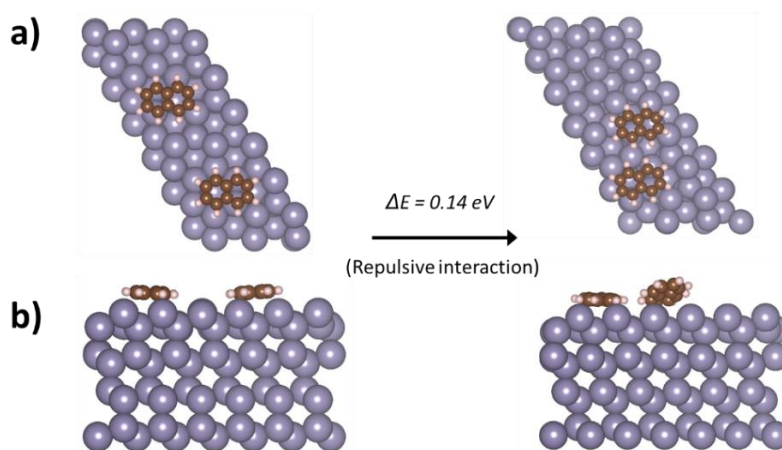
Fig B13. Difference of lateral interaction energy between naphthalene (a) top-down view and (b) lateral view
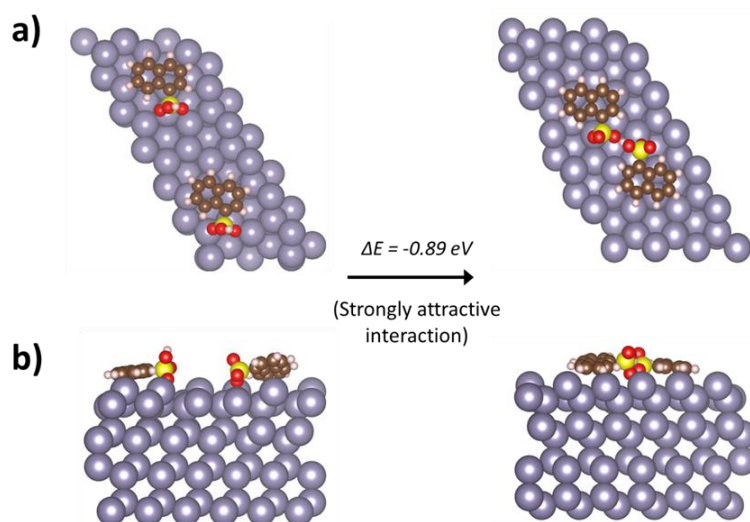
Fig B14. Difference of lateral interaction energy between naphthalenesulfonate (a) top-down view and (b) lateral view

B.6 Shift of the peak A2 is not kinetic in nature

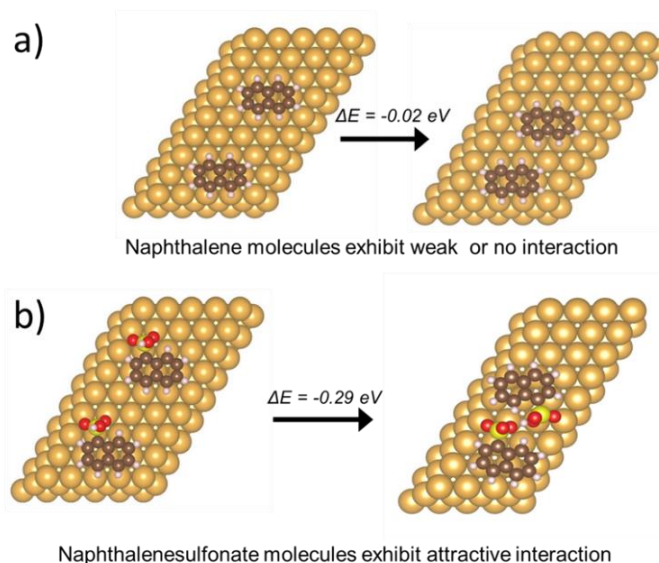Figure B15 shows the measurements of the scan rate dependence in the presence of naphthalenesulfonate. It is observed that peak A2 is not affected by the scan rate. Peak positions stay almost at the same potential, showing that the phenomenon is not related to a kinetic effect (or to diffusion from the bulk to the surface), instead is related to the thermodynamics of the process, a change in the composition of the Au-Sn alloy is likely.

Inset of the Fig. B15 shows the EDX spectrum for a nanoparticle of the tin deposit, showing small amounts of oxygen and sulfur in the deposit. Oxygen is not a surprise; it must be incorporated during the transfer to the SEM equipment due to the oxidative nature of tin.
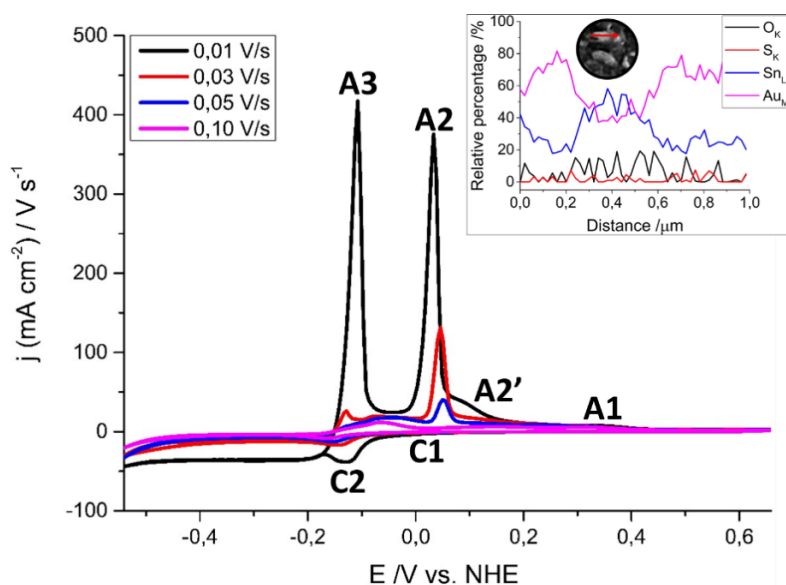
Fig B15. Cyclic voltammogram of tin electrodeposition on RDE polycrystalline gold, 0.1 M H_2SO_4, 200 µM $C_{10}H_7NaO_3S$ at different scan rates, 30 mV s^{-1} and 1600 rpm. Inset shows the spectrum of the EDX microanalysis of a nanoparticle in the tin deposit.

B.7 Number of Sn ML on the gold substrate

Fig. B16 shows the linear sweep voltammetry and the transient recorded during the tin deposition in the absence and presence of naphthalene-based additives. Transients recorded in the absence and presence of NPTS and HNPTS exhibit almost identical current, with a small difference seen in the presence of NPT, due to a slight variation of the Sn (II) concentration in the solution. Furthermore, in the presence of ENSA, a strong decrease in the current is seen in agreement with the strong inhibition of tin deposition.
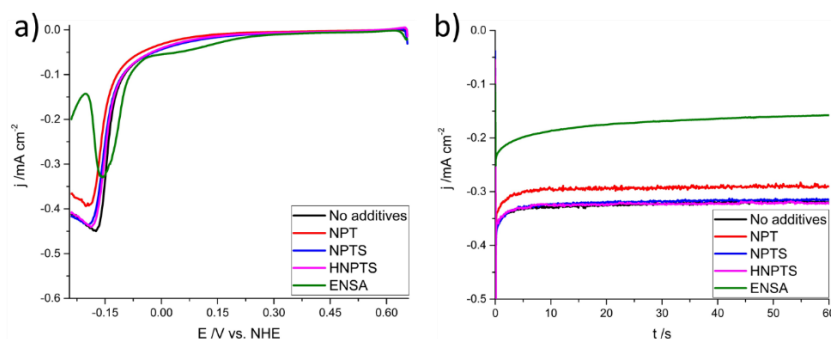
Fig B16. Linear sweep voltammetry and subsequent chronoamperometry of tin electrodeposition on RDE polycrystalline gold, 0.1 M H_2SO_4, 0.6 mM $SnSO_4$ in the absence and presence of 200 µM of: NPT, NPTS HNPTS and ENSA at 1600 rpm.

_____

B.8 Scanning electron micrographs of gold substrates
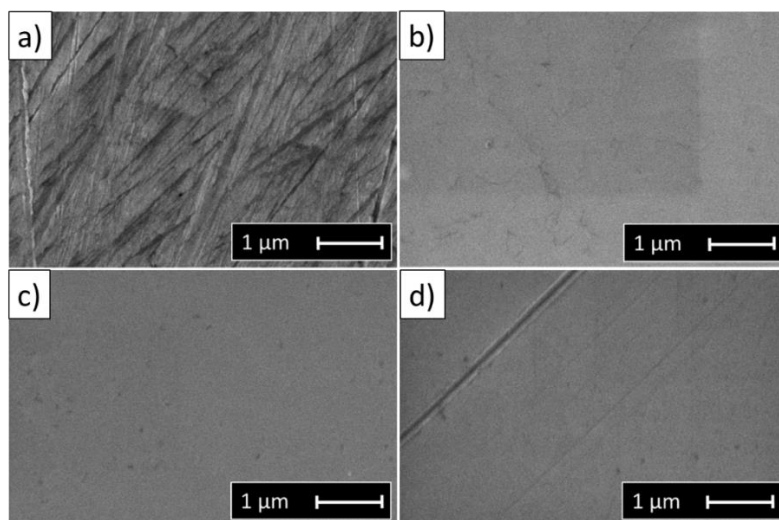
Fig B17. Scanning electron micrographs of: (a) polycrystalline gold (b) Au (100) (c) Au (110) (d) Au (111)

C

Supporting information to Chapter 4:

The effect of naphthalene-based additives
on the kinetics of tin electrodeposition on
a boron doped diamond electrode

_____

C.1 Effect of naphthalene-based additives on the tin (II) diffusion coefficient

Table C1 show the tin (II) diffusion coefficients in the absence and presence of different concentrations of NPT, NPTS and HNPTS. Values were calculated at high negative potential by fitting the current transient to the Cottrell equation.

Table C1. Tin (II) diffusion coefficient ($D_{Sn^{2+}}$) in the absence and presence of naphthalene-based additives at different concentrations, at -0.460 V.

| Additive	Concentration / mM	$D_{Sn^{2+}}$ / $cm^2 s^{-1}$
NPT	0	$7.7 \pm 0.2 \times 10^{-6}$
	0.1	8.0×10^{-6}
	0.5	6.8×10^{-6}
	1.0	6.8×10^{-6}
NPTS	0	$7.7 \pm 0.23 \times 10^{-6}$
	0.1	7.2×10^{-6}
	0.5	5.8×10^{-6}
	1.0	7.0×10^{-6}
HNPTS	0	$7.7 \pm 0.2 \times 10^{-6}$
	0.1	5.3×10^{-6}
	0.5	5.6×10^{-6}
	1.0	7.3×10^{-6}

Table C2 show the tin (II) diffusion coefficients in the absence and presence of different concentrations of NPT, NPTS and HNPTS. Values were calculated at lower negative potentials by fitting the current transient to the Cottrell equation.

Table C2. Diffusion coefficients ($D_{Sn^{2+}}$) in the absence and presence of naphthalene-based additives at different concentrations at different applied potentials.

-E /V	No additives $D_{Sn^{2+}}$ / $cm^2 s^{-1}$	NPT (1 mM) $D_{Sn^{2+}}$ / $cm^2 s^{-1}$	NPTS (1 mM) $D_{Sn^{2+}}$ / $cm^2 s^{-1}$	HNPTS (1 mM) $D_{Sn^{2+}}$ / $cm^2 s^{-1}$
-0.340	7.3×10^{-6}	7.8×10^{-6}	7.5×10^{-6}	6.4×10^{-6}
-0.365	7.8×10^{-6}	7.3×10^{-6}	7.8×10^{-6}	6.9×10^{-6}
-0.390	7.7×10^{-6}	6.5×10^{-6}	9.5×10^{-6}	7.3×10^{-6}
-0.415	7.4×10^{-6}	6.3×10^{-6}	9.5×10^{-6}	7.6×10^{-6}
-0.440	7.2×10^{-6}	7.0×10^{-6}	6.6×10^{-6}	6.5×10^{-6}

C.2 Effect of naphthalene-based additives on the nucleation mode of tin deposits on a boron doped diamond electrode
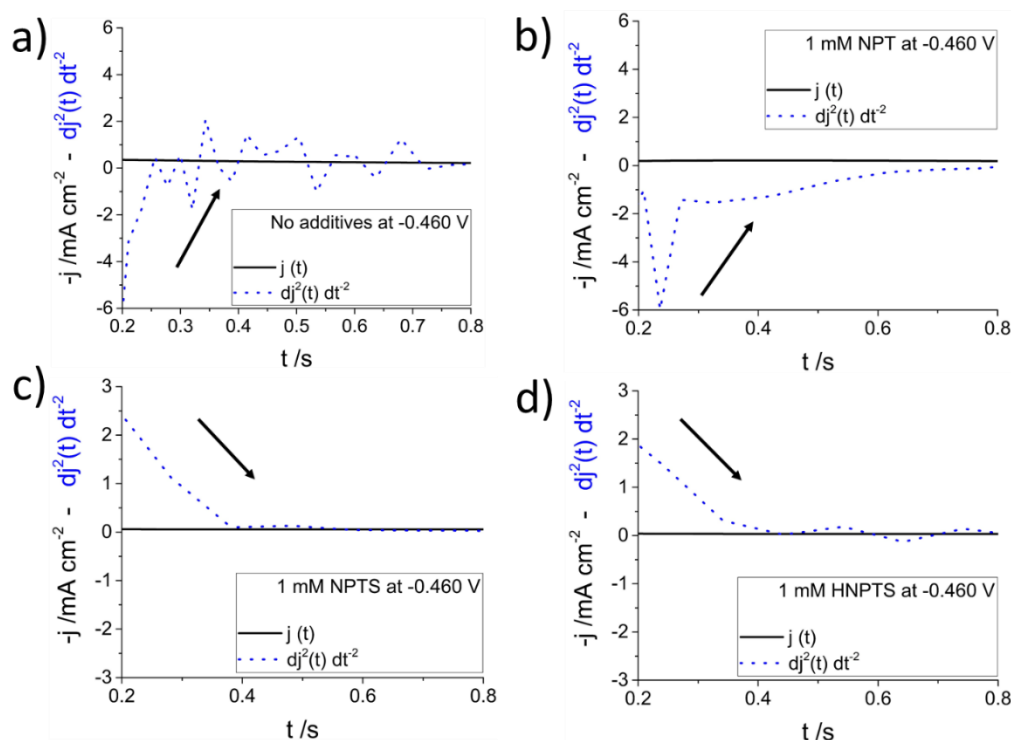
Figure C1. Current transient j(t) and second derivative $\frac{d^2 j(t)}{dt^2}$ for current transients recorded in 0.1 M H₂SO₄, 0.5 Mm SnSO₄ at -0.460 V in the (a) absence, and the presence of 1 mM (b) NPT, (c) NPTS, and (d) HNPTS

Current transients recorded at -0.460 V (the highest negative potential) in the absence of additives and presence of NPT, figures C1a and C1b respectively, exhibit a negative second derivative at short times, characteristic of instantaneous nucleation mode. The measurements in the presence of NPTS and HNPTS, fig C1c and C1d respectively show a positive second derivative, characteristic of progressive nucleation mode. Results show that NPT does not change the tin nucleation mode on BDD, in contrast to NPTS, and HNPTS that change the nucleation mode from instantaneous to progressive.

C.3 Effect of naphthalene-based additives on the morphology of tin deposits on a boron doped diamond electrode

Figure C2, C3, C4, C5 and C6 show the scanning electron micrographs of tin deposits on a boron doped diamond electrode grown in the absence and in the presence of NPT, NPTS, HNPTS and ENSA, respectively.

Figure C2. Scanning electron micrographs of tin electrodeposited on a boron doped diamond surface in 0.1 M H_2SO_4 and 0.5 mM SnSO4. Potential was held at -0.266 V for 10 s where nucleation and early growth happened, subsequently potential was held at -0.230 V during 60 s where the nuclei were grown.
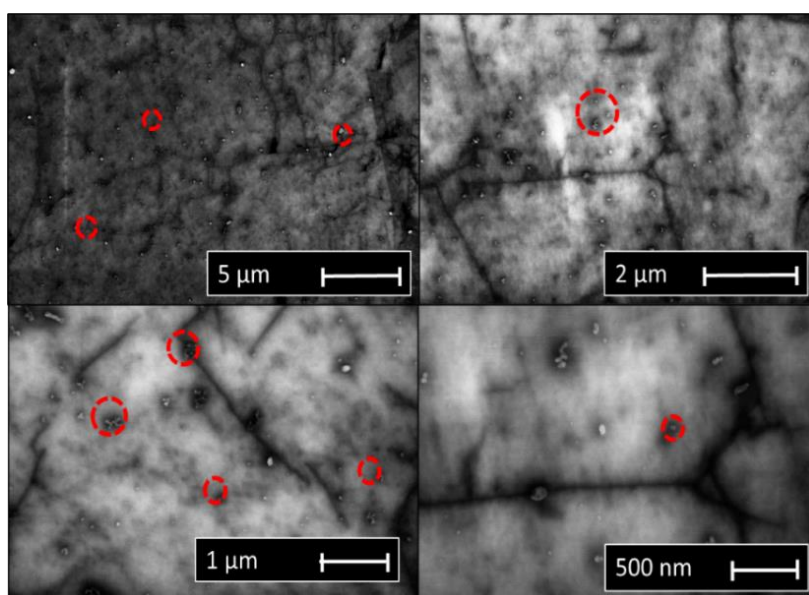
Figure C3. Scanning electron micrographs of tin electrodeposited on a boron doped diamond surface in 0.1 M H_2SO_4 and 0.5 mM SnSO4 and in the presence 1 mM of NPT. Potential was held at -0.266 V for 10 s where nucleation and early growth happened, subsequently potential was held at -0.230 V during 60 s where the nuclei were grown.

_____

Figure C4. Scanning electron micrographs of tin electrodeposited on a boron doped diamond surface in 0.1 M H_2SO_4 and 0.5 mM SnSO₄ and in the presence 1 mM of NPTS. Potential was held at -0.266 V for 10 s where nucleation and early growth happened, subsequently potential was held at -0.230 V during 60 s where the nuclei were grown.
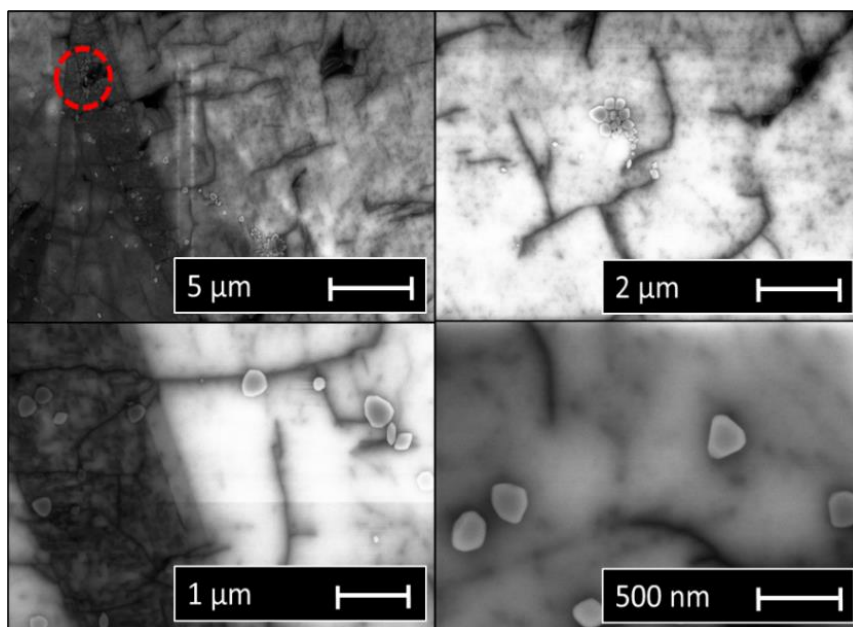
Figure C5. Scanning electron micrographs of tin electrodeposited on a boron doped diamond surface in 0.1 M H_2SO_4 and 0.5 mM SnSO₄ and in the presence 1 mM of HNPTS. Potential was held at -0.266 V for 10 s where nucleation and early growth happened, subsequently potential was held at -0.230 V during 60 s where the nuclei were grown.

_____

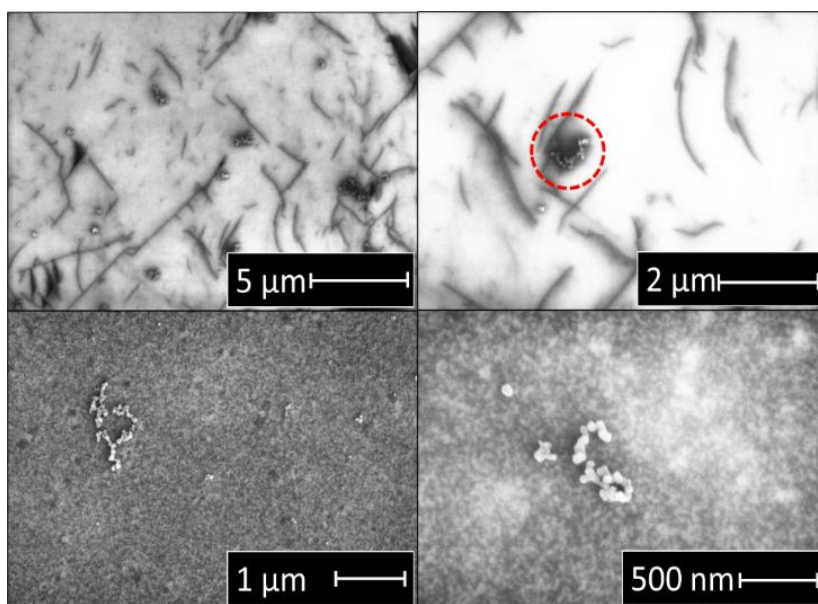**Figure C6**. Scanning electron micrographs of tin electrodeposited on a boron doped diamond surface in 0.1 M H_2SO_4 and 0.5 mM SnSO₄ and in the presence 1 mM of ENSA. Potential was held at -0.266 V for 10 s where nucleation and early growth happened, subsequently potential was held at -0.230 V during 60 s where the nuclei were grown.
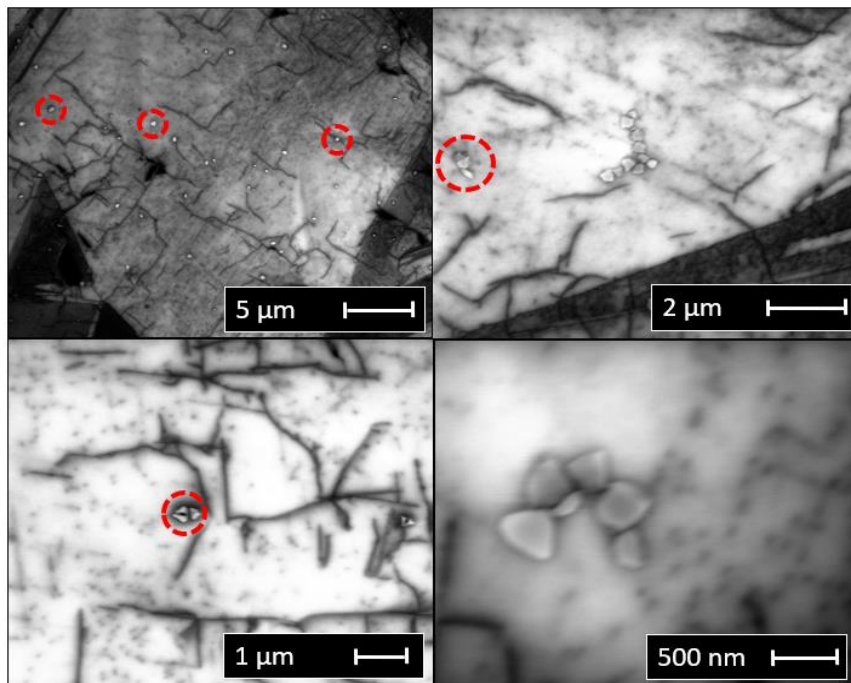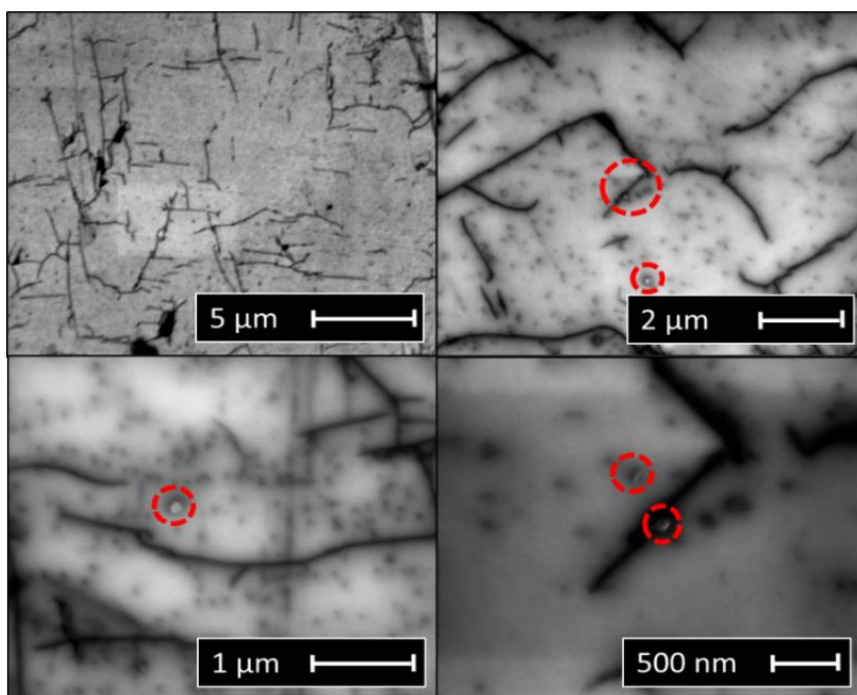
_____

Summary and outlook

Tin electrodeposition applications have rapidly evolved in the past 25 years. Usage of tin coatings has advanced from being mainly used for corrosion protection and decorative purposes, to being used in modern technology such in electronic devices, photovoltaic cells and Li – ion batteries. The new tin coating applications have also come with challenges that require the production of nanostructured deposits, multilayers coatings and composites. Furthermore, the need to reduce energy and source consumptions, and the implementation of more environment-friendly processes, require detailed and fundamental knowledge of the electrodeposition process.

The emphasis throughout this thesis is therefore to obtain detailed mechanistic information of tin electrodeposition process. The experimental and theoretical work presented in this thesis attempts to understand the mechanism of tin electrodeposition, and the effect of electrolyte anions and naphthalene-based additives, during the early and subsequent stages of the process. The experimental approach includes conventional electrochemical techniques, in-situ spectro-electrochemical and ex-situ microscopy techniques, and density functional theory studies.

Chapter 1 presents an introduction to the tin electrodeposition process, including its history and evolution. The composition of the electroplating baths is highlighted, as it is basic in the understanding of the tin electrodeposition process.

In Chapter 2, we study the tin electrodeposition mechanism on polycrystalline gold electrodes from two different electrolytes: sulfuric and methanesulfonic acid. We show the presence of at least three different tin deposition mechanisms on gold: irreversible adsorption, underpotential and overpotential deposition. Furthermore, evidences of the intricate tin underpotential deposition on gold are presented, associating it with island formation and surface alloying. We also compare the effect of sulfuric and methanesulfonic acid on the tin electrodeposition, showing that the coverage of underpotential deposited tin in the presence of methanesulfonic acid is slightly higher than in sulfuric acid. We demonstrate that kinetics of tin bulk electrodeposition in methanesulfonic acid are slower than in sulfuric acid, presumably due to Sn-MSA complex formation. Additionally, the lower tin deposition rate in methanesulfonic acid also leads to a more homogeneous coverage of the gold by tin. Moreover, our results show that Au-Sn surface alloy formation is more prominent in the presence of methanesulfonic acid, concluding that the lower deposition rate leads to a relatively more prominent surface alloying.

With the mechanism of tin electrodeposition on polycrystalline gold electrodes and the effect of sulfate and methanesulfonate anions studied, and the assignment of the peaks in the voltammetric profile done, we extended our study and focus on the effect of naphthalene-

based additives: naphthalene (NPT), naphthalenesulfonate (NPTS), hydroxynaphthalenesulfonate (HNPTS) and ethoxylated α-napthalenesulfonic acid (ENSA, a commonly used additive in the tin electroplating industry), on the tin electrodeposition process on gold electrodes. In Chapter 3, we present the results of a detailed study using spectro-electrochemical and microscopic techniques and density functional theory calculations. We conclude the formation of condensed films of NPT, NPTS, HNPTS and ENSA, where NPT and NPTS lie flat on the gold surface and HNPTS and ENSA undergo oxidative polymerization. We demonstrate that NPTS forms a denser film due to attractive interactions via hydrogen bonding between the adsorbed molecules. Considering the density functional theory studies, we claim that naphthalene-based additive films are not very sensitive to the nature of the electrode material. NPT and NPTS bind to the gold and tin electrode surfaces mainly through Van der Waals interactions and HNPTS and ENSA undergo oxidative polymerization which is generally not very sensitive to the nature of the electrode material.

Furthermore, in chapter 3 we also show tin electrodeposition is strongly affected by the presence of the NPT, NPTS, HNPTS, and ENSA films. Our results show that tin bulk electrodeposition is inhibited in the presence of NPT and NPTS, but promoted in the presence of HNPTS. Regarding the morphology of the tin deposits, NPT and NTPS exhibit a similar morphology, but tin deposit grown in the presence of HNPTS exhibits markedly smaller features. We show that the presence of sulfonated additives during tin electrodeposition on gold leads to some form of sulfur incorporation in the AuSn alloys, with thiosulfate identified as a possible intermediate in the reaction. Furthermore, we determine that ENSA exhibits a similar behavior to NPT and NPTS during the tin deposition process: a suppression of the bulk Sn electrodeposition, but essentially no effect on the AuSn alloy formation, besides sulfur incorporation. Lastly, the lack of a strong effect of naphthalene-based additives on the AuSn alloying process is ascribed to the slow nature of Sn UPD on gold and AuSn alloying process.

Following the studies of the effect of naphthalene-based additives on tin electrodeposition on gold electrodes, Chapter 4 focuses on the effect of naphthalene-based additives on the kinetics of tin electrodeposition process. Owing to the complexity of the early stages of tin electrodeposition and its fast kinetics on gold, a change of the substrate from gold electrodes to boron doped diamond (BDD) electrodes was made.

In Chapter 4, we study the effect of naphthalene-based additives on the kinetics of tin electrodeposition on a boron doped diamond electrode. Current transients in the presence of NPT, NPTS and HNPTS were analyzed with the standard Scharifker-Hills model: the steady state nucleation rate (AN_0) and the number density of nucleation sites (N_0) were determined at different applied potentials. In the absence of additives, the nucleation and growth process is shown to transition from progressive to instantaneous with increasingly negative potential. A decrease in the nucleation kinetics of tin deposition on BDD was observed in the presence of naphthalene-based additives: NPT showed the smallest effect on the reduction of the kinetics, followed by NPTS, and the strongest effect was observed in the presence of HNPTS. Moreover, we show that Sn (II) is not complexed by the additives (NPT, NPTS, HNPTS, and

_____

presumably neither by ENSA-6) and charge transfer kinetics is not influenced by the presence of the additives. Additives only affect the nucleation process. Furthermore, the behavior of ethoxylated α-napthalenesulfonic acid (ENSA) exhibits an identical behavior that on gold, i.e., a strong inhibition of the tin deposition process.

Lastly, in Chapter 5 we use the gathered knowledge of the effect of naphthalene-based additives on tin electrodeposition on more stable substrates, i.e., gold and boron doped diamond electrodes, to provide insights of the interaction of the additives with iron and their effect on the overall tin deposition process on an iron electrode. We showed the effect of NPT and NPTS on tin electrodeposition remains mainly independent of the substrate. HNPTS shows a stronger decrease of tin deposition, according to what has been previously observed on tin deposition on a BDD electrode. Furthermore, we showed that transport of Sn (II) ions from the bulk to the electrode surface is not affected by NPT, NPTS and HNPTS. We verified that ENSA-6 forms a thick film on the iron surface, a behavior correlated the strongest inhibition of tin deposition on gold, BDD and iron electrodes.

Outlook

This thesis has shown that kinetics of the tin deposition is strongly affected by the presence of the different species in solution. Nonetheless, little attention has been paid to the chemistry of the complexes that exists in the bulk solution of the electroplating baths. Despite large number of studies acknowledge the importance of complexes, there are virtually no studies that identify in detail the speciation of the tin electroplating solutions. The identification of the species in solution would allow to explain differences in the kinetics, but also in the thermodynamics of the tin deposition process.

Attention should be given to understand the interaction of single and mixtures of molecules used as additives with the substrate; more in-situ spectro-electrochemical studies are required. These studies are crucial to comprehend the role of additives during the nucleation and growth of tin deposits.

Moreover, this thesis has shed light on the importance and also the complexity of understanding the mechanism of tin electrodeposition and the effect of the substrate. Future research should make use of in-situ microscopic techniques such as scanning tunneling microscopy and atomic force microscopy, in order to get information at atomic-scale of the early stages of the tin electrodeposition. The use of well-defined surfaces (single crystals) would help to interpret the data. Furthermore, considering the increase of tin coating, tin-composites and tin alloys applications, it is also very important to study the tin deposition on multiple substrates, including highly reactive surfaces such as iron and steel.

_____

Samenvatting en vooruitzicht

Toepassingen gerelateerd aan het afzetten van een laagje tin (tin-elektrodepositie) zijn de afgelopen 25 jaar veel verder ontwikkeld. Origineel werden tin laagjes voornamelijk als bescherming tegen corrosie of voor decoratieve doeleinden. Na verdere ontwikkeling van de techniek wordt tin-elektrodepositie tegenwoordig ook gebruikt in bv. elektronische apparaten, zonnecellen en lithium batterijen. Deze nieuwe toepassingen gepaard met nieuwe uitdagingen, bijvoorbeeld in de vorm van het maken van afzettingen met specifieke nanostructuren, beschermingslaagjes welke meerdere dik zijn, en laagjes bestaande uit composieten. Tevens is het belangrijk energie- en materiaalverbruik verminderen en milieuvriendelijkere processen te ontwikkelen, waarvoor we gedetailleerde en fundamentele kennis van het elektrodepositieproces nodig hebben.

De nadruk in dit proefschrift ligt op het verkrijgen van gedetailleerde informatie over het elektrodepositieproces van tin. Het experimentele en theoretische werk dat hier wordt gepresenteerd, probeert het mechanisme van tin-elektrodepositie, en het effect van elektrolytanionen en naftaleen-gebaseerde additieven, tijdens de vroege en latere fasen van het proces te begrijpen. De experimentele benadering omvat onder andere; algemene elektrochemische technieken, in-situ spectro-elektrochemische technieken en ex-situ microscopietechnieken, en onderzoek middels theoretische (Density Functional Theory, DFT) berekeningen.

Hoofdstuk 1 is een inleiding voor het afzetten van tin, inclusief haar geschiedenis en de ontwikkeling van het veld. De samenstelling van de galvaniseerbaden wordt benadrukt, aangezien deze de basis vormt voor het begrijpen van het tin-elektrodepositieproces.

In Hoofdstuk 2 bestuderen we tinelektrodepositie-mechanismen op polykristallijne goudelektroden in twee verschillende elektrolyten: zwavelzuur en methaansulfonzuur. We tonen de aanwezigheid aan van ten minste drie verschillende mechanismen voor de elektrodepositie van tin op goud: irreversibele adsorptie afzetting bij potentialen positief t.o.v. de Nernst evenwichtspotentiaal van tin (onderpotentiaal), en afzetting bij potentialen negatief t.o.v. de Nerst evenwichtspotentiaal (overpotentiaal). Verder worden bewijzen gepresenteerd betreffende het mechanisme van elektrodepositie bij potentialen positief t.o.v. de evenwichtspotentiaal, waarbij we laten zien dat het afzetten van tin in dit potentiaalgebied gepaard gaat met de formatie van eilanden en oppervlaktelegeringen. We vergelijken ook het effect van zwavelzuur en methaansulfonzuur op de elektrodepositie van tin, wat aantoont dat de bedekkingsgraad van tin dat afgezet wordt in het UPD gebied in methaansulfonzuur iets hoger is dan in zwavelzuur. We tonen aan dat de kinetiek van tin-elektrodepositie in methaansulfonzuur langzamer is dan in zwavelzuur, vermoedelijk als gevolg van de vorming van Sn-complex. Bovendien leidt de lagere afzettingssnelheid van tin in methaansulfonzuur ook tot een meer homogene bedekking van het goud met tin.

Bovendien laten onze resultaten zien dat er meer legeringsvorming plaatsvindt in de aanwezigheid van methaansulfonzuur, waaruit we concluderen dat een lagere snelheid van tinafzetting leidt tot een relatieve toename van de hoeveelheid legeringsvorming.

Na het onderzoek naar het mechanisme van de elektrodepositie van tin op polykristallijne gouden elektrodes, waarbij we de pieken in het cyclisch voltammogram hebben toegewezen, en het effect van sulfaat- en methaansulfonaat anionen hebben bestudeerd, hebben we ons onderzoek verder uitgebreid naar naftaleen-gebaseerde additieven, en hun effect op tin electrodepositie op polykristallijn goud. We hebben de effecten van naftaleen (NPT), naftaleensulfonaat (NPTS), hydroxynaftaleensulfonaat (HNPTS) en geëthoxyleerd α-naftaleensulfonzuur (ENSA, een veelgebruikt additief in de tin-galvanisatieindustrie) bestudeerd. In Hoofdstuk 3 presenteren we de resultaten van een studie waarin fotospectro-elektrochemische en microscopische technieken worden gebruikt, samen met DFT berekeningen. Met deze studie bevestigen we de vorming van een dun membraam van NPT, NPTS, HNPTS en ENSA op het oppervlak; waarbij NPT en NPTS plat op het goudoppervlak liggen, en HNPTS en ENSA oxidatieve polymerisatie ondergaan. We laten zien dat NPTS moleculen dichter bij elkaar liggen vanwege de gunstige intermoleculaire interacties in de vorm van waterstofbindingen tussen de geadsorbeerde moleculen. Uit DFT berekeningen concluderen we dat naftaleen-gebaseerde oppervlaktemembranen niet erg gevoelig zijn voor de aard van het elektrodemateriaal. Namelijk, NPT en NPTS binden zich voornamelijk aan de goud- en tinelektrode-oppervlakken door middel van Van der Waals-interacties, terwijl HNPTS en ENSA oxidatieve polymerisatie ondergaan, wat over het algemeen niet gevoelig is voor de aard van de elektrode.

Verder laten we in hoofdstuk 3 zien dat tin-elektrodepositie sterk wordt beïnvloed door de aanwezigheid van de NPT-, NPTS-, HNPTS- en ENSA-oppervlaktemembranen. Onze resultaten tonen aan dat de elektrodepositie van tin in bulk wordt geremd in aanwezigheid van NPT en NPTS, maar wordt bevorderd in aanwezigheid van HNPTS. Betreffende de oppervlaktestructuur van de de tin-afzettingen vertonen NPT en NTPS een vergelijkbare morfologie, maar de tin afzettingen die vormen in de aanwezigheid van HNPTS zijn aanzienlijk kleiner. We tonen aan dat de aanwezigheid van additieven met sulfonaat functionaliteit tijdens de elektrodepositie van tin op goud, leidt tot opname van zwavel in de Sn-Au-legeringen; thiosulfaat wordt voorgesteld als een mogelijk tussenproduct in de reactie. Verder stellen we vast dat ENSA een soortgelijk gedrag vertoont als NPT en NPTS tijdens het afzetten van tin: er is een onderdrukking van de bulk tin-elektrodepositie, het leidt tot de opname van zwavel in de legering, maar verder heeft het nauwelijks effect op de vorming van de legering. Uiteindelijk wijden we de afwezigheid van een sterke invloed van naftaleen-gebaseerde additieven op de vorming van Sn-Au legeringen aan de langzame aard van tin elektrodepositie op goud bij potentialen positief t.o.v. de evenwichtspotentiaal, en dat het legeringsproces langzaam is.

Als vervolg op het onderzoek naar het effect van naftaleen-gebaseerde additieven op de tin-elektrodepositie op goudelektroden, richt hoofdstuk 4 zich op het effect van naftaleen-

_____

gebaseerde additieven op de kinetiek van het tin-elektrodepositieproces. De complexiteit van de vroege stadia van tin-elektrodepositie op goud en zijn snelle kinetiek, vereisen dat we het originele substraat moeten vervangen met een diamant elektrode welke gedoseerd is met boor (BDD elektrode).

In Hoofdstuk 4 bestuderen we het effect dat naftaleen-gebaseerde additieven hebben op de kinetiek van tin-elektrodepositie op een BDD elektrode. Tijdsafhankelijke stroommetingen in de aanwezigheid van NPT, NPTS en HNPTS hebben we geanalyseerd middels het standaard Scharifker-Hills model, waarmee we de nucleatiesnelheid bij stationaire omstandigheden en de dichtheid aan nucleatieplekken bij verschillende opgelegde potentialen hebben bepaald. In de afwezigheid van additieven laten we zien dat het mechanisme van de nucleatie en groei van tin veranderd van progressief naar instantaan, als we steeds negatievere potentialen aanleggen. De snelheid van nucleatie van tin op BDD nam af in de aanwezigheid van naftaleen-gebaseerde additieven; NPT had het minste effect, waarna NPTS, terwijl het sterkste effect werd gevonden de aanwezigheid van HNPTS. Tevens laten we zien dat Sn (II) geen complex vormt met de additieven (NPT, NPTS, HNPTS en, waarschijnlijk, ook niet met ENSA-6), en dat de kinetiek van de overdracht van lading ook niet wordt beïnvloed door de aanwezigheid van de additieven. Verder laten we zien dat geëthoxyleerd α-naftaleensulfonzuur identiek gedrag vertoont als aan goud, te wezen een sterke inhibitie van de elektrodepositie van tin.

Maken we in Hoofdstuk 5 gebruik van de opgedane kennis betreffende de effecten van naftaleen-gebaseerde additieven op tin-elektrodepositie op oppervlakken met hogere stabiliteit; goud en BDD elektroden, om verder inzicht te verkrijgen in hun interactie met een ijzer oppervlak, en het effect dat ze in op tin-elektrodepositie op ijzer elektroden in hun algemeen. We laten zien dat de effecten van NPT en NPTS voor tin-elektrodepositie voornamelijk substraat-onafhankelijk zijn. We tonen aan dat HNPTS leidt tot een afname in tin afzetting, in lijn met wat we eerder zagen op een BDD elektrode. Ook laten we zien dat het transport van Sn(II) ionen van de bulk oplossing naar het elektrode oppervlak niet beïnvloed is door de aanwezigheid van NPT, NPTS en HNPTS. Verder hebben we geverifieerd dat ENSA-6 een dik oppervlaktemembraan vormt op het ijzer-oppervlak, gedrag dat correleert met een sterke inhibitie van tin afzetting op goud, BDD en ijzer electroden.

Vooruitzicht

Dit proefschrift heeft aangetoond dat de kinetiek van de tinafzetting sterk wordt beïnvloed door de aanwezigheid van verschillende soorten additieven in oplossing. Desalniettemin is er in het verleden weinig aandacht besteed aan de chemie van de complexen die aanwezig zijn in de bulkoplossing van de galvaniseerbaden. Ondanks de consensus in de literatuur over het belang van deze complexen, bestaan er vrijwel geen publicaties waarin ze de complexvorming van tin in galvaniseerbaden nader. De identificatie van de verschillende complexen in oplossing zou het mogelijk maken om verschillen in de kinetiek, maar ook in de thermodynamica van het tin-afzettingsproces, te verklaren.

Er zal ook aandacht moeten worden besteed aan het begrijpen van de interactie van afzonderlijke moleculen en mengsels van moleculen die als additieven worden gebruikt met het substraat; hier zijn meer in-situ spectro-elektrochemische studies voor nodig. Deze studies zijn cruciaal om de rol van additieven tijdens de nucleatie en groei van tin-afzettingen te begrijpen.

Verder heeft dit proefschrift nieuw licht geworpen op het belang en ook de complexiteit van het begrijpen van het mechanisme van tin-elektrodepositie en het substraateffect op dit mechanisme. Toekomstig onderzoek zou gebruik kunnen maken van in-situ microscopische technieken zoals 'scanning tunneling microscopy' en 'atomic force microscopy', om op atomaire schaal informatie te verkrijgen over de vroege stadia van de tin-elektrodepositie. Het gebruik van goed gedefinieerde oppervlakken (eenkristallen) zou kunnen helpen met het interpreteren van de gegevens. Bovendien, gezien de toename van toepassingen voor tin-beschermingslaagjes, tin-composieten en tin-legeringen, is het ook erg belangrijk om de tin-afzetting op meerdere substraten te bestuderen, inclusief zeer reactieve oppervlakken, zoals bijvoorbeeld ijzer en roestvrij staal.

_____

List of publications

This thesis is based on the following publications

Chapter 2

D. Aranzales, J.H.O.J. Wijenberg and M. T. M. Koper. Voltammetric Study of Tin Electrodeposition on Polycrystalline Gold from Sulfuric and Methanesulfonic Acid, J. Electrochem. Soc. **2019** volume 166, issue 8, D283-D289

Chapter 3

D. Aranzales, I. Briliani, I. T. McCrum, J.H.O.J. Wijenberg, A.C.A. de Vooys and M.T.M. Koper. The effect of naphthalene-based additives on tin electrodeposition on a gold electrode. Electrochimica Acta **2021** volume 368, 137606.

Chapter 4

D. Aranzales, J.H.O.J. Wijenberg and M. T. M. Koper. The effect of naphthalene-based additives on the kinetics of tin electrodeposition on a boron doped diamond electrode. Submitted to ChemElectroChem **2021**.

Other publications

K. Ojha, N. Arulmozhi, **D. Aranzales** and M.T. M. Koper. Double layer of Pt (111) aqueous electrolyte interface: Potential of Zero Charge and Anomalous Gouy - Chapman Screening. Angew. Chem. Int. Ed. **2020** volume 59, 711-715

D. Aranzales, C. Blay, E. Claramonte, J.E. Primo, A. Sanz, M. Sospedra, A. Torres, D. Ventura, M. Cabello, H., A simple approach to understand materials chemistry by studying materials present in electronic lighters. Proceedings of EDULEARN15 Conference 6th-8th July, 2015. Barcelona, Spain.

_____

Curriculum vitae

Diana Aranzales was born on the 27th of October 1988 in Bogotá, Colombia and grew up in Soacha, where she attended the Cosmos high school and finished it in 2005. After finishing high school, she got a technical degree in chemistry between 2006 – 2008 at the National learning service (SENA). On August 2008, she started studying chemistry at National University of Colombia and finished it on August of 2013, during her bachelor she received the distinction as honor bachelor in 2009. During September 2013 to August 2014, she worked as analytical chemist at the industry performing chemical analysis for water quality.

In June 2014, she was awarded with the Grisolia grant from Generalitat Valenciana from Spain to study a master program. In August 2014, she moved to Spain to obtain her master's degree in Applied Chemistry at Jaume I University in Castellon de la Plana. The topic of her master thesis project was "Synthesis and characterization of graphene oxide for photovoltaic applications" supervised by Prof. Dr. Juan Carda Castelló and Dr. Teodora Stoyanova. She finished her master studies on July 2016.

In August 2016, she started her PhD studies at Leiden University under the supervision of Prof. Dr. Marc Koper to work in the project "Robust production of ultra-thin tin coated steel strip by fundamental understanding of the tin deposition process (ThinTin)" sponsored by Tata Steel Nederland Technology B.V. through the Materials Innovation Institute M2i and the Technology Foundation TTW. The main goal of the project was the fundamental understanding of the initial stages of the tin electrodeposition process and the study of the influence of different parameters involved in the nucleation and growth of tin such as electrolyte and additives effect. The results of this work are presented in this thesis and parts of the work have been published and presented at several international conferences.